Inputs Drive Cell Phenotype Variability
Supplemental Information

James Park[1,2†], Anthony Brureau[1†], Kate Kernan[3], Alexandria Starks[1], Sonali Gulati[1], Babatunde Ogunnaike[2], James Schwaber[1,2*], Rajanikanth Vadigepalli[1,2*]

[1]Daniel Baugh Institute for Functional Genomics and Computational Biology, Department of Pathology, Anatomy and Cell Biology, Jefferson Medical College, Thomas Jefferson University, Philadelphia, PA 19107

[2]Department of Chemical and Biochemical Engineering, University of Delaware, Newark, Delaware 19716

[3]Department of Pediatrics, Washington University Saint Louis, Saint Louis, Missouri 63130

* Correspondence to: James.Schwaber@jefferson.edu
Rajanikanth.Vadigepalli@jefferson.edu

† contributed equally to the present work

Material and Methods

Animals

Male, Sprague-Dawley rats (270-280g, Charles River, Wilmington, MA) were housed two per cage in the Thomas Jefferson animal facility. Facilities were maintained at constant temperature and humidity with 12/12 hour light cycles (lights on at Zeitgeber time 0).

The TJU Institutional Animal Care and Use Committee approved all protocols.

Acute Hypertension Challenge

Each rat was placed into an induction chamber to induce anaesthesia (isoflurane 5% in oxygen), Piramal, Bethlehem, PA). Once the rat was anethetized, he was moved to the surgical station and remained under anaesthesia throughout the procedure (isoflurane 2% in oxygen). The common iliac vein and artery were cannulated for delivery of pharmaceuticals (phenylephrine, or saline solution) and blood pressure measurement.

The fur around the incision site was shaved with a non-irritating electric razor, and the area was disinfected with Betadine (Purdue Products LP, Stamford, CT). A single incision was made and the subcutaneous fat and fascia was cleared away. The ascending branch of the internal iliac artery was tied off and cut to prevent blood flow and to provide access to the common iliac artery and vein. Sterile packs of braided silk (Harvard Apparatus, Holliston, MA) were used to tie off these vessels and for all other processes in the surgery. The common iliac artery and vein are separated from each other and from the sciatic nerve. Any other small feed sources to either the vein or artery within the region to be cannulated were tied off and cut. The artery was then tied closed at the distal end and clamped with a hemostat approximately half an inch proximally. The artery was sliced open and a cannula was inserted. This cannula contains 4U per mL heparin (APP Pharmaceuticals, Schaumburg, IL) to prevent coagulation in saline. Then the cannula was tied securely in place within the vessel. The cannulation procedure was repeated for the common iliac vein with a cannula containing only saline. The cannulae were then tied firmly in place. To prevent the animal from pulling out or chewing through the cannulae, a small incision was made in the skin between the scapulae and the cannulae are fed subcutaneously to this exit incision. The leg wound was sutured closed and 2% lidocaine gel was applied topically. Lidocaine was also applied topically to the small wound between the scapulae, and the animal was returned to a bedded box to recover from the anesthetic. During this recovery period, the animal was housed alone.

The animal was allowed to move freely in the bedded box for at least one hour to recover from anesthesia. The animal's blood pressure was monitored (LabView, National Instruments, Austin, TX) and recorded during this time and throughout the experiment via the arterial cannula. Unprovoked increases in blood pressure were avoided as potentially indicating increased pain or distress for the animal.

The animals fell within two experimental groups: hypertensive (n=4) and baseline normotensive (n=2). During the infusion period (1h), the hypertensive animal received phenylephrine and the control animal received an equivalent amount of saline without phenylephrine. Both solutions were delivered via the venous cannula. In the hypertensive animal, hypertension was induced and maintained using a phenylephrine concentration that was titered to maintain a blood pressure level 40mmHg higher than baseline. The infusion rate and dosage were maintained by an adjustable pump: the rate of delivery was adjusted as needed.

NTS Tissue Sections

Once the desired time point is reached, the rat was sacrificed via rapid decapitation and the brainstem was immediately frozen in OCT block (TissueTek, QIAGEN, Valencia, CA). The brainstem blocks were sectioned at 10µm, and thaw mounted on glass slides. Tissue sections were taken throughout the intermediate levels of the NTS co-extensive with the *area postrema* using a cryostat.

Immunohistochemistry Staining

To preserve RNA, immunostaining was performed within 30 minutes using an accelerated protocol. Slides were first fixed in cold Acetone and hydogen peroxide Sigma-aldrich, 50ml: 50µl) for 1 minunte, then blocked and permeabilized with PBS containing 2% BSA (Sigma–Aldrich) for 30 seconds. Afterwards, brain sections were incubated with the primary antibody anti-Tyrosine Hydroxylase (TH) 1/25 (Pel-Freez® Biologicals, Roger, AR) or anti-*c-Fos* for 2 minutes at room temperature. Then the slides were washed, and were incubated for 3 minutes at room temperature in the dark with the secondary antibody Alexa-488 anti-rabbit 1/50 (Life Technologies, Grand Island, NY) with PBS containing 2% BSA. Then slides were rinsed with PBS and dehydrated in graduated ethanol concentrations and in xylene for 5 min.

Laser Capture Microdissection (LCM)

The LCM process was performed using a PixCell system and CapSure Macro LCM caps (Arcturus Engineering, Mountain View, CA). The NTS was localized using anatomical landmarks and cells with positive staining (*Th*+ or *c-Fos*+) were lifted individually on caps.

The annulus for the Laser was adjusted to the size of immuno-labeled neurons, the neuron was lifted and screened for quality as a whole cell on the cap after capture and only accepted if the cell target was fully lifted. During single cell sampling both the tissue and the corresponding cap were inspected for the removed cell body to ensure that the fluoresced neuron of interest is collected, as demonstrated in Fig. 1A and Fig. 2A-B. The precise nature of the near-IR laser allowed us to collect an intact cell body 7.5μm in diameter from the 10μm thick tissue slices. The pre- and post-laser-microdissection inspections in conjunction with the precise nature of the near-IR laser minimized the possibility of any gross contamination from occurring.

Lysis buffer was added onto the single cell on the cap (5.5µl; Life Technologies, Grand Island, NY) and cooled on ice before storage at -80°C. Approximately 10 single NTS neurons were lifted from each immuno-stained tissue section.

High-throughput quantitative PCR

Our sample preparation does not isolate RNA from a single cell sample, but processes the single neurons directly in a reverse transcriptase reaction, which is followed by real-time PCR for targeted amplification and detection using the Roche Universal Probe Library based approach. In this PCR scheme, the signal is derived from a fluorescently labeled probe that binds to the amplicon of interest, providing additional specificity beyond the typical intercalated dye based approaches to detect the PCR amplified product.

Intron-spanning PCR primers and probes for every assay were designed using Roche's Universal Probe Library Assay Design Center (www.universalprobelibrary.com) Table S3). The standard BioMark™ protocol was used to pre-amplify cDNA samples for 20 cycles using TaqMan® PreAmp Master Mix per the manufacturer's protocol (Applied Biosystems, Foster City, CA). qPCR reactions were performed using 96.96 BioMark™ Dynamic Arrays (Fluidigm®, South San Francisco, CA) enabling quantitative measurement of multiple mRNAs and samples under identical reaction conditions (Spurgeon et al. 2008). Each run consisted of 40 amplification cycles (15s at 95°C, 5s at 70°C, 60s at 60°C). C_t values were calculated by the Real-Time PCR Analysis Software (Fluidigm).

Four 96.96 BioMark^{TM} Arrays were used to measure gene expression across the 300 single cell samples. The same serial dilution sample set was included to verify reproducibility and test for technical variability. A chip to chip comparison of the serial dilution samples demonstrates that the BioMark^{TM} Dynamic Arrays are capable of high reproducibility with minimal technical variability (Fig. S1).

Data Normalization

Individual qRT-PCR results were examined to determine the quality of the qRT-PCR. An initial pass-fail-no call assessment was made for each reaction based on the qualitative nature of the reaction curves obtained from the PCR. Following this initial review, both *samples* and *gene assays* having greater than 30% failed reactions were excluded from the present analysis. The "failure" criteria for a sample or gene assay was set fairly low in order to ensure that these failures would not bias the subsequent data analysis and further increase the quality and confidence in the data used for analysis. A total of 192 single cell samples (41 normotensive samples and 151 hypertensive samples) and 81 different gene assays were included in the present analysis.

Raw C_t values for individual samples were normalized against an average expression level between *Actb* and *Rpl19* to obtain - ΔC_t. A -ΔC_t value (Spurgeon et al. 2008) was used in order to relate this value to actual gene expression (e.g. a -ΔC_t value of 10 in one cell has higher gene expression than a cell with a -ΔC_t value of -2 in a particular gene). The following equations were used to calculate -ΔC_t values for each gene:

$$-\Delta C_t^{gene} = average\left(C_t^{Actb}, C_t^{Rpl19}\right) - C_t^{gene} \qquad (1)$$

Actb and *Rpl19*, included as part of a set of potential reference genes, were selected based on previously developed data normalization methods (Vandesompele et al. 2002; Andersen et al. 2004). These two genes proved to have the lowest stability measures (i.e. most stable behavior) across samples when analyzed by these established methods (Fig. S4). The $-\Delta C_t$ values were used as a measure for relative gene expression and used as the basis for the analytical methods utilized in this report.

Due to the nature of the multiplex gene expression data obtained, several multivariate analytical techniques were utilized. Analysis initially focused on single cells from rats exposed to hypertension in order to identify transcriptional signatures that would distinguish neurons based on their respective input-type. The analysis was then expanded to include the set of single cells obtained from the normotensive baseline condition.

Principal Component Analysis (PCA)

PCA is a mathematical technique that has a wide range of applications including analysis of high dimensional data sets produced by DNA microarrays and other high-throughput technologies. PCA is a technique that reduces the dimensionality of data while retaining most of the variation in the data set. The reduction of data is accomplished by identifying directions, or principal components, along which the variation in the data is maximal, with each subsequent principal component capturing the next largest amount of variation remaining in the data.

Single cell clustering and contributing genes

PCA was used as an unsupervised method to identify variables, specifically which genes from the initial set of 81 genes, which contributed to the variation, or separation of single cell populations along the principal components. PCA was performed on gene expression data for the hypertensive single cell samples. Multiple principal components were analyzed and genes were selected for further investigation based on their loading values for the principal components analyzed. This process resulted in a subset of 48 genes that was used to define and characterize the transcriptional behavior of the single cells described in the main text.

Gene selection criteria

In order to determine which genes had significant contributions to each principal component, genes were rank ordered based on their loading values, which were determined from PCA. The five highest and lowest ranked genes (10 genes total) from the first five principal components, which accounted for 49% of the variability in the data (based on the cumulative sum of their respective eigenvalues), were identified as genes of interest for subsequent analysis. Additionally, various subsets of the single cell data were analyzed based on gene functions (Table S3). These subsets were analyzed in order to identify any other genes contributing to the variability that may have been overshadowed by a few genes. In other words, these functional gene subsets were analyzed through PCA in order to identify less dominant sources of variability. Some of

the functional categorizations used to subset gene groups included ion channels, neuromodulatory regulators, and intracellular signaling. The full list of specific gene categorizations is listed in Table S3.

A rank ordered list of genes along the first five principal components and the respective gene functional subsets in which the single cell data was analyzed is tabulated in Table S4. The highlighted genes in Table S4 represent 30 of the final 48 genes selected that created the 48-gene dimensional data set on which further multivariate analysis was performed. The additional 18 genes were selected on the basis of their loading values from PCAs performed on the various subsets of data as described previously. As several genes were repeatedly identified as either a high or low ranking gene along multiple principal components (Fig. S5 and Table S4), a final set of 48 genes was selected.

Spearman Rank Correlation Coefficient, Dissimilarity Distance, and Multidimensional Scaling (MDS)

Several statistical and visualization techniques were used to analyze single cell populations across the multiplex set of genes identified via PCA.

Spearman Rank Correlation & Dissimilarity Distance

Relative distances between single cells were determined using the spearman rank correlation coefficient, which in this case is a nonparametric measure of association between two single cells and is based on the rankings of the 48 genes used to define the transcriptional state of a single cell. The Spearman correlation coefficient is defined by the following equation:

$$\rho = \frac{\sum_i (x_i - \bar{x}_i)(y_i - \bar{y}_i)}{\sqrt{\sum_i (x_i - \bar{x}_i)^2 \sum_i (y_i - \bar{y}_i)^2}} \qquad (2)$$

Where ρ is the Spearman rank correlation coefficient (ranging from -1 to 1) and x_i and y_i correspond to the rank order of the i^{th}gene of the expression level (i.e. $-\Delta C_t$) in single cell x and single cell y respectively. Parameters $\bar{x}_i$ and $\bar{y}_i$ correspond to the mean of all rank values in single cell x and y respectively. This coefficient value is then used to determine the dissimilarity distance between two cells:

$$d = 1 - \rho \qquad (3)$$

Dissimilarity distance d corresponds to the Spearman rank dissimilarity distance (ranging from 0 to 2) between two cells. A larger d value corresponds to two cells being more dissimilar to each other. The relative distances between all possible pairs of analyzed single cell samples was determined using the R statistical software (R Core Team 2013).

Multidimensional Scaling (MDS)

Non-metric MDS was performed in order to map the high-dimensional data set of dissimilarity values to a new set of "configuration" points $x_i, \ldots, x_n$ in a lower k-dimensional space such that the rank-order of the dissimilarity values between a pair of

single cells is well-approximated by the rank-order of distance values in the lower k-dimensional space. MDS is a technique that has been used extensively for classification in gene expression studies (Ross et al. 2003; Taguchi and Oono 2005; Fuller et al. 2002). Consequently the MDS technique maps these dissimilarity values into a lower dimensional space by interpreting the dissimilarity values as distances, which in this case equates to coordinate distances in a 3-D space. Therefore the Euclidean distance between each pair of spheres (i.e. single cells) represents the difference in their relative gene expression behavior. The closer the cells are in this projected space, the more similar they are in their transcriptional behavior. MDS aids in the visualization of the dissimilarity value between pairs of single cells and the distances between each mapped single cell approximates the calculated pair-wise dissimilarity calculated among the single cell samples. This mapping procedure occurs while minimizing the error between the actual distances in the original n-dimensional space and the lower dimensional space (i.e. minimizing the stress) (Van Deun and Delbeke 2000). This error, or stress (S), is defined as:

$$S = \sqrt{\frac{\sum_{ij}\left(d_{ij} - d_{ij}^{*}\right)^{2}}{\sum_{ij} {d_{ij}^{*}}^{2}}} \qquad (4)$$

Where d_{ij} is the target distance in the original n-dimensional space and d_{ij}^{*} is the configuration distance in the lower k-dimensional space.

Configuration points were determined using the *isoMDS* function within the *MASS* package provided by R (R Core Team 2013).

Single Cell Subtypes

As mentioned in the main text, input-type cell group definition focused on the extreme groups, cells with either *Th* expression or *Fos* expression. A rank ordering of the *Th* levels ($-\Delta C_t$) showed a significant decrease in $-\Delta C_t$ values within the lower 15% quantile. A similar approach was applied to *Fos* expression levels, however the lower 30% quantile showed a significant drop in expression levels within the subset of hypertensive samples. Thus single cells that fell within the lower 15% and 30% quantiles for *Th* and *Fos* expression ranges were deemed as *Th*-/*Fos*+ and *Th*+/*Fos*- respectively (Fig. S8-11).

The remaining single cells were considered to have dual expression of *Th* and *Fos* and could be potentially be classified as either a catecholaminergic cell receiving higher-order inputs or a hypertension-response cell responding to baroreceptor inputs via interneurons. In order to address the multiple possible categorizations for these cells, a combinatorial approach was used for classification of these intermediate-expressing cells. The $-\Delta C_t$ ranges for *Th* and *Fos* for these double positive cells were split into two groups respectively. A 30% quantile value of the *Th* expression range was used to define a threshold diving Th^{high} and Th^{low} cells while the median expression of the intermediate range of *Fos* expression levels was used to determine Fos^{high} and Fos^{low} cells. Using this binary classification of expression levels, the remaining double positive

cells could be classified in one of 4 groups, *Th*^{low}/*Fos*^{low}, *Th*^{low}/*Fos*^{high}, Th^{high}/*Fos*^{low}, and *Th*^{high}/*Fos*^{high} as indicated in Fig. 5A in the main text and in Fig. S8A-S11A and Fig.S8B-11B.

Testing Th and Fos quantile limits

The quantile limits used to define the various input-type groups resulted in the extreme subtypes (*Th*+/*Fos*- and *Th*-/*Fos*+) forming extreme clusters in MDS space (Fig. 4) with the intermediate input-type groups forming intermediate clusters in-between the extreme cluster of single cells. In order to test whether or not the organization of single cells is strictly dependent on the specific thresholds used, various threshold values were used to define the six input-type groups (Fig. S8-S11). Threshold ranging from a 5% quantile limit to a 25% quantile limit were used to redefine the subtypes (Fig. S8A/B, S9A/B, S10A/B and S11A/B). Using the new subtype classification, it is clear that regardless of the quantile limit used, cells classified in the extreme subtypes continue to cluster into extreme groups in the MDS space while the intermediate groups remain clustered in-between these extreme groups (Fig. S8D, S9D, S10D and S11D). The persistent placement of single cells at the extreme regions in the MDS space indicates that this multiplex gene gradient behavior across single cells is indeed strongly correlated to the strength and magnitude of the inputs received.

Statistical Significance of Subtype Clusters and *Th* and *Fos* expression limits

In order to determine the statistical significance of the extreme clusters, we determined the likelihood of similar extreme sub-type groups forming randomly from the existing data set. This probability was determined by performing the same statistical analysis (pairwise spearman rank correlation across single cells and MDS visualization of the dissimilarity data) on random permutations of the 48-gene “vectorized” data set of the single cells analyzed.

A random permutation of the data consisted of randomly shuffling the gene expression values ($-\Delta C_t$) within a single cell sample. For example, the original *Fos* expression value would be randomly switched with the expression value of *Atf2*, *Th* switched with *Tac1*, and so on and so forth. This random shuffling of gene expression data was performed on each single cell resulting in a single iteration of a random permutation of the data. Using this randomly shuffled data set, all possible pairwise comparisons between single cells were made to determine the Spearman rank correlation coefficient (2). This was then converted into a distance metric (3). This distance data matrix was then projected into a three dimensional space via multidimensional scaling (Fig. 4).

The same *Th* and *Fos* quantile limits were used to define the two extreme sub-types identified in our original analysis (*Th*+ limit: 15% quantile, *Fos*+ limit: 30% quantile). Thus the 15% quantile limit was defined by the randomized set of *Th* and *Fos* expression values. The dissimilarity values based on all possible pairwise-comparisons of the permuted data were projected into the 3D MDS space for visualization of the high dimensional distance data set. The input-type annotation was then applied to the projected data for the extreme *Th*+/*Fos*- and *Th*-/*Fos*+ cell groups. We then characterized the two extreme cell groups using two typical statistical measures,

centroid distance and minimum distance, to define how these extreme cell groups were positioned relative to each other. In this case the centroid distance is defined as the distance between the central point (i.e., centroid) of the cluster of cells within a subtype (using cells falling within the 95% of the density distribution for the respective subtype). The minimum distance is simply the minimum distance between these two clusters. We repeated this permutation and cluster characterization process 1000 times with the existing data set.

We then posed the null hypothesis that the Euclidean distance (centroid or minimum distance) between the original extreme cell groups (within the MDS space) is no different than the distance measure obtained from the randomly shuffled data set. The alternative hypothesis indicates that these distance measures are greater than the distances from the shuffled data set. The 1000 iterations performed show that only one permutation of the data was able to achieve a centroid distance between the extreme cell subtypes equal to or greater than the centroid distance between the originally defined *Th*+/*Fos*- and *Th*-/*Fos*+ cell groups (Fig. S7E). Moreover, none of the permutations were able to achieve a minimum distance greater than the minimum distance between the original groups. Thus the empirically defined p-value of the centroid and minimum distance between the *Th+/Fos*- and *Th-/Fos*+ cell groups are 0.001 and 0 respectively allowing us to reject the null hypothesis. These values give no reason to suspect that these extreme subtypes or clusters are a result of random chance (Fig. S7E-F).

Gene Correlation Networks

The gene expression heat maps of Fig. 4D and Fig. 5C indicate substantial correlation of gene expression across the various subsets of single cells. In Fig. 4D the heat map is divided into top and bottom rows for what appears as two distinct gene correlational clusters, which we have termed “modules”. We used a Spearman rank correlation coefficient approach to produce a quantitative representation of these pair-wise comparisons of gene-gene correlations and the two modules across the various subsets of single cells. These results were visualized in Fig. 4C. Then the correlational results were visualized as network structures – as described below.

Spearman rank correlation coefficient

The $-\Delta C_t$ values for the set of 192 single cell samples (151 hypertensive and 41 control single cells) and subset of the 48 genes identified by PCA were used to determine possible correlative relationships between genes across single cell samples. Individual reactions that failed were interpreted to represent either too low or no measurable amount of cDNA in the amplified sample. Therefore a “minimum-1” value was substituted for that particular sample-gene qRT-PCR reaction (the minimum value being the lowest -ΔCt value across all samples for a particular gene) (Bergkvist et al. 2010). The Spearman correlation coefficient shared between two genes was calculated using equation (2). In this case x_i and y_i corresponds to the rank order of gene x and gene y for the i^{th} single cell sample. Therefore two genes having a high ρ value indicate that the two genes that have similar rank ordering across the set of single cells analyzed. Spearman rank correlation coefficients were calculated for all possible pair-wise

comparisons of the 48 genes identified from PCA across single cells within each of the input-type sub-types identified. Only gene-to-gene correlation coefficients >= 0.4 were used to define whether or not two genes shared a correlative relationship and were included in the correlational network diagram.

The target genes are separated into transcription modules identified by their Spearman rank correlation across single cells (Fig. 4C). This structure allows for an easier visualization and interpretation of how the pairwise functional relationships change under physiological perturbations (baseline normotensive group and hypertensive sub-groups).

Gene network diagram structure
The connectional relationships among genes were represented as connections between members of three circles, in a tri-circular manner. The objects in the top circle in each panel are transcription factors (TFs) and the bottom circles represent the genes of each gene expression module (Fig. 6).

The correlative network structures represent correlative relationships shared between TFs and target genes of each module across the three cell types: baseline *Th*, hypertension *Th*, hypertension *Fos*. This structure and the three constituent parts provide an efficient way to visualize differences in correlative relationships and connectivity across the modules and cell types.

In this context, we note that the number of correlational relationships between TFs and target genes from module 1 and module 2, is much higher in the baseline group of cells (obtained from normotensive rats), and decreases in the hypertensive group of cells (obtained from hypertensive rats) shown (Fig. 6). The *Th* hypertension cells share network properties that are intermediate, with commonalities with both the other cell types, which are most different from one another. Additionally, the number of correlations between genes of module 1 and module 2 decreases in the perturbed (hypertensive) groups of cells.

Contour Plots and Dynamic Landscape
The contour plots and 2-dimensional figures are used to help illustrate the concepts of distinct cell states and the influence inputs have in determining these states. The contour pots are a projection of the single cells in the 3D MDS space onto a 2D plane (Fig. 7A and 7B). This perspective provides a further reduction of the high-dimensional dissimilarity data set. Moreover, the contour plots provide a simplified perspective on how the various input-type groups are positioned relative to one another. The placement of the *Th+/Fos-* and *Th-/Fos+* groups are clearly positioned at the extremes of the entire region, or landscape, while the intermediate groups occupy the intermediate region in-between the two extreme groups. This schematic also illustrates the idea of how a single cell may transition between respective cell states and the likelihood of such a transition occurring. Cell states that share a high degree of overlap, as is the case with the *Th+/Fos-* and Th^{high}/Fos^{low} are more likely to have single cells transition between these states as opposed to distinct states that are much farther apart. The various

colored contours represent the 65th, 95th, and 99th percentile of the single cells for any given input-type group. Outliers, defined as cells falling outside of the 95th percentile of all single cells classified within a subtype, were not included in defining the 65th, 95th, 99th percentile. The majority of cells lie within the inner most contour region in this topology (65th percentile) (Fig. 7A and 7B).

To further emphasize the dominant transcriptional states and how these states relate to one another, a landscape topography was created. The landscape topography is based on an inversion of the probability densities of single cells. When there is a greater concentration of cells in a particular region, such as those found in the 65th percentile of a particular input-type group, the probability density is much higher and decreases as one moves away from these regions of high single cell concentration. A topographical plot based on the probability densities was then inverted in order to create regions of lower values or valleys in this landscape to highlight the stability associated with these dominant transcriptional or potential "attractor"-like states. As a single cell moves away from the inner most contour or deep well, it is transitioning away from the well and climbing up towards a less stable state, which is less occupied by the single cells. Depending on the inputs received, single cells may occupy these various stable valleys and intermediate levels within these valleys.

Contour plots and landscape topography figures were based on the projected point values in the 3D MDS space (Fig. 7A and 7B). The plotrix, gplots, and graphics packages that were used to generate the figures are in the R statistical software (R Core Team 2013).

Cross-Contamination Analysis of LCM Single Cell Samples

In order to investigate the likelihood of adjacent cell contamination in LCM single cell samples, gene expression levels were measured from a separate set of single neuron and astrocyte samples collected from the NTS of a naïve rat. Due to the high density of astrocytes and their close proximity to neurons, this cell-type and associated genes were selected to test for possible cross-contamination in single neuron samples. Single cell samples were obtained using the following methods:

Tissue Sections

Coronal 10μm sections from the naïve rat were obtained using the same procedures outlined in the "NTS Tissue Sections" text.

Cell-Type Specific Immunohistochemistry Staining

Following the accelerated protocol outlined in the "Immunohistochemistry Staining" section, brain tissue sections were incubated with the primary antibody anti-Tyrosine Hydroxylase (TH) 1/25 (Pel-Freez® Biologicals) or anti-Glial Fibrillary Acidic Protein (GFAP) (Invitrogen^{TM}). Due to availability issues, TH-tissue sections were incubated with the secondary antibody Cy3 anti-rabbit (Jackson ImmunoResearch Laboratories, Inc.) instead of Alexa-488 anti-rabbit. GFAP-tissue sections were incubated with the secondary antibody Alexa-488 anti-mouse (Jackson ImmunoResearch Laboratories, Inc.).

Single Neuron and Astrocyte LCM Sampling

The same procedures and settings outlined in the "Laser Capture Microdissection (LCM)" were used to obtain single neuron and single astrocyte samples. Cells with positive staining (TH+, GFAP+) were lifted individually on caps. Pre- and post-laser-microdissection inspections of the tissue slice and cap were performed for each single cell collected to ensure that no gross contamination was present in a sample. Once each cell was screened for quality as a whole cell on the cap after capture, lysis buffer was dropped onto the single cell on the cap (5.5µl; Life Technologies, Grand Island, NY) and cooled on ice before storage at -80°C.

Single Neuron and Astrocyte qRT-PCR

Intron-spanning PCR primers for genes enriched in astrocyte, microglial, and endothelial cells were designed using QuantPrime (www.quantprime.de) and PrimerBLAST (www.ncbi.nlm.nih.gov/tools/primer-blast). The same reverse-transcription and pre-amplification procedures outlined in the "High-throughput quantitative PCR" section were used for the single neuron and astrocyte sample set. Eva Green® dye was used for DNA binding during the PCR cycle due to its high binding sensitivity, which would minimize the chance of false negatives (e.g. GFAP non-expression in a neuron sample) as a result of technical issues. Runs were 40 cycles (15s at 95°C, 5s at 70°C, 60s at 60°C). C_t values were calculated by the Real-Time PCR Analysis Software (Fluidigm).

Data Normalization for Neuron and Astrocyte LCM samples

Raw C_t values for individual samples within a particular assay were normalized against the median expression level across all neuron sample replicate 2 raw C_t values within the respective assay. The following equations were used to calculate $-\Delta C_t$ values for each gene:

$$-\Delta C_t^{gene} = median\left(C_{t,\ i-rep2}^{gene}\right) - C_t^{gene} \qquad (5)$$

where i is the i^{th} single neuron sample from replicate set 2 ($rep2$).

Supplemental Table and Figure Legends

Table S1. Raw Ct data of quality controlled single cell samples.

Table S2. Normalized $-\Delta C_t$ data of quality-controlled single cell samples.

Table S3. Specific gene categorizations, related primer sequences, and gene entrez ID.

Table S4. Selection of genes contributing to variability. Genes are rank ordered based on their loading values along the first principal component. The highlighted loading values indicate genes that were selected based on their high or low loading values along each respective principal component.

Fig. S1. High-throughput qPCR reproduciblity. A serial dilution sample set of mRNA extracted from tissue punches from the nucleus tractus solitarius (NTS) of a Sprague Dawley rat was assayed on each 96.96 BioMark™ dynamic array. A pairwise comparison among all dynamic arrays shows that the measured C_t values for the serial dilution sample sets fall along the 45 degree line (red dashed line) with minimal deviation. The slope and R^2 values are nearly 1 for all graphs indicating that the arrays are capable of measuring gene expression values, over 5 orders of magnitude, consistently with minimal technical variability.

Fig. S2. High-throughput qPCR analysis of LCM collected single neurons and astrocytes. (A) Heat map representing gene expression levels of single neuron and astrocyte samples obtained via BioMark™ (Fluidigm©; reference Materials and Methods High-throughput qPCR for additional details). Raw C_t values are visualized in the heat map. Ten single neuron and eight single astrocyte samples were collected and measured. Two sets of technical replicates across samples and four technical replicates across each assay were measured. Assays measuring the expression of housekeeping genes (*Gapdh, Rpl19*) and cell-type enriched genes were used. Cell-type enriched assays include an astrocyte-enriched gene (*Gfap*), neuron-enriched genes (*Cacna1d, Th*), microglia-enriched gene (*Itgam*), and endothelial-enriched genes (*Lamb3, Pecam1*). Rat whole brain RNA extract was included as a positive control while DNA suspension buffer was included as a negative control. Expression of housekeeping genes occurs in both types of single cells (neurons and astrocytes) as expected. *Gfap* expression is present in all astrocyte samples while it is either low or non-existent in single neuron samples, which suggests minimal cross-contamination of astrocytes in neuron samples. Expression of *Cacna1d* and *Th* is present in all neuron samples while it is non-existent in single astrocyte samples indicating no cross-contamination of neurons in astrocyte samples. Additionally, expression of microglia and endothelial-enriched genes is non-existent in either neuron or astrocyte samples, which indicates no cross-contamination of microglial or endothelial cell-types in either neuron or astrocyte samples collected by LCM. **(B)** A plot of sample (technical) replicate 1 versus sample (technical) replicate 2 shows the highly-reproducible nature of the high-throughput qPCR BioMark™ platform and demonstrates the low technical variability

affecting gene expression measures of single cell samples. **(C)** Representative qPCR amplification curves from the same single cell samples used in the gel-electrophoresis run (ref Fig. S2C). **(D)** Heat map representing median centered $-\Delta C_t$ values. Raw C_t values were subtracted from the corresponding median C_t value of neuron replicate sample set 2 within each assay. Neuron samples show higher normalized expression of *Cacna1d* and *Th* (neuron-enriched assays) than astrocyte samples and minimal to no normalized expression of *Gfap* (astrocyte-enriched assay).

Fig. S3. Assay technical replicates. All possible pairwise comparisons of assay technical replicates measured for single neuron and astrocyte LCM samples (Fig 2). All possible pairwise combinations show minimal technical variability which further supports the highly reproducible nature of the high-throughput qPCR measurements obtained from the single cell samples.

Fig. S4. Reference gene stability. (A) Stability measures of the four potential housekeeping genes as determined by the geNorm method developed by Vandesompele et al., (2002). The variability measure indicates a gene that has lower gene expression variation across the samples and conditions measured. **(B)** Variability of the four potential housekeeping genes as determined by the NormFinder method developed by Andersen et al., (2004). Similarly a lower variability value indicates more stable gene expression behavior across samples and conditions measured. In both cases, *Actb* and *Rpl19* exhibited the most stable behavior.

Fig. S5. Contribution of genes to variability. Ranked loading values for all 81 genes analyzed across multiple principal components (PCs). **(A)** PC 3, **(B)** PC 4, and **(C)** PC 5 are included. Different genes have greater (or lower) contributions to the variation in data along each principal component.

Fig. S6. Multiple angles of 3D MDS visualization. Various angles are included to provide additional perspective on how single cells of **(A,C,E)** extreme groups and **(B,D,F)** intermediate groups are projected into the 3D MDS space (based on their similarity in rank ordered gene expression). Cells not included in the extreme *Th+/Fos-* and *Th-/Fos+* groups are represented by smaller more transparent grey spheres in (**A**). Conversely, cells not included in the intermediate groups (Th^{high}/Fos^{low}, Th^{high}/Fos^{high}, Th^{low}/Fos^{low}, Th^{low}/Fos^{high}) are represented as smaller more transparent spheres in (**B**).

Fig. S7. Statistical significance of *Th+/Fos-* and *Th-/Fos+* thresholds. Normalized gene expression data was permuted over 1000 iterations to determine the possibility of similar extreme groups forming randomly. The centroid distance and minimum distance between the extreme subtypes were used to characterize their relative positioning. The centroid distance is the distance between central points of each group in the 3D MDS space while minimum distance is the distance between the two closest points between the two groups. **(A)** *Intergroup distance (centroids).* The minimum distance (green dashed line segment) between the two extreme subtypes from the original data set. **(B)** *Intergroup distance (closest points).* The minimum distance (green dashed line segment) between the two extreme subtypes from the original data set. **(C)** *Intergroup*

distance of permuted data (centroids). A representative example of a permuted data set and the resulting *Th+/Fos-* (orange spheres) and *Th-/Fos+* (blue spheres) groups. The green dashed line represents the centroid distance while the green dashed line in **(D)** *Intergroup distance of permuted data (closest points).* The minimum distance between clusters generated from the permuted data set. **(E)** Distribution of the centroid distances calculated from the 1000 iterations performed. Only 1 random permutation achieved the formation of two extreme groups having a centroid distance equal to or greater than the distance found in the original data, shown by the red dashed line (p=.001). **(F)** Distribution of the minimum distances calculated from a permutation step. None of the iterations produced a minimum distance as large as the distance found in the original data set, shown by the red dashed line (p=0.000). Refer to *Statistical Significance of Subtype Clusters and Th and Fos expression limits* section of Supplementary Information for additional detail.

Fig. S8. Varying *Th+/Fos-* and *Th-/Fos+* thresholds (5% quantile limits). Specified quantile values were used to define the limits used to categorize single cells within the subtypes. Single cell projections in the MDS space were examined under various quantile limits used to categorize single cells in the two extreme subtypes. **(A)** 5% quantile limit for *Th+* expression is represented by the blue dashed line. Cells below the blue dashed line are categorized as *Th-*/*Fos+* cells. Single cells above the blue dashed line are categorized as either Th^{high} or Th^{low} cells. The green dashed line represents the 30% quantile limit used to determine which cells are Th^{high} (above green line) or Th^{low} (below green line). **(B)** 5% quantile limit for *Fos+* expression is represented by the orange dashed line. Single cells below the orange line are categorized as *Th+/Fos-* cells. The green dashed line represents the median expression value of the remaining single cells and is used to determine which remaining single cells are Fos^{high} or Fos^{low}. **(C)** The resulting bivariate plot showing the scatter of single cells and what cells are categorized in the two extreme subtypes. **(D)** The resulting 3D MDS visualization of single cell correlations (or dissimilarity) based on rank ordered gene expression. Note how the newly defined single cells continue to be projected at opposite extremes of the MDS space. **(E)** The corresponding rearranged heat map representing the scaled gene expression data. Rows represent genes while columns represent single cells. Single cells within each subtype are rank ordered by their respective *Th* or *Fos* expression level.

Fig. S9. Varying *Th+/Fos-* and *Th-/Fos+* thresholds (10% quantile limits). Stepwise process of defining expression limits for *Th* and *Fos* and how the resulting cells are projected into the 3D MDS space based on their similarity (or dissimilarity) in rank ordered gene expression of the 48 genes identified from PCA. Annotation is identical to Fig. S8.

Fig. S10. Varying *Th+/Fos-* and *Th-/Fos+* thresholds (15% quantile limits). Stepwise process of defining expression limits for *Th* and *Fos* and how the resulting cells are projected into the 3D MDS space based on their similarity (or dissimilarity) in rank ordered gene expression of the 48 genes identified from PCA. Annotation is identical to Fig. S8.

Fig. S11. Varying *Th*+/*Fos*- and *Th*-/*Fos*+ thresholds (15% and 25% quantile limits). Stepwise process of defining expression limits for *Th* and *Fos* and how the resulting cells are projected into the 3D MDS space based on their similarity (or dissimilarity) in rank ordered gene expression of the 48 genes identified from PCA. A 15% quantile value is used to define *Th*+ cells while a 25% quantile value is used to define *Fos*+ cells. Annotation is identical to Fig. S8.

Fig. S12. Gene-to-gene spearman rank correlations. Spearman rank correlation coefficients were calculated for pairwise comparisons of the subset of 48 genes across single cells having expression of both *Th* and *Fos* (i.e., cells in the intermediate groups). The spearman correlation coefficients (ranging from -1 to 1) between all pairs are shown in the heat map. Genes within transcription module 1 have a slightly higher correlation coefficient with each other than with those in module 2 and vice versa. However, the overall values of the spearman correlation coefficients are lower than those calculated between genes across single cells of the extreme subtypes (*Th*+/*Fos*- and *Th*-/*Fos*+ groups).

Fig. S13. Constrained transcriptional behavior of hypertensive cells. A projection of the similarity values of single cells (based on rank ordered gene expression of the 48 genes identified in PCA). Normotensive *Th*+ single cells (green spheres) are included along with hypertensive *Th*+/*Fos*- single cells (orange spheres) and *Th*-/*Fos*+ single cells (blue spheres). The ellipsoids represent the 65^{th} percentile of the single cell density for each subtype. Outliers within each subtype (single cells outside of the 95^{th} percentile density for each subtype) were not included when defining these ellipsoids. In the case of the normotensive ellipsoids, two ellipsoids were included to represent the space occupied the normotensive single cells. The hypertensive *Th*+/*Fos*- cells occupy a smaller constrained space than their normotensive counterparts.

Fig. S14. Subtype clusters maintained across animal subjects. Single cells in the 3D MDS space are annotated with the respective animal subjects from which they were taken from. Ellipsoids were added to represent the input-type defined subtypes originally identified (orange: *Th*+/*Fos*-, red: Th^{high}/Fos^{low}, yellow: Th^{high}/Fos^{high}, cyan: Th^{low}/Fos^{low}, grey: Th^{low}/Fos^{high}, blue: *Th*-/*Fos*+). The ellipsoids represent the 65^{th} percentile of the single cell density for each subtype. Outliers within each group (single cells outside of the 95^{th} percentile population density for each subtype) were not included when defining these ellipsoids. Single cells from their respective animal subjects are scattered throughout all subtypes and are not concentrated to one particular ellipsoid indicating that these clusters are *not* an artifact of animal variability.

Supplemental References

Andersen CL, Jensen JL, Ørntoft TF. 2004. Normalization of real-time quantitative reverse transcription-PCR data: a model-based variance estimation approach to identify genes suited for normalization, applied to bladder and colon cancer data sets. *Cancer Res* **64**: 5245–50.

Bergkvist A, Rusnakova V, Sindelka R, Garda JMA, Sjögreen B, Lindh D, Forootan A, Kubista M. 2010. Gene expression profiling--Clusters of possibilities. *Methods* **50**: 323–35.

Van Deun K, Delbeke L. 2000. Multidimensional Scaling. http://www.mathpsyc.uni-bonn.de/doc/delbeke/delbeke.htm.

Fuller GN, Hess KR, Rhee CH, Yung WKA, Sawaya R a, Bruner JM, Zhang W. 2002. Molecular classification of human diffuse gliomas by multidimensional scaling analysis of gene expression profiles parallels morphology-based classification, correlates with survival, and reveals clinically-relevant novel glioma subsets. *Brain Pathol* **12**: 108–16.

R Core Team. 2013. R: A Language and Environment for Statistical Computing. http://www.r-project.org/.

Ross ME, Zhou X, Song G, Shurtleff S a, Girtman K, Williams WK, Liu H-C, Mahfouz R, Raimondi SC, Lenny N, et al. 2003. Classification of pediatric acute lymphoblastic leukemia by gene expression profiling. *Blood* **102**: 2951–9.

Spurgeon SL, Jones RC, Ramakrishnan R. 2008. High throughput gene expression measurement with real time PCR in a microfluidic dynamic array. *PLoS One* **3**: e1662.

Taguchi Y-H, Oono Y. 2005. Relational patterns of gene expression via non-metric multidimensional scaling analysis. *Bioinformatics* **21**: 730–40.

Vandesompele J, De Preter K, Pattyn F, Poppe B, Van Roy N, De Paepe A, Speleman F. 2002. Accurate normalization of real-time quantitative RT-PCR data by geometric averaging of multiple internal control genes. *Genome Biol* **3**: RESEARCH0034.

Table S3. Specific gene categorizations, related primer sequences, and gene entrez ID.

Entrez ID	Gene	Primer Design Forward	Primer Design Reverse	UPL#	Gene Functional Categorization
24310	Ace	GACAACTATCCAGAGGGAATTGA	CACAACACCTTGGCTGTCC	25	Angiotensin System
81822	Actb	CTGGCTCCTAGCACCATGA	TAGAGCCACCAATCCACACA	63	housekeeping
25238	Adrbk1	AAGAAGATCCTGCTGCCAGA	CCGGAAAAGCAGGTATCCTA	89	Signaling feedback
24179	Agt	CACCTACGTTCACTTCCAAGG	AGAACTCATGGAGCCCAGTC	7	Angiotensin System
24180	Agtr1a	GGCTAGCCAAAGGAAGAGTCA	CTGCCAGCGAACTGTTTTC	42	Angiotensin System
24182	Agtr2	GAACAGAATTACCCGTGACCA	ATGAATGCCAACACAACAGC	121	Angiotensin System
298646	Agtrap	CCATCTTCAGCTTGCTGCT	CCTGAGAAGGTCCGAAGAAA	2	Angiotensin System
24185	Akt1	AACGACGTAGCCATTGTGAA	CCATCATTCTTGAGGAGGAAGT	71	Intracellular Signaling
64363	Araf	GAAGACAAGCCCAAGATGGA	GACTGGGCAGGTGCCATA	77	Intracellular Signaling
25387	Arrb1	GGGAGACCTTGCATCCAGT	GGAGTCTCGCTCTCTGGAAC	76	Signaling feedback
25388	Arrb2	GATCCTGTCGATGGTGTGGT	GGAAAGACAGGCCCAGTACA	98	Signaling feedback
81647	Atf2	CTGGTGGCTGAAAGGAACAT	TCCCAAGTTGCCATCTAGTGT	85	transcriptional regulators
29716	Cacna1d	GGCAGAAGACATAGATCCTGAGA	ACTGGTGGGCATGCTAGTGT	55	Ion Channel
24241	Calca	CAGATGAAAGTCAGGGAGCTG	CAGGATCTCTTCTGGGCAGT	63	neuromodulatory regulator
314322	Fos	CAGCCTTTCCTACTACCATTCC	ACAGATCTGCGCAAAAGTCC	67	transcriptional regulators
81646	Creb1	CTAGTGCCCAGCAACCAAGT	GGAGGACGCCATAACAACTC	9	transcriptional regulators
81648	Crh	CAACCTCAGCCGATTCTGAT	GCGGGACTTCTGTTGAGGT	69	neuromodulatory regulator
25699	Dbh	ACTACTGTCGCCACGTGCT	ACCGGCTTCTTCTGGGTAGT	81	neuromodulatory regulator
116663	Dusp6	TCTCTGATCACTGGAGCCAAA	GTTTTTGCCTCGGGCTTC	123	Intracellular Signaling
24330	Egr1	CGAACAACCCTACGAGCAC	GCGCCTTCTCGTTATTCAGA	114	transcriptional regulators
114090	Egr2	CTACCCGGTGGAAGACCTC	TCAATGTTGATCATGCCATCTC	60	transcriptional regulators
25148	Egr3	CAATCTGTACCCCGAGGAGA	CCGATGTCCATCACATTCTCT	7	transcriptional regulators
314436	Elk1	CACCAGTCCAAACCCCTTAG	TCAACTCTTCAGATTTCTGGTTTG	16	transcriptional regulators
25445	Fosl1	GCAGAAACCGAAGAAAGGAA	TCCTCCAACTTGTCGGTCTC	4	transcriptional regulators
29705	Gabra1	CGATCCTCTCTCCCACACTT	TCTTCATCACGGGCTTGTC	50	neuromodulatory targets - Ion Channel
289606	Gabra2	GGTTTCCGCTGCTTGTTCT	TTCTTGGATGTTAGCCAGCAC	20	neuromodulatory targets - Ion Channel
140675	Gabra4	GTACCTGCGATCGTGCTGT	CTGTCCTGGGGATTCGTTTA	98	neuromodulatory targets - Ion Channel
24922	Gabrb3	TCATGGGTGTCCTTCTGGAT	ATGGTGAGCACGGTGGTAAT	84	neuromodulatory targets - Ion Channel
65187	Gabrq	GCGGAGAATCGTGTATTTCAA	GCTGCTGTTGTGGTAAGTCG	123	neuromodulatory targets - Ion Channel
24379	Gad1	TACAACCTTTGGCTGCATGT	TGAGTTTGTGGCGATGCTT	77	neuromodulatory regulator
29141	Gal	TGGAGTTTCTCAGTTTCTTGCAC	GGTGTGGTCTCAGGACTGCT	10	neuromodulatory regulator
29627	Gria2	GCCAAGGACTCGGGAAGTA	CCCCCGACAAGGATGTAGA	67	neuromodulatory targets - Ion Channel
29628	Gria3	TTCAACAAAAGAATTTTTCAGACG	CCGTCAGCTGTTGTTTTGG	21	neuromodulatory targets - Ion Channel
24409	Grin2a	CGTCATGGTCTCCAGGAGTAA	GAGGCACTGAAGGGTTCG	94	neuromodulatory targets - Ion Channel
24408	Grin1	GCTTTTGCAGCCGTGAAC	GGGCTCTGCTCTACCACTCTT	69	neuromodulatory targets - Ion Channel
24410	Grin2b	TCCTGCAGCTGTTTGGAGAT	GCTGCTCATCACCTCATTCTT	106	neuromodulatory targets - Ion Channel
24411	Grin2c	GGCACTCCTGCAACTTCTG	GTTCTGGCAGATCCCTGAGA	78	neuromodulatory targets - Ion Channel

.

Table S3. Specific gene categorizations, related primer sequences, and gene entrez ID.

Entrez ID	Gene	Primer Design Forward	Primer Design Reverse	UPL#	Gene Functional Categorization
24412	Grin2d	GCCCTGCTGCGAGACTAT	CGGTTATCCCAGGTGATGTT	67	neuromodulatory targets - Ion Channel
59075	Grk5	CCACCAAAGAAAGGGCTGT	TCTTGGAATTGTTTTGATGCTG	124	Signaling feedback
59076	Grk6	ATGTCTTTGGGCTGGATGG	CAGTTCCCACAGCAATCCTT	85	Signaling feedback
114244	Hcn2	CACCCCTACAGCGACTTCAG	TTTCCCACCATGAACAACAG	95	neuromodulatory targets - Ion Channel
24465	Hprt1	GACCGGTTCTGTCATGTCG	ACCTGGTTCATCATCACTAATCAC	95	housekeeping
293621	Hras	TCACAGTAAATTATTTGATGGTCTTGA	CCACAGGCACTACACCTCCT	20	Intracellular Signaling
25262	Itpr1	CATCACAGCCCTCATCCTTAAC	GGAGTAGCTTTGAAGCATTGTTCT	60	Intracellular Signaling
25679	Itpr3	GTGATGGAGACCAAGCTGAAG	TAGTCTAGGCGCACGTTGAG	80	Intracellular Signaling
24516	Jun	TTCTGACCAACTGCCTGGAT	GAAGGGACTCTCCAAGTGCTC	17	transcriptional regulators
24517	Junb	GGGAGCTGAGAGAAGAGACG	TGGTAGCTGTGCGTAAAAGC	50	transcriptional regulators
24518	jund	CAAGCTGGAGCGTATCTCG	CGGTGTTCTGGCTTTTGAG	25	transcriptional regulators
29712	Kcnj2	GCTGCCTTCCTCTTCTCCAT	TCGGGCACTCGTCTGTAAC	115	neuromodulatory targets - Ion Channel
170851	Map2k1	GGCCTGGTTATGGCTAGGA	GATGATCTGGTTCCGGATTG	80	Intracellular Signaling
287398	Map2k4	AACAAAATGGTCCACAAACCA	TTTTTCATCCACAAGTTGATCGT	118	Intracellular Signaling
363855	Map2k7	TCAGGGGACTTCCAGTCATT	GATGAAGCTGTGTTCAAGTAGTTTG	114	Intracellular Signaling
309168	Map3k11	CGGGAAGAGACACGTGGA	CCAGGAGCAGAGCGTGATA	22	Intracellular Signaling
25579	Map3k12	CCTCTCACCTCCATTCCTGA	AGCCAGGTGTGCTGAGTAGC	3	Intracellular Signaling
116596	Map3k8	ACCTCCGGGGAACAGAGA	GCCTGTCTGCATGTGAATGA	125	Intracellular Signaling
116590	Mapk1	TGAAGTTGAACAGGCTCTGG	TGAATGGTGCTTCAGCAATG	1	Intracellular Signaling
50689	Mapk3	GGAGGTGGAGGTGGTGAA	GCACGTGGTCATATGCTGAG	46	Intracellular Signaling
114509	Mapk7	ACCCAGCAACTGTCCAAGTC	GGTCAAAGCCAACACCGTAG	16	Intracellular Signaling
116554	Mapk8	GCAGCCGTCTCCTTTAGGT	CATTGACAGACGGCGAAGA	89	Intracellular Signaling
24604	Npy	ATCCCTGCTCGTGTGTTTG	CTGGCCATGTCCTCTGCT	129	neuromodulatory regulator
29358	Npy1r	CTGCAACCACAATCTGCTGT	TGACGCAGGTGGAGATCAT	53	neuromodulatory regulator
29431	Pak1	TCGAGAAGATTGGACAAGGTG	GCCCTGTGGCTACATCCAT	98	Intracellular Signaling
81745	Pdpk1	AAAACTTTCTTCGTCCACACG	GGACTGCTCTGGTACTGTTGC	79	Intracellular Signaling
29542	Pebp1	CGGACCTCCCAAAGACAC	AGAGGCTGCTCCTGCTCATA	20	Intracellular Signaling
364152	Phox2b	GAGAGTCCAGGTGTGGTTCC	GGCTTCTTTGCTCTCGTCAT	70	transcriptional regulators
60664	Pik3r3	ATCCCAAACTTGATGTGAAGC	TTATCTTCTTTTACCAACTGATCCTG	130	Intracellular Signaling
24680	Prkca	TACGGCGTGCTCCTGTATG	CTTGGCAGGGTGTTTGGT	44	Intracellular Signaling
24654	Plcb1	CGCCAAAAAGGATAGCAAGA	GCGGATGAGCCATGATCT	3	Intracellular Signaling
29322	Plcb3	CTTCACACAATACCTATCTCACTGC	CGGTACATCTCCACTGACGA	20	Intracellular Signaling
25594	Ppp1cb	TGAACGTGGACAGCCTCAT	ACAATTTTTCCCGGACGAC	67	Intracellular Signaling
24669	Ppp1cc	GGCGGATATCGATAAACTCAA	TGGCTTGGACCCTCTCACT	66	Intracellular Signaling
117281	Ppp2r1a	GCTACATGGTGGCAGACAAA	TAGTGATCTCAGGCCCAACTG	50	Intracellular Signaling
65179	Ppp5c	CCGAAGGCACTCTGAAGC	TGATAGCGTTCTCGTAGTCCTTG	82	Intracellular Signaling
29340	Prkce	TCTACCCTGTCTGGCTTAGCA	CGGGTTCTTGGTCATGAAAG	89	Intracellular Signaling
50646	Ptk2b	CAATCTGCTGGCTCCTAAGC	TAGGAGAGCTGGCACACAGA	85	Intracellular Signaling
24697	Ptpn1	GGAACAGGTACCGAGATGTCA	AGTCATTATCTTCCTGATGCAATTT	114	Intracellular Signaling
117063	Ptpn2	AGGCTACAACCGCTCAGAAG	CATTTAGGTGTCTGTCAATCTTGG	84	Intracellular Signaling
24703	Raf1	TTTCTTGCCGAATAAGCAAAG	CAGTCGTGCAAGCTCATCC	114	Intracellular Signaling

.

Table S3. Specific gene categorizations, related primer sequences, and gene entrez ID.

Entrez ID	Gene	Primer Design Forward	Primer Design Reverse	UPL#	Gene Functional Categorization
25676	Rasa1	CATCTAATAAACGCCTTCGTCA	TGGTAGTTTATGAGCTTCTTCAATATG	66	Intracellular Signaling
192213	Rasgrf1	GGCTGGTCTCAAACTTAGGATG	TCATGCCTGTAATCCCAGCTA	49	Intracellular Signaling
114513	Rasgrf2	AGGAGCAAGCAGGGAAAGA	TCTCAATCAAAATGTCTGCGTAA	58	Intracellular Signaling
29434	Rasgrp1	GTTCATCCATGTGGCTCAGA	ACAGCCATTAGCGTGTTGAA	22	Intracellular Signaling
54289	Rgs1	GCAAGAAGAACAGGGTGAGG	CACTGTATTTCATGACAGTACCACA	12	Signaling feedback
84583	Rgs2	AACTTTTATCAAGCCTTCTCCTGA	ACGCTCTGAATGCAGCAAG	113	Signaling feedback
54293	Rgs3	CCGGAAGAGAAAGAGCAAAAA	GGCCCCAGGAGATTCATT	124	Signaling feedback
29480	Rgs4	CAAGATGTGCAAAGGACTCG	CCAGCCGATGTTTCATATCC	4	Signaling feedback
54294	Rgs5	CCAGAGAAGCCTGCCAAG	GAAGTTTGTCCAGGGATTGG	25	Signaling feedback
81767	Rpl19	TGCCGGAAGAACACCTTG	GCAGGATCCTCATCCTTCG	85	housekeeping
157074	Sdha	TGCCATCCATTACATGACAGA	AAATCCTCCCATCTTCAGTCC	16	housekeeping
83612	Slc32a1	AGGCTCGGAAACTTGACCTT	GACGCAGTAGATTCCAAGCAC	76	neuromodulatory targets - Ion Channel
83511	Slc6a2	AGTGAAGACATCGGGAAAGG	AACCAGGAGCACAAAGAGGA	76	neuromodulatory targets - Ion Channel
59114	Slc9a3r1	CAGGACCGGATTGTGGAG	AGCAGCTTGGCTTCATCAC	121	neuromodulatory targets - Ion Channel
24797	Sst	AGCCCAACCAGACAGAGAAC	CCTCATCTCGTCCTGCTCA	1	neuromodulatory regulator
24949	Syn1	GGACGGAAGGGATCACATTA	TGGTGATCCCCAATGAGTG	25	neuromodulatory targets - Ion Channel
24806	Tac1	CAGAAAGGCTGCTGTGAGG	GAAGCGCAAGACACACAGG	13	neuromodulatory regulator
25085	Th	GGGAGCTGAAGGCTTATGGT	CCTCTGACAGGGAGTGCAG	66	neuromodulatory regulator

.

Table S4. Selection of genes contributing to variability.

No.	Gene Symbol	PC1 loadings	PC2 loadings	PC3 loadings	PC4 loadings	PC5 loadings
1	Th	**0.444**	**-0.137**	**0.208**	-0.218	0.051
2	Dbh	**0.317**	**-0.068**	0.107	**-0.258**	0.005
3	Gabrq	**0.228**	**-0.006**	0.101	0.040	0.081
4	Gal	**0.212**	0.016	0.095	-0.117	**0.144**
5	Rgs4	**0.202**	0.002	0.102	0.069	0.024
6	Slc6a2	0.186	**-0.053**	0.121	-0.165	-0.055
7	Phox2b	0.162	0.089	0.057	0.040	**-0.105**
8	Rasgrp2	0.148	0.004	0.034	0.035	0.116
9	Gria3	0.141	**0.215**	-0.173	-0.090	0.015
10	Gria2	0.133	0.160	-0.105	-0.017	-0.009
11	Rgs2	0.132	0.049	0.106	0.048	-0.067
12	Rasgrf2	0.131	0.055	0.052	0.008	0.139
13	Cacna1d	0.128	0.074	0.080	0.059	0.077
14	Grin 2a	0.128	0.098	-0.048	0.062	0.106
15	Dusp6	0.115	0.047	0.072	-0.058	-0.009
16	Prkca	0.101	**0.227**	**-0.435**	-0.192	-0.082
17	Ppp5c	0.099	0.113	-0.139	-0.017	-0.025
18	Hprt1	0.097	0.081	0.016	**0.115**	0.019
19	Grin1	0.088	0.094	0.146	**0.166**	-0.007
20	Atf2	0.088	0.096	-0.007	0.069	0.052
21	Fosl1	0.086	**0.068**	0.113	-0.098	-0.218
22	Araf	0.085	0.062	-0.011	0.083	0.016
23	Ptpn1	0.085	0.050	0.093	-0.049	0.071
24	Map2k1	0.085	0.064	0.009	**0.116**	0.017
25	Grin2b	0.084	0.112	0.021	0.012	0.048
26	Mapk1	0.083	0.096	-0.041	0.100	0.042
27	Ace	0.082	0.038	0.103	0.001	0.084
28	Rgs3	0.079	0.059	**-0.172**	-0.194	0.069
29	Gabra2	0.070	0.120	-0.003	0.113	0.102
30	Gabra4	0.069	0.066	0.018	0.145	0.089
31	Pak1	0.064	0.065	0.032	0.093	0.050
32	Syn1	0.050	0.119	0.045	0.076	0.052
33	Ppp2r1a	0.048	0.062	0.039	0.102	0.050
34	Adrbk1	0.044	0.106	-0.019	0.038	0.030
35	Raf1	0.043	0.196	**-0.275**	-0.166	0.035
36	Pdpk1	0.041	0.130	-0.027	0.001	0.066
37	Elk1	0.039	0.192	-0.060	-0.088	0.083
38	Akt1	0.039	0.065	-0.003	0.043	0.082
39	Prkce	0.037	0.103	0.111	0.082	0.067
40	Jund	0.036	0.033	0.099	0.051	0.002
41	Map2k7	0.032	0.062	-0.064	0.047	0.044
42	Rasa1	0.028	0.100	-0.063	0.016	0.092
43	Ppp1cc	0.024	0.083	0.072	0.024	0.059
44	Map3k12	0.022	0.107	0.085	0.038	0.117
45	Grin2c	0.021	0.061	0.000	-0.122	-0.019

Table S4. Selection of genes contributing to variability.

No.	Gene Symbol	PC1 loadings	PC2 loadings	PC3 loadings	PC4 loadings	PC5 loadings
46	Ppp1cb	0.020	0.071	0.013	0.024	0.023
47	Arrb1	0.017	0.100	0.022	0.041	0.077
48	Gabra1	0.016	0.196	-0.099	**0.315**	**0.144**
49	Pik3r3	0.014	0.088	-0.020	0.006	0.123
50	Hcn2	0.014	0.075	-0.112	-0.071	0.037
51	Rpl19	0.004	0.012	-0.034	-0.032	-0.008
52	Ptpn2	0.002	0.047	0.092	-0.032	0.021
53	Creb1	0.000	0.079	0.076	-0.061	0.070
54	Itpr1	-0.001	0.058	0.091	-0.073	0.123
55	Mapk7	-0.003	0.055	0.047	-0.083	0.058
56	Actb	-0.004	-0.012	0.034	0.032	0.008
57	Mapk3	-0.005	0.042	-0.085	-0.014	0.037
58	Jun	-0.005	0.126	0.117	0.018	-0.066
59	Egr1	-0.006	**0.284**	0.113	0.013	**-0.369**
60	Plcb1	-0.011	**0.231**	**-0.165**	-0.049	0.122
61	Agt	-0.015	0.021	0.127	0.050	0.061
62	Arrb2	-0.017	0.109	-0.001	0.098	0.010
63	Agtrap	-0.017	0.063	-0.011	-0.045	0.076
64	Pebp1	-0.019	0.051	0.002	0.087	0.014
65	Agtr1a	-0.021	0.029	0.136	-0.182	0.096
66	Fos	-0.034	0.341	**0.192**	-0.036	**-0.556**
67	Map3k11	-0.041	0.054	0.006	-0.114	0.091
68	Grk5	-0.063	0.077	0.002	-0.062	0.100
69	Rasgrf1	-0.075	0.105	0.126	-0.140	0.050
70	Gad1	-0.077	0.157	**0.165**	0.104	0.141
71	Slc9a3r1	-0.081	0.035	0.057	-0.104	0.077
72	Hras	-0.083	0.061	0.079	**-0.228**	0.104
73	Npy1r	-0.092	0.054	0.143	-0.120	**0.149**
74	Junb	-0.092	0.209	0.100	-0.035	**-0.186**
75	Kcnj2	-0.105	0.116	0.037	**-0.277**	0.057
76	Rgs1	-0.105	0.026	0.113	**-0.221**	0.066
77	Crh	**-0.119**	0.068	0.056	**-0.248**	0.045
78	Npy	**-0.129**	0.088	**0.231**	0.114	0.030
79	Slc32a1	**-0.141**	0.118	**0.222**	0.046	**0.168**
80	Tac1	**-0.145**	0.115	0.139	-0.109	0.092
81	Sst	**-0.289**	0.159	0.029	-0.043	**0.168**

Figure S1

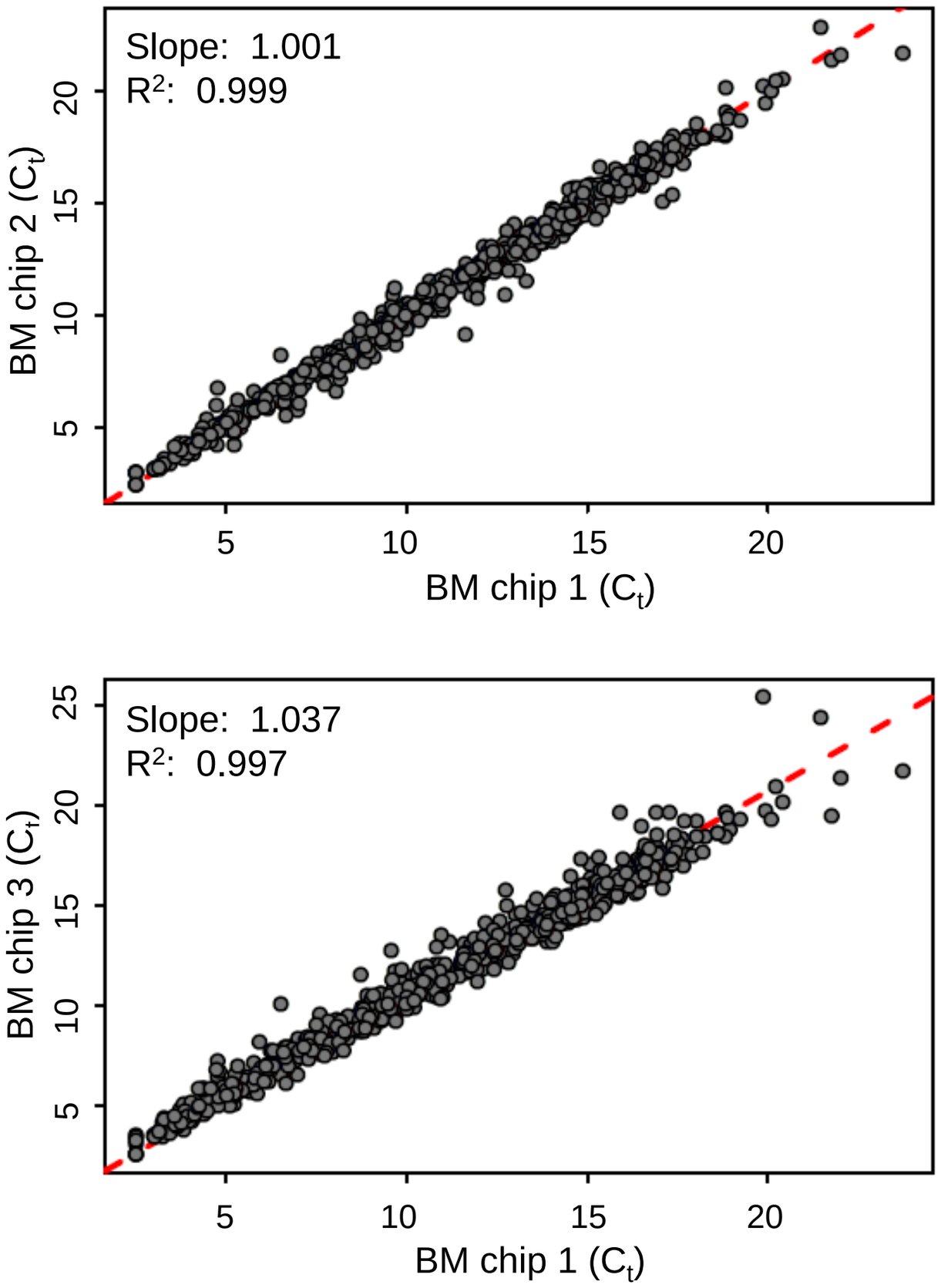
Slope: 1.001
R²: 0.999
BM chip 2 (Ct)
BM chip 1 (Ct)

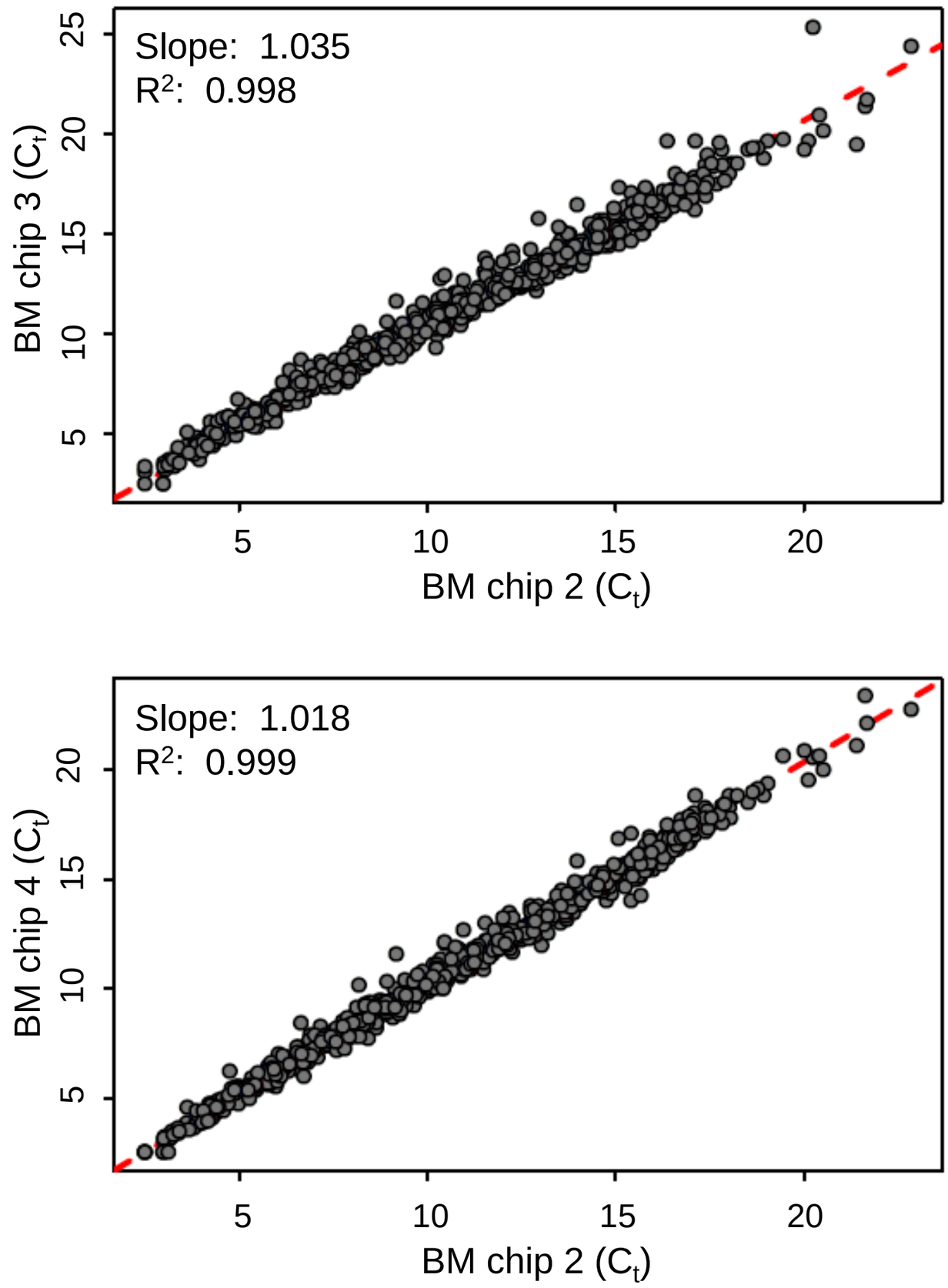
Slope: 1.035
R²: 0.998
BM chip 3 (Ct)
BM chip 2 (Ct)

Slope: 1.037
R²: 0.997
BM chip 4 (Ct)
BM chip 1 (Ct)

Slope: 1.018
R²: 0.999
BM chip 4 (Ct)
BM chip 2 (Ct)

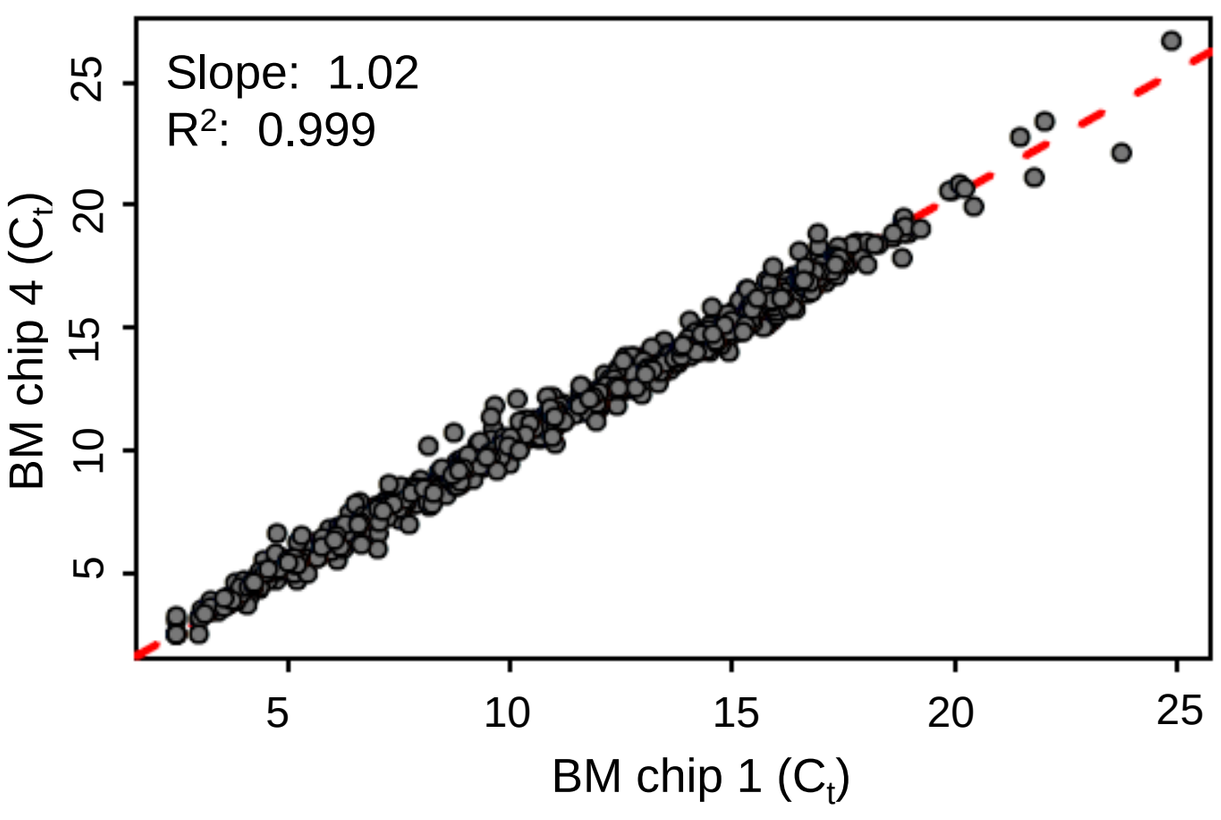
Slope: 1.02
R²: 0.999
BM chip 4 (Ct)
BM chip 1 (Ct)

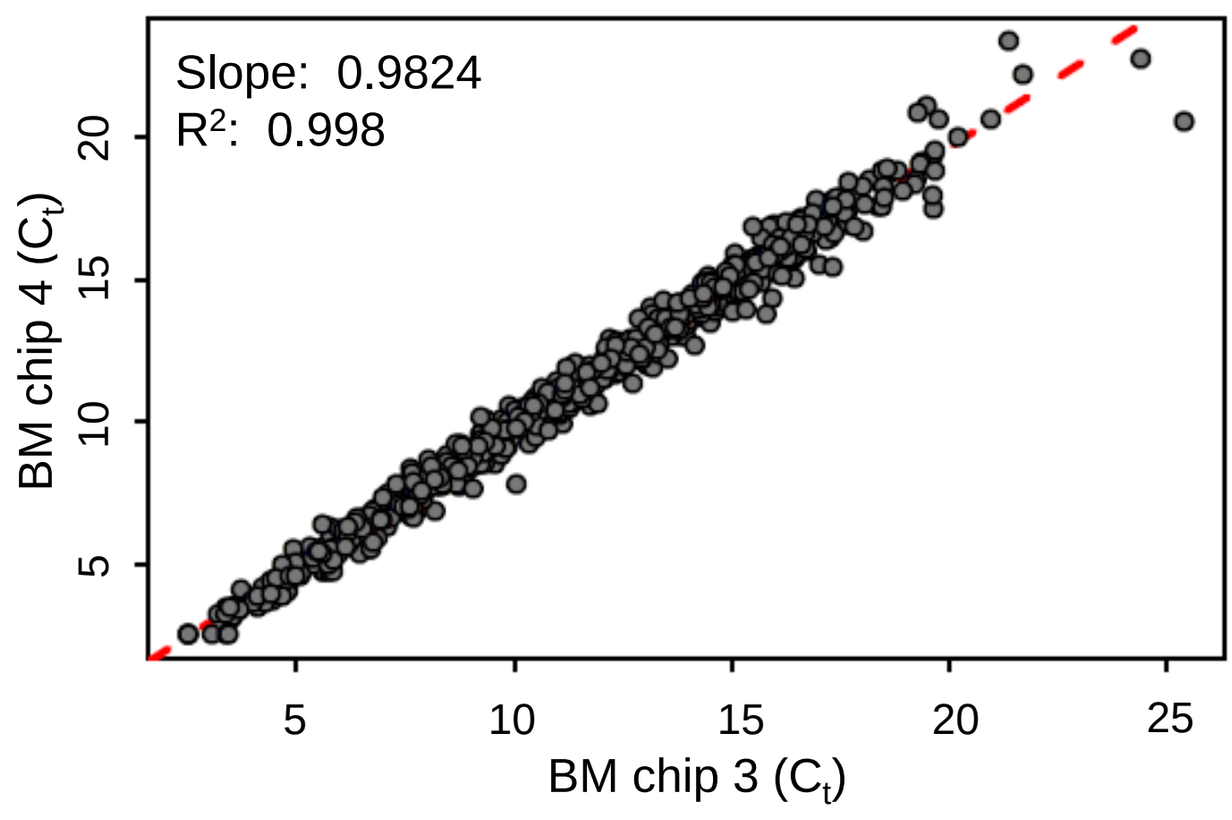
Slope: 0.9824
R²: 0.998
BM chip 4 (Ct)
BM chip 3 (Ct)

Figure S2

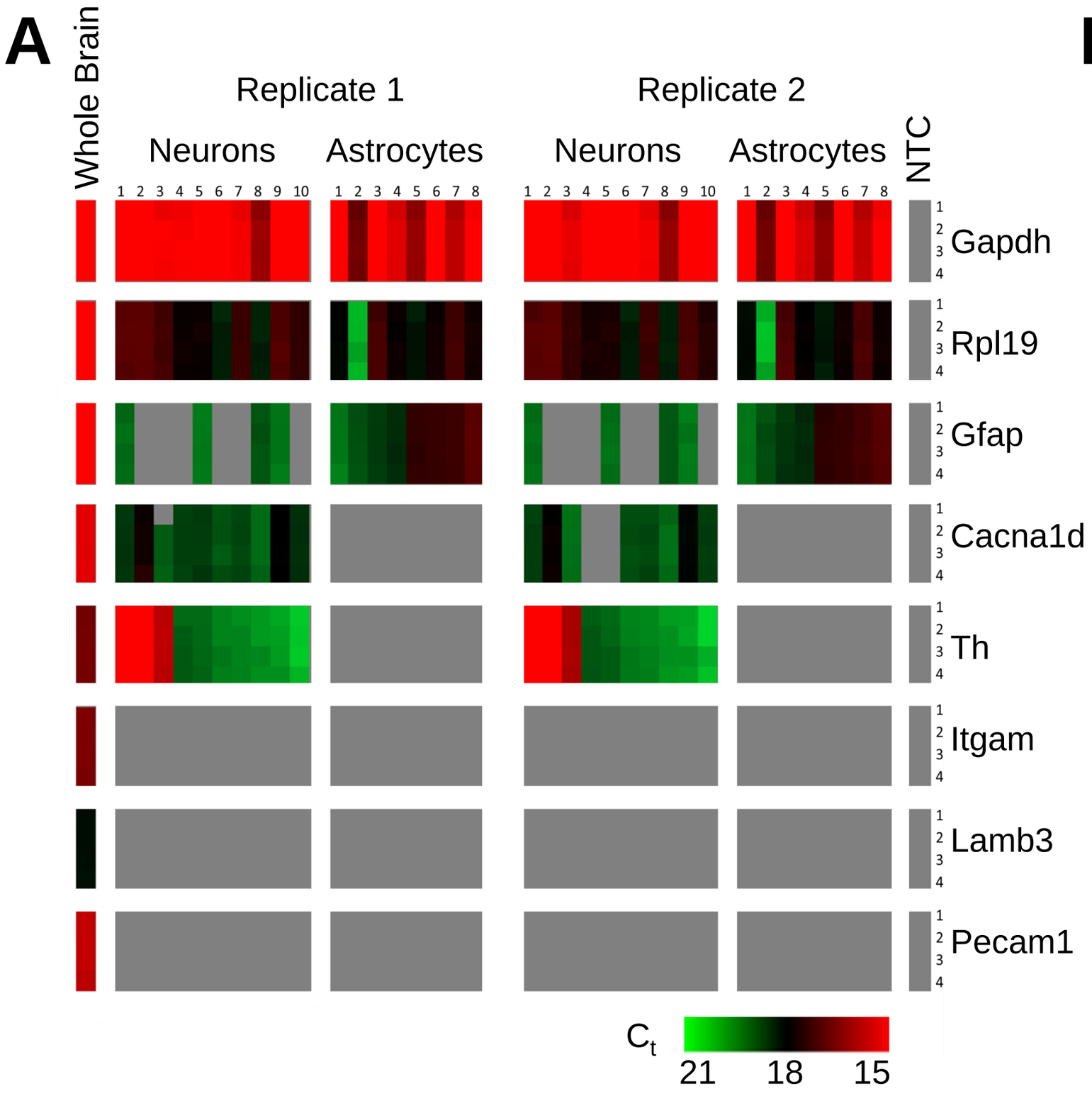
A
Whole Brain
Replicate 1
Replicate 2
Neurons
Astrocytes
Neurons
Astrocytes
NTC
1 2 3 4 5 6 7 8 9 10
1 2 3 4 5 6 7 8
1 2 3 4
Gapdh
Rpl19
Gfap
Cacna1d
Th
Itgam
Lamb3
Pecam1
Ct
21 18 15

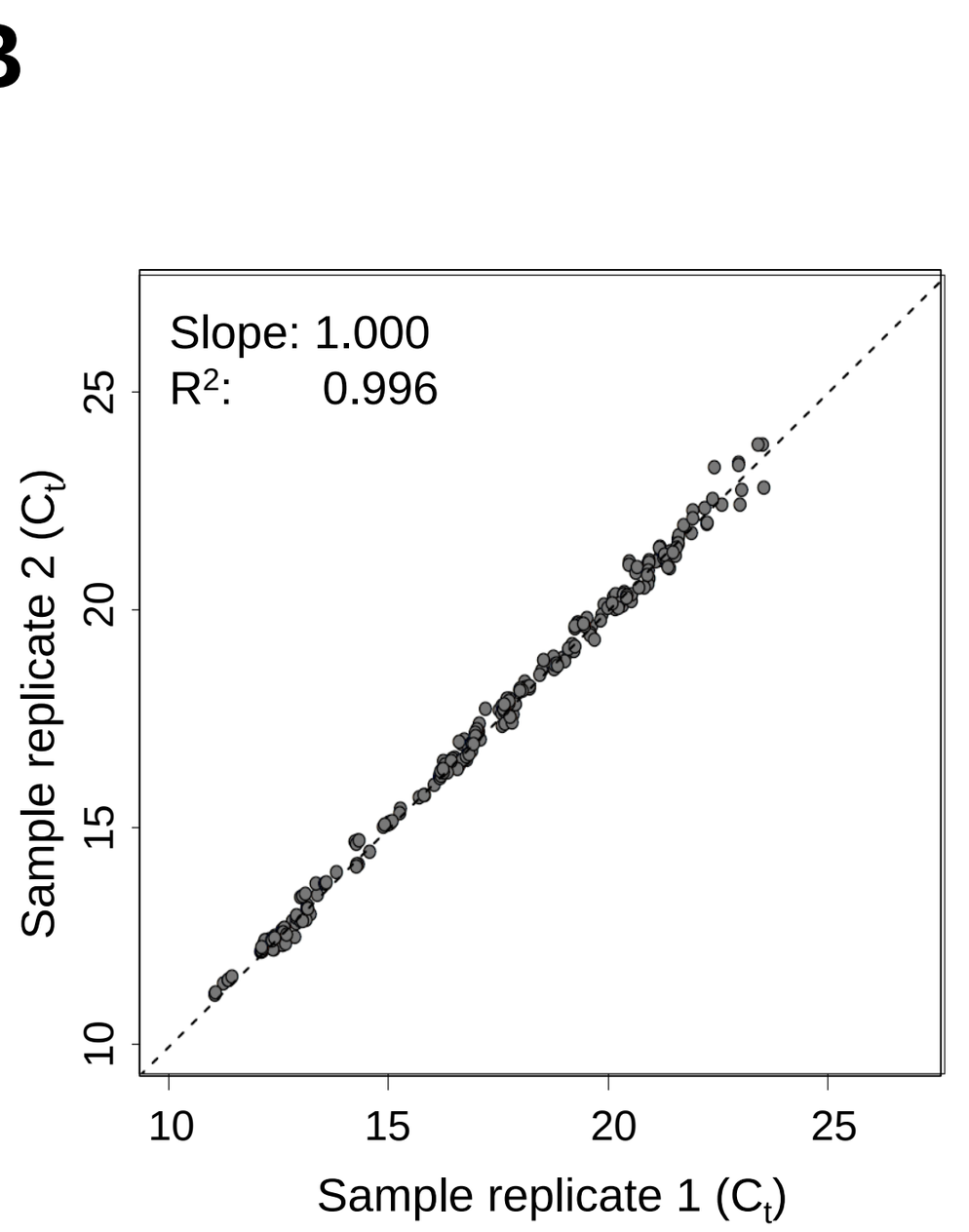
B
Slope: 1.000
R2: 0.996
Sample replicate 2 (Ct)
Sample replicate 1 (Ct)
10
15
20
25

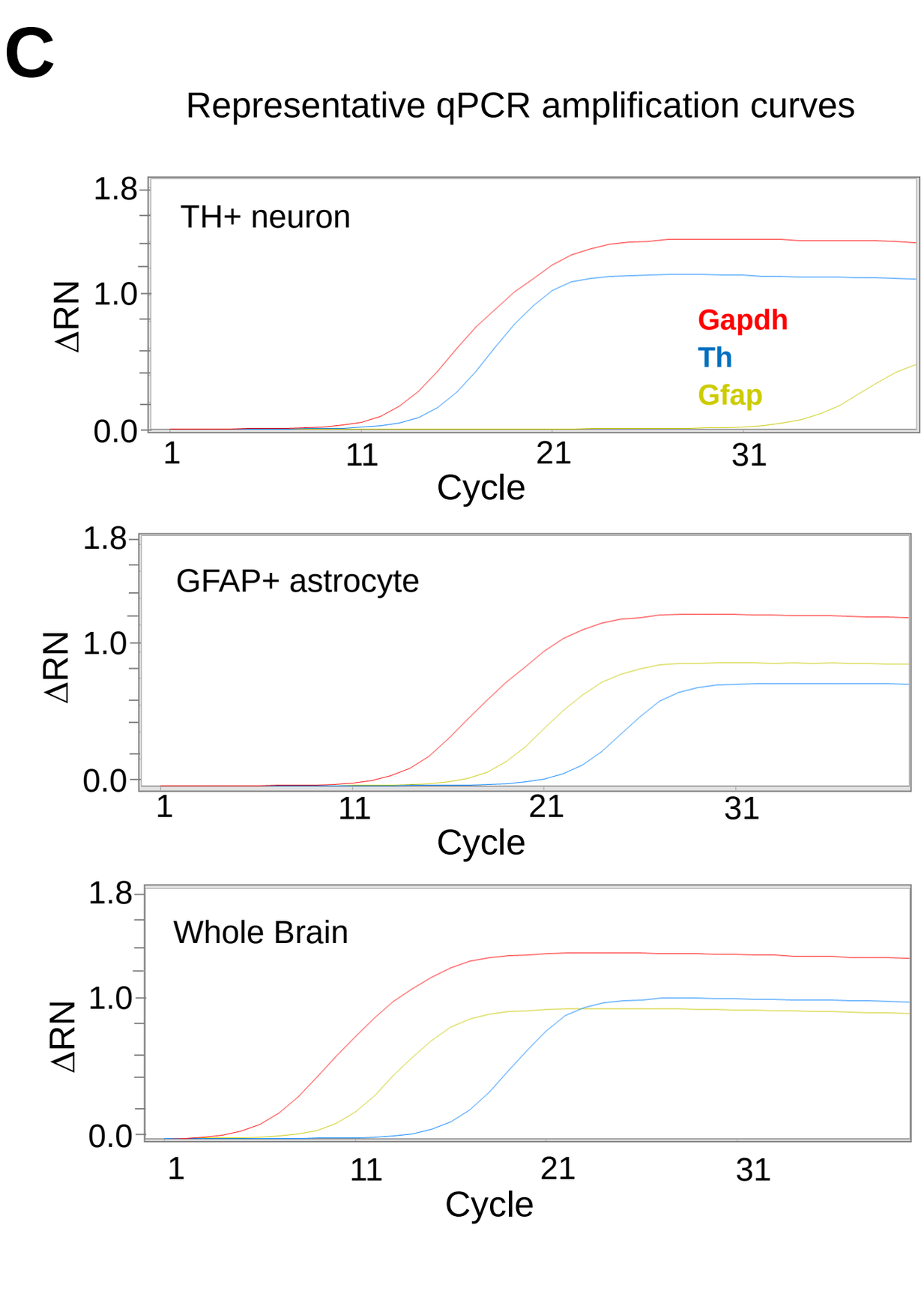
C
Representative qPCR amplification curves
TH+ neuron
GFAP+ astrocyte
Whole Brain
ΔRN
Cycle
1.8
1.0
0.0
1
11
21
31
Gapdh
Th
Gfap

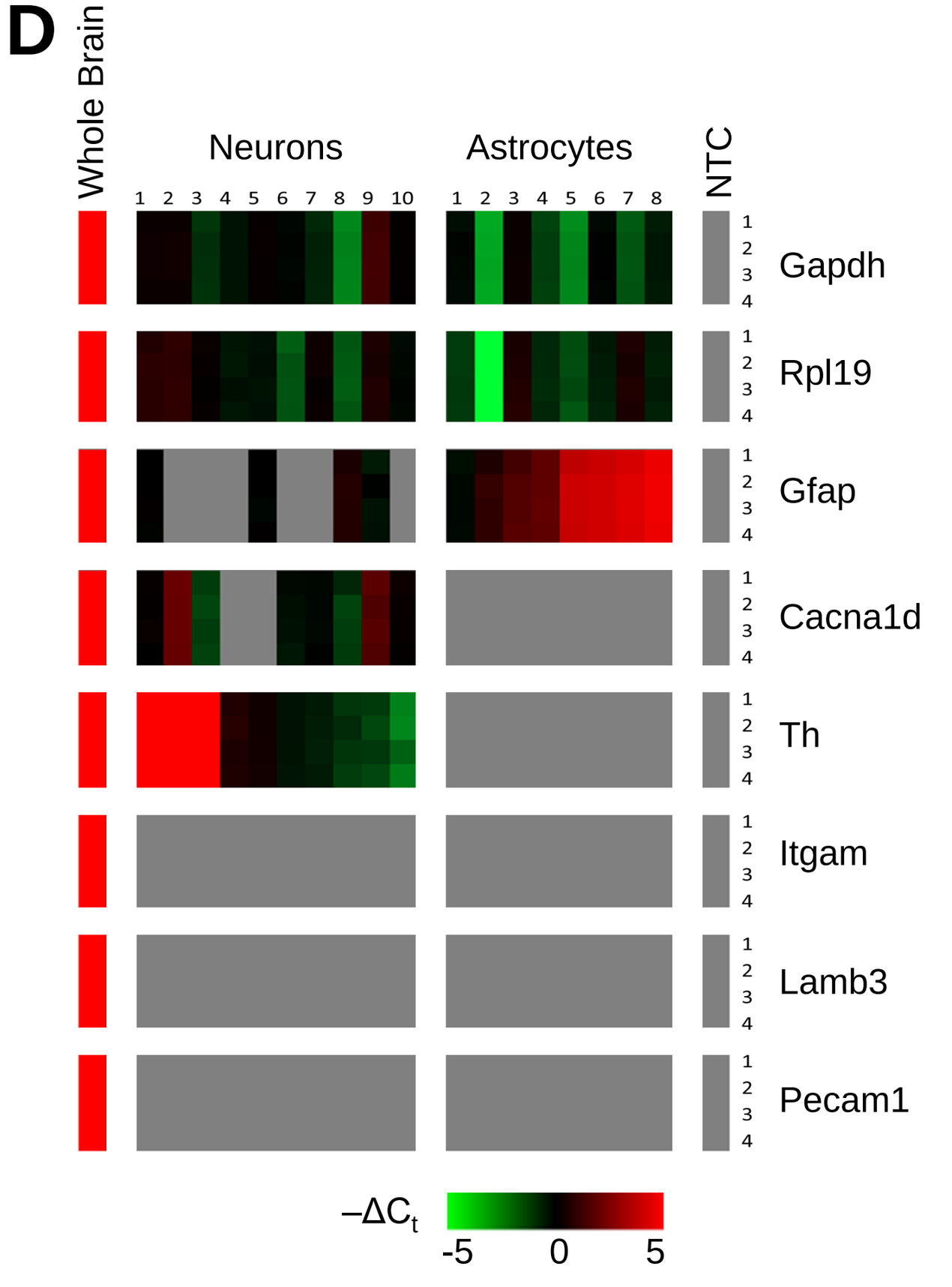
D
Whole Brain
Neurons
Astrocytes
NTC
1 2 3 4 5 6 7 8 9 10
1 2 3 4 5 6 7 8
1 2 3 4
Gapdh
Rpl19
Gfap
Cacna1d
Th
Itgam
Lamb3
Pecam1
–ΔCt
-5 0 5

Figure S3

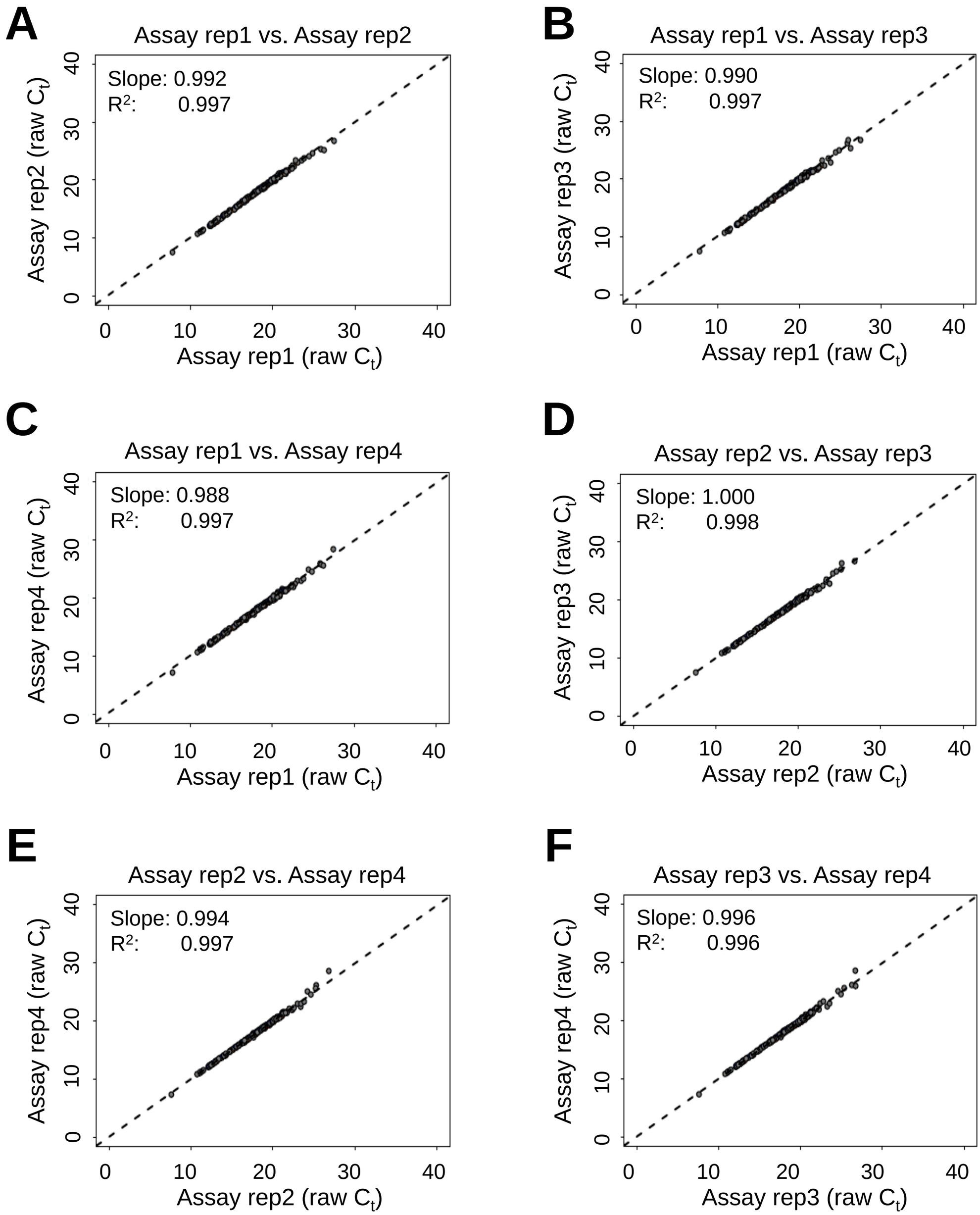
A
Assay rep1 vs. Assay rep2
Slope: 0.992
R2: 0.997
Assay rep2 (raw Ct)
Assay rep1 (raw Ct)
B
Assay rep1 vs. Assay rep3
Slope: 0.990
R2: 0.997
Assay rep3 (raw Ct)
Assay rep1 (raw Ct)
C
Assay rep1 vs. Assay rep4
Slope: 0.988
R2: 0.997
Assay rep4 (raw Ct)
Assay rep1 (raw Ct)
D
Assay rep2 vs. Assay rep3
Slope: 1.000
R2: 0.998
Assay rep3 (raw Ct)
Assay rep2 (raw Ct)
E
Assay rep2 vs. Assay rep4
Slope: 0.994
R2: 0.997
Assay rep4 (raw Ct)
Assay rep2 (raw Ct)
F
Assay rep3 vs. Assay rep4
Slope: 0.996
R2: 0.996
Assay rep4 (raw Ct)
Assay rep3 (raw Ct)
0
10
20
30
40

Figure S4

A

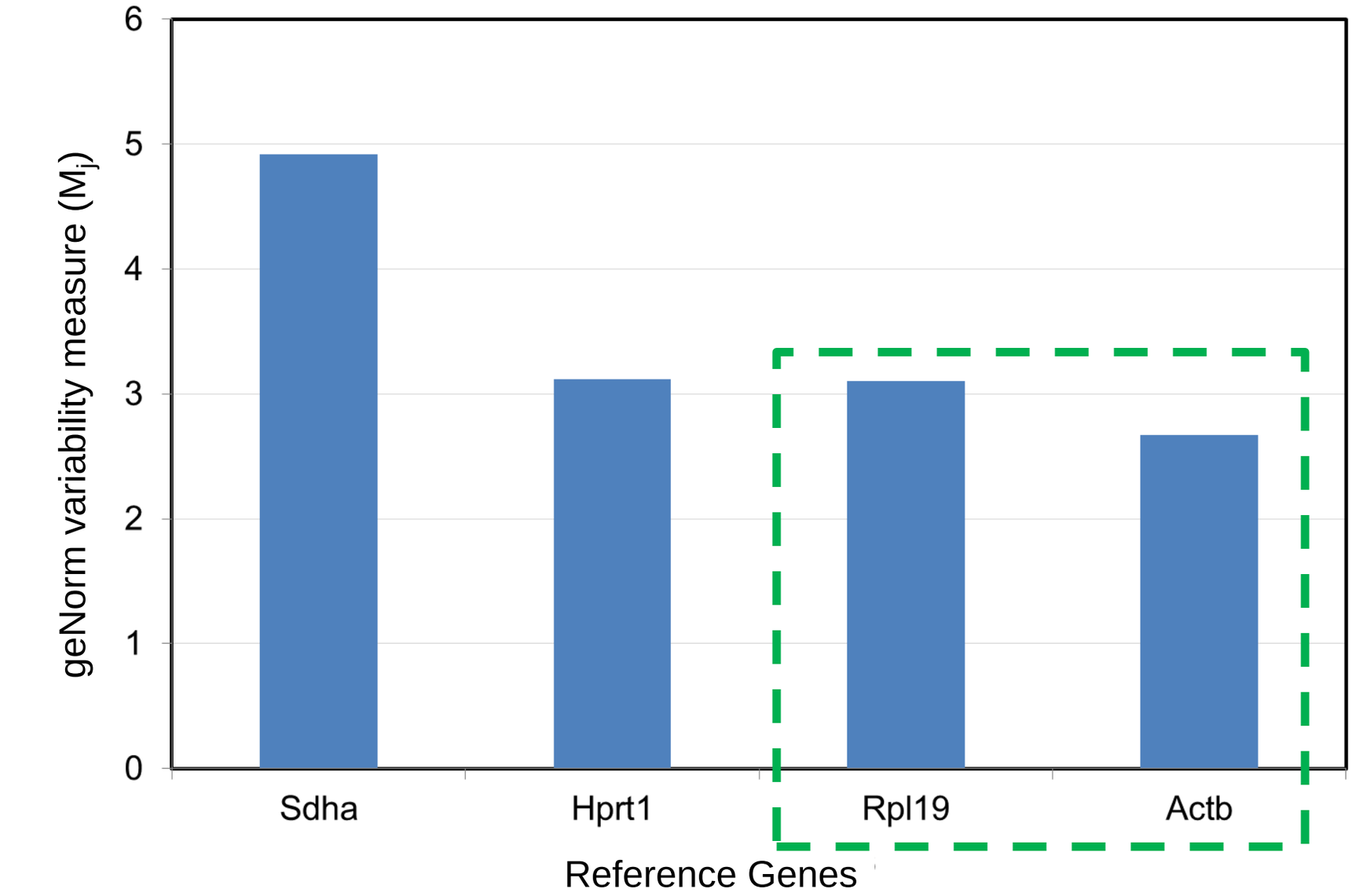
6
5
4
3
2
1
0
geNorm variability measure (Mj)
Sdha
Hprt1
Rpl19
Actb
Reference Genes

B

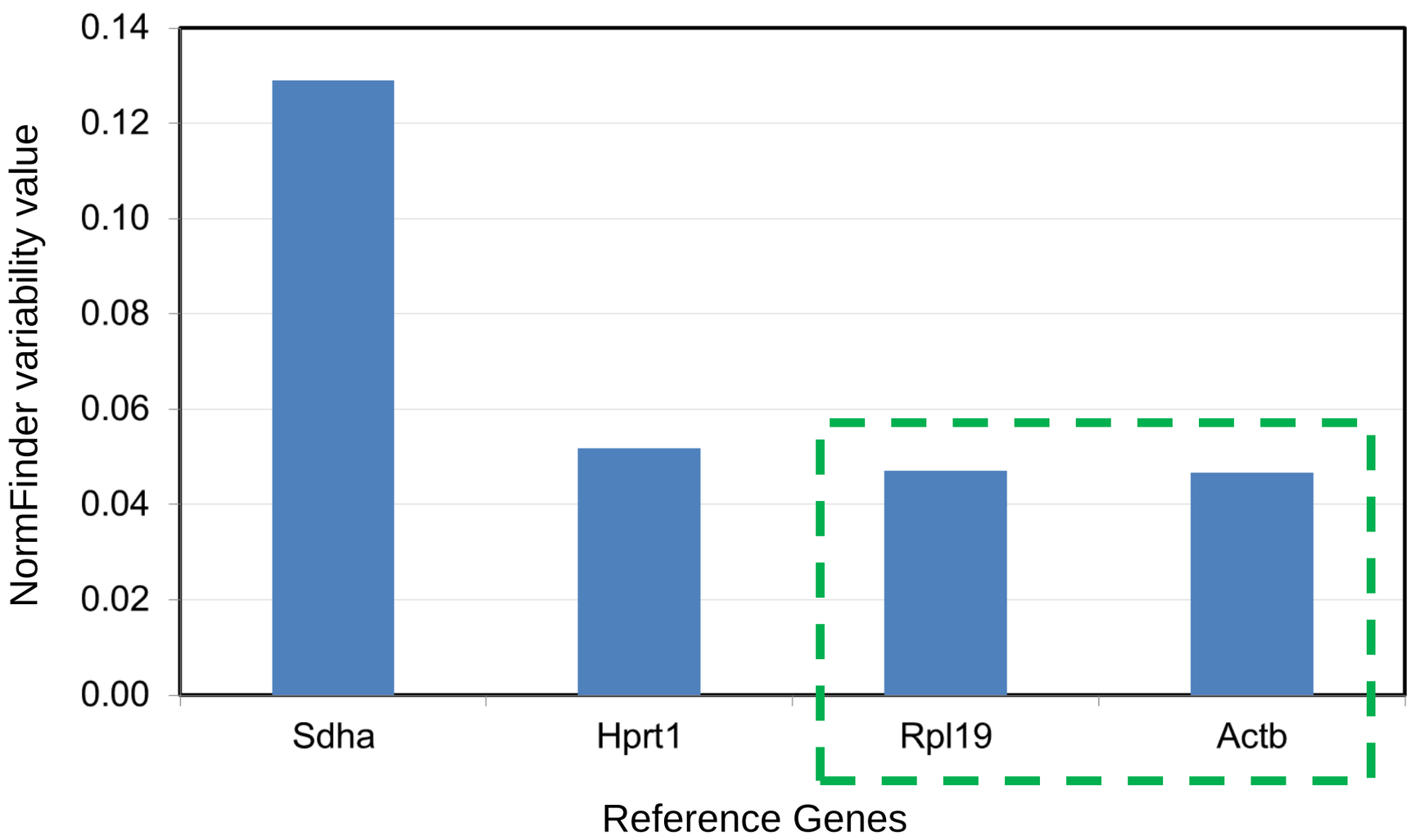
0.14
0.12
0.10
0.08
0.06
0.04
0.02
0.00
NormFinder variability value
Sdha
Hprt1
Rpl19
Actb
Reference Genes

Figure S5

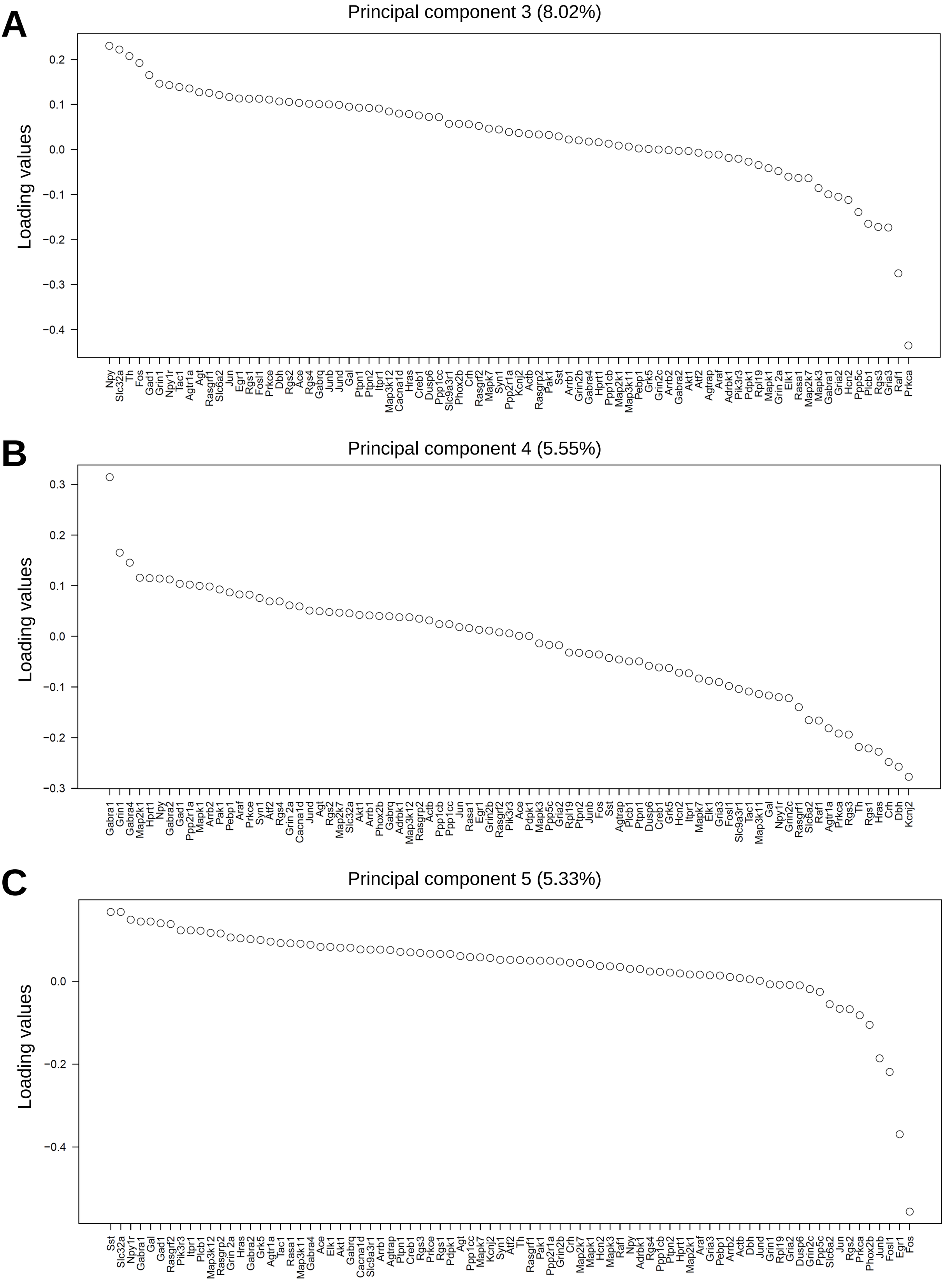
A
Principal component 3 (8.02%)
Loading values
0.2
0.1
0.0
−0.1
−0.2
−0.3
−0.4
Npy
Slc32a
Th
Fos
Gad1
Grin1
Npy1r
Tac1
Agtr1a
Agt
Rasgrf1
Slc6a2
Jun
Egr1
Rgs1
Fosl1
Prkce
Dbh
Rgs2
Ace
Rgs4
Gabrq
Junb
Jund
Gal
Ptpn1
Ptpn2
Itpr1
Map3k12
Cacna1d
Hras
Creb1
Dusp6
Ppp1cc
Slc9a3r1
Phox2b
Crh
Rasgrf2
Mapk7
Syn1
Ppp2r1a
Kcnj2
Actb
Rasgrp2
Pak1
Sst
Arrb1
Grin2b
Gabra4
Hprt1
Ppp1cb
Map2k1
Map3k11
Pebp1
Grk5
Grin2c
Arrb2
Gabra2
Akt1
Atf2
Agtrap
Araf
Adrbk1
Plk3r3
Pdpk1
Rpl19
Mapk1
Grin 2a
Elk1
Rasa1
Map2k7
Mapk3
Gabra1
Gria2
Hcn2
Ppp5c
Plcb1
Rgs3
Gria3
Raf1
Prkca
B
Principal component 4 (5.55%)
Loading values
0.3
0.2
0.1
0.0
−0.1
−0.2
−0.3
Gabra1
Grin1
Gabra4
Map2k1
Hprt1
Npy
Gabra2
Gad1
Ppp2r1a
Mapk1
Arrb2
Pak1
Pebp1
Araf
Prkce
Syn1
Atf2
Rgs4
Grin 2a
Cacna1d
Jund
Agt
Rgs2
Map2k7
Slc32a
Akt1
Arrb1
Phox2b
Gabrq
Adrbk1
Map3k12
Rasgrp2
Actb
Ppp1cb
Ppp1cc
Jun
Rasa1
Egr1
Grin2b
Rasgrf2
Pik3r3
Ace
Pdpk1
Mapk3
Ppp5c
Gria2
Rpl19
Ptpn2
Junb
Fos
Sst
Agtrap
Plcb1
Ptpn1
Dusp6
Creb1
Grk5
Hcn2
Itpr1
Mapk7
Elk1
Gria3
Fosl1
Slc9a3r1
Tac1
Map3k11
Gal
Npy1r
Grin2c
Rasgrf1
Slc6a2
Raf1
Agtr1a
Prkca
Rgs3
Th
Rgs1
Hras
Crh
Dbh
Kcnj2
C
Principal component 5 (5.33%)
Loading values
0.0
−0.2
−0.4
Sst
Slc32a
Npy1r
Gabra1
Gal
Gad1
Rasgrf2
Pik3r3
Itpr1
Plcb1
Map3k12
Rasgrp2
Grin 2a
Hras
Gabra2
Grk5
Agtr1a
Tac1
Rasa1
Map3k11
Gabra4
Ace
Elk1
Akt1
Gabrq
Cacna1d
Slc9a3r1
Arrb1
Agtrap
Ptpn1
Creb1
Rgs3
Prkce
Rgs1
Pdpk1
Agt
Ppp1cc
Mapk7
Kcnj2
Syn1
Atf2
Th
Rasgrf1
Pak1
Ppp2r1a
Grin2b
Crh
Map2k7
Mapk1
Hcn2
Mapk3
Raf1
Npy
Adrbk1
Rgs4
Ppp1cb
Ptpn2
Hprt1
Map2k1
Araf
Gria3
Pebp1
Arrb2
Actb
Dbh
Jund
Grin1
Rpl19
Gria2
Dusp6
Grin2c
Ppp5c
Slc6a2
Jun
Rgs2
Prkca
Phox2b
Junb
Fosl1
Egr1
Fos

Figure S6

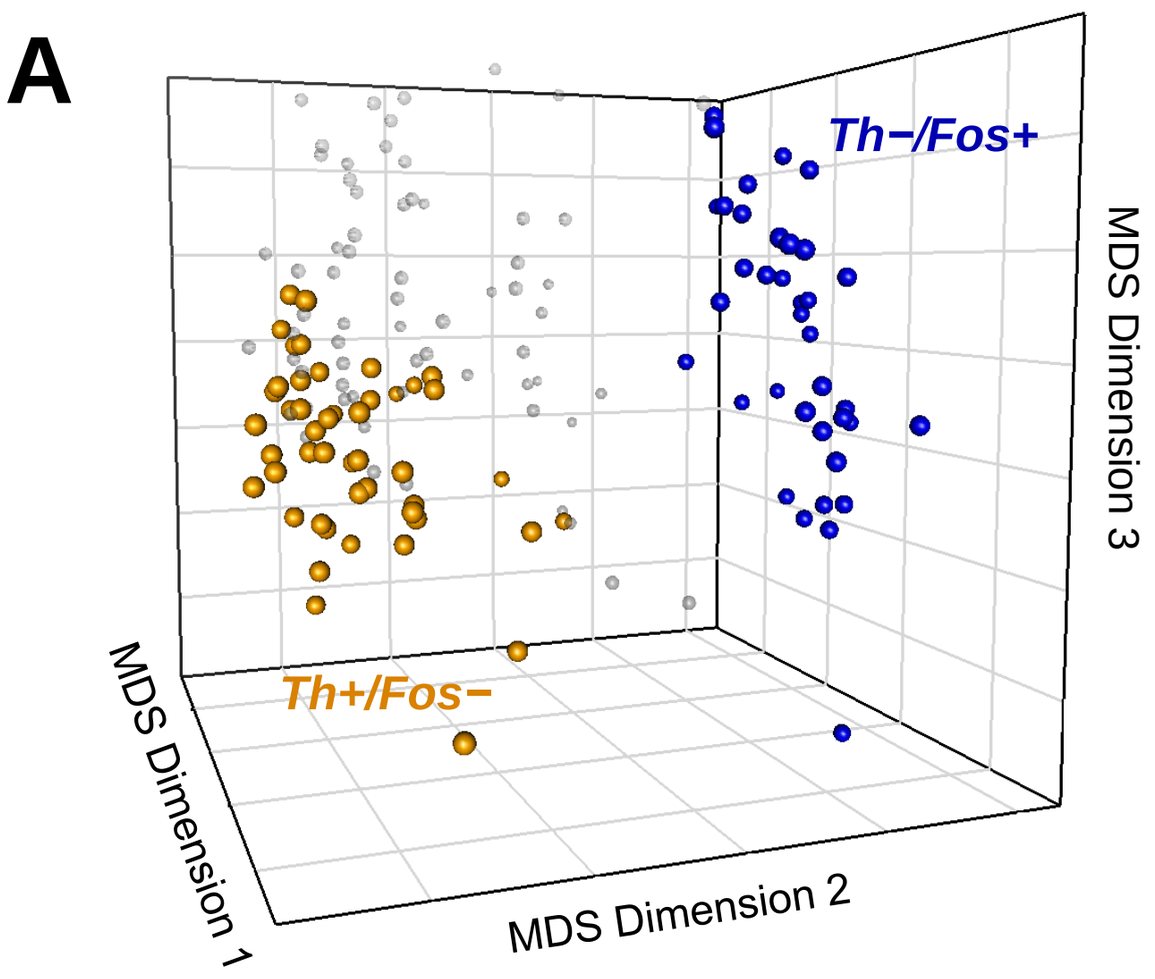
A
Th−/Fos+
Th+/Fos−
MDS Dimension 1
MDS Dimension 2
MDS Dimension 3

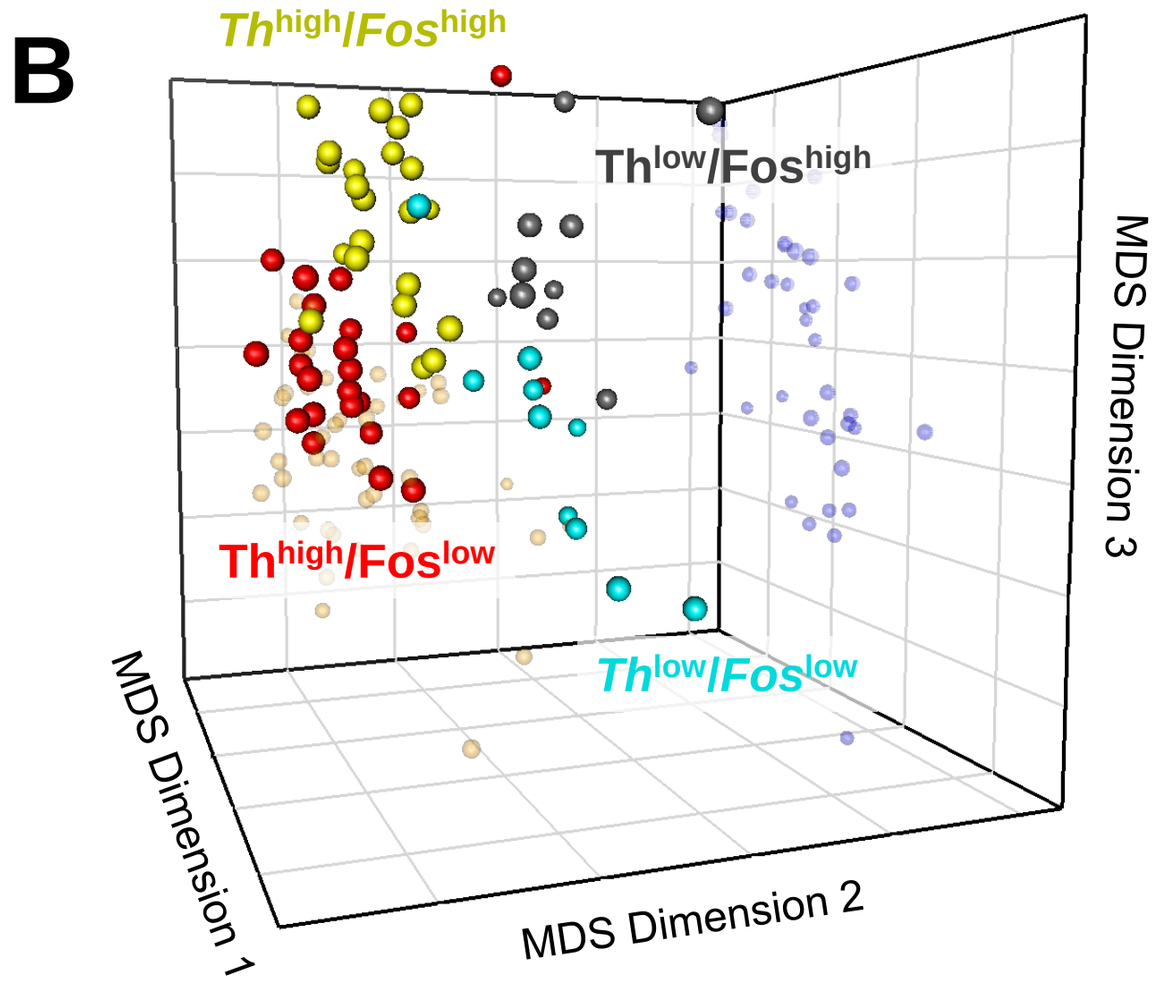
B
Thhigh/Foshigh
Thlow/Foshigh
Thhigh/Foslow
Thlow/Foslow
MDS Dimension 1
MDS Dimension 2
MDS Dimension 3

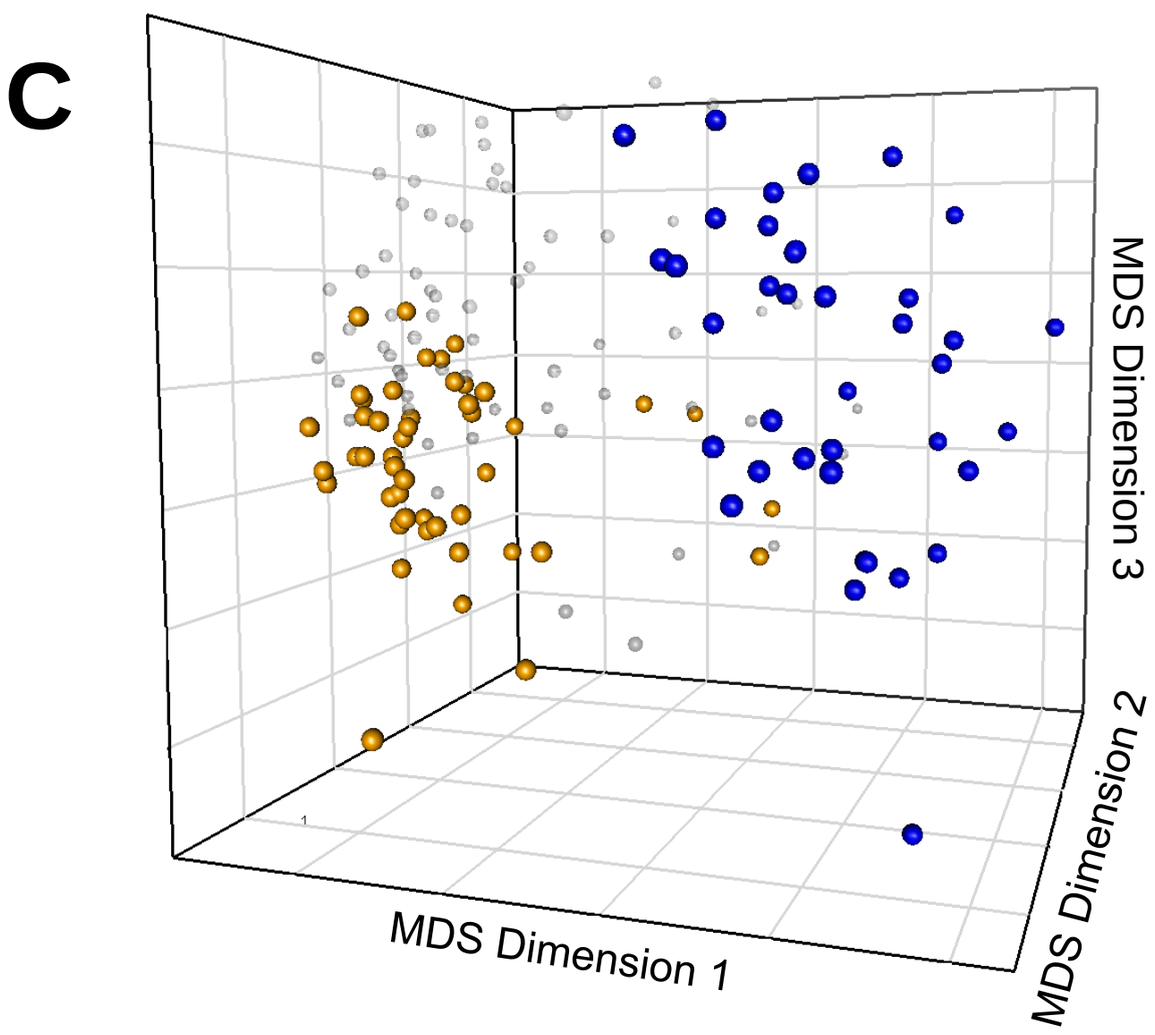
C
MDS Dimension 1
MDS Dimension 2
MDS Dimension 3

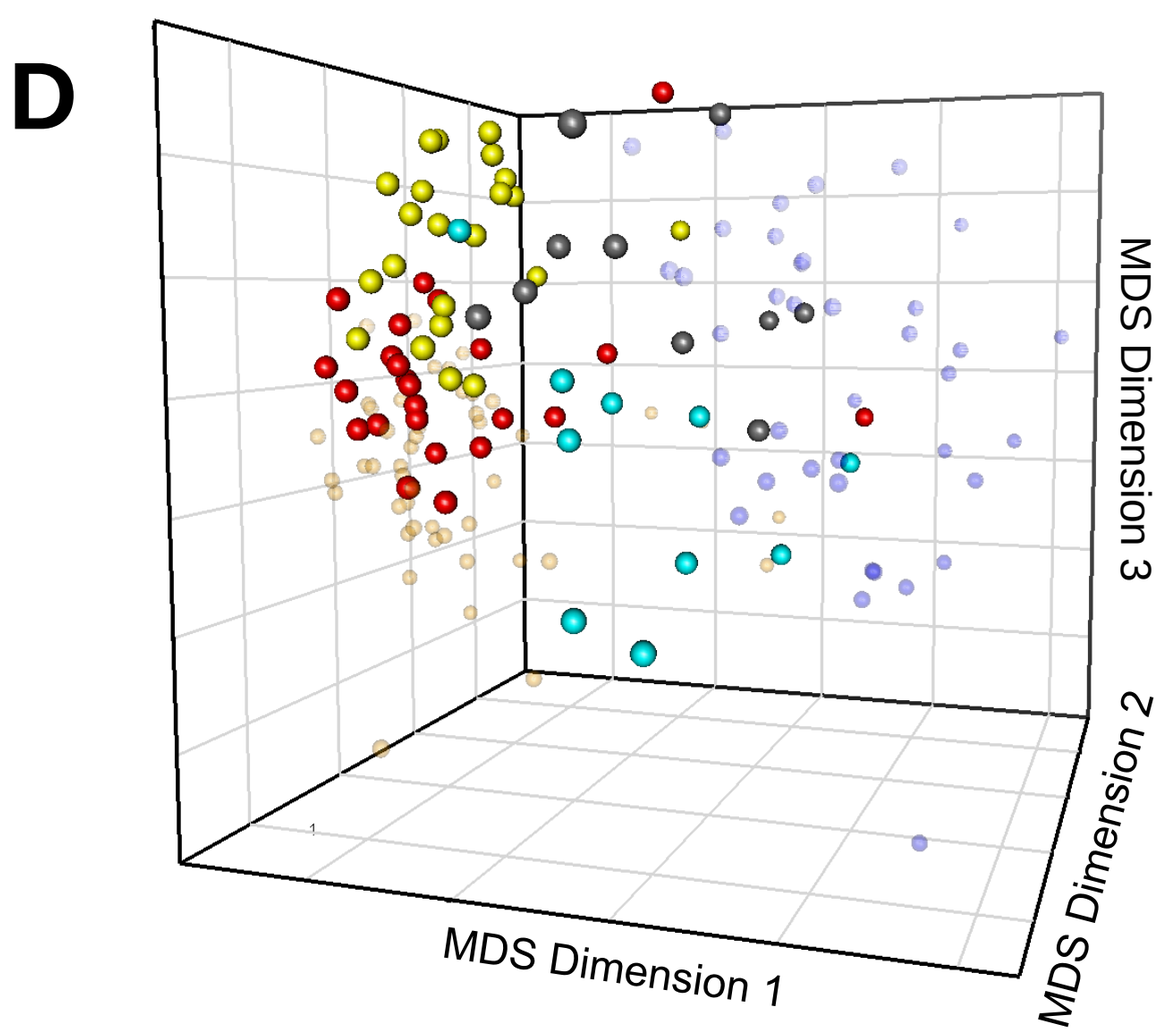
D
MDS Dimension 1
MDS Dimension 2
MDS Dimension 3

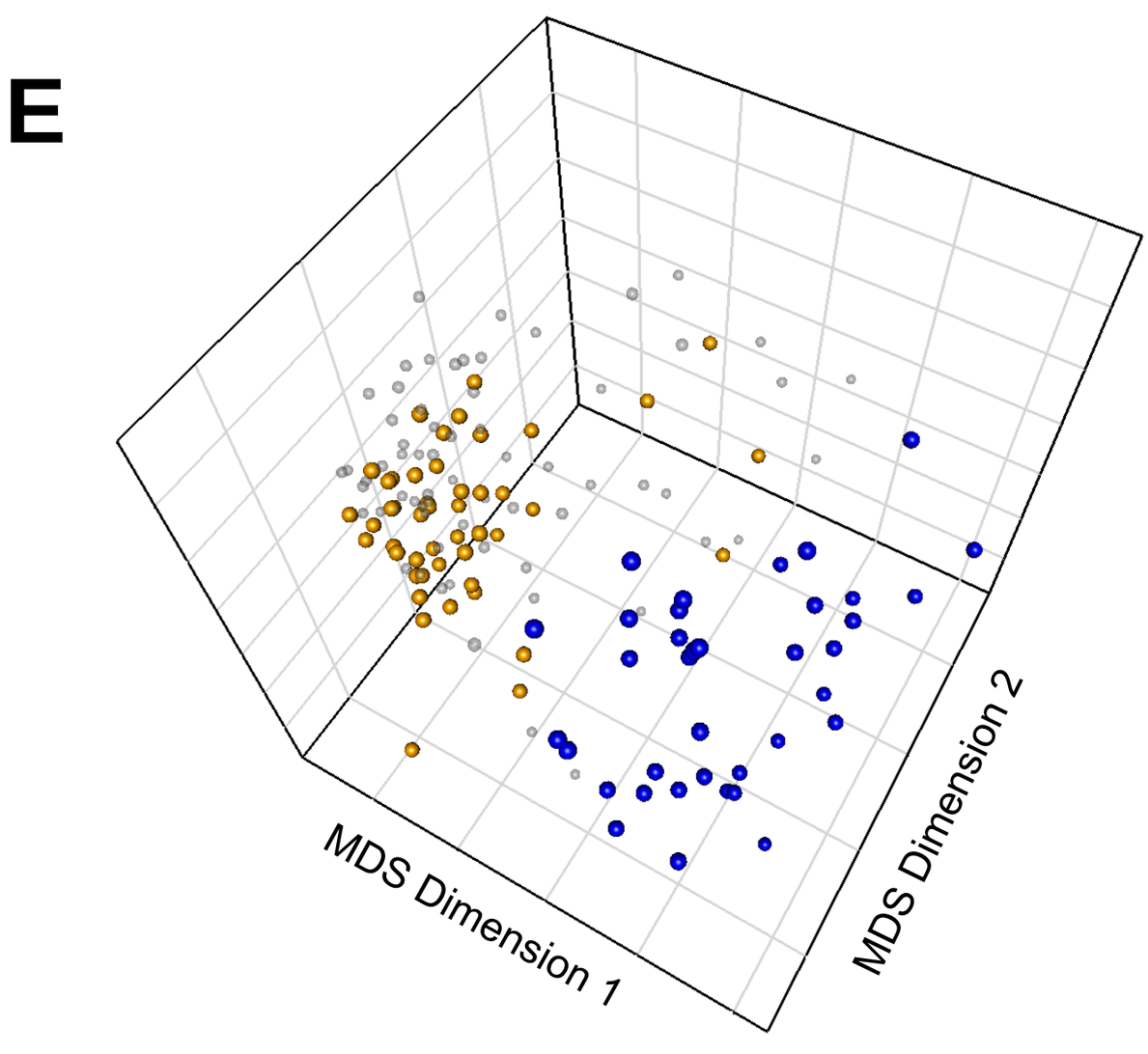
E
MDS Dimension 1
MDS Dimension 2
MDS Dimension 3

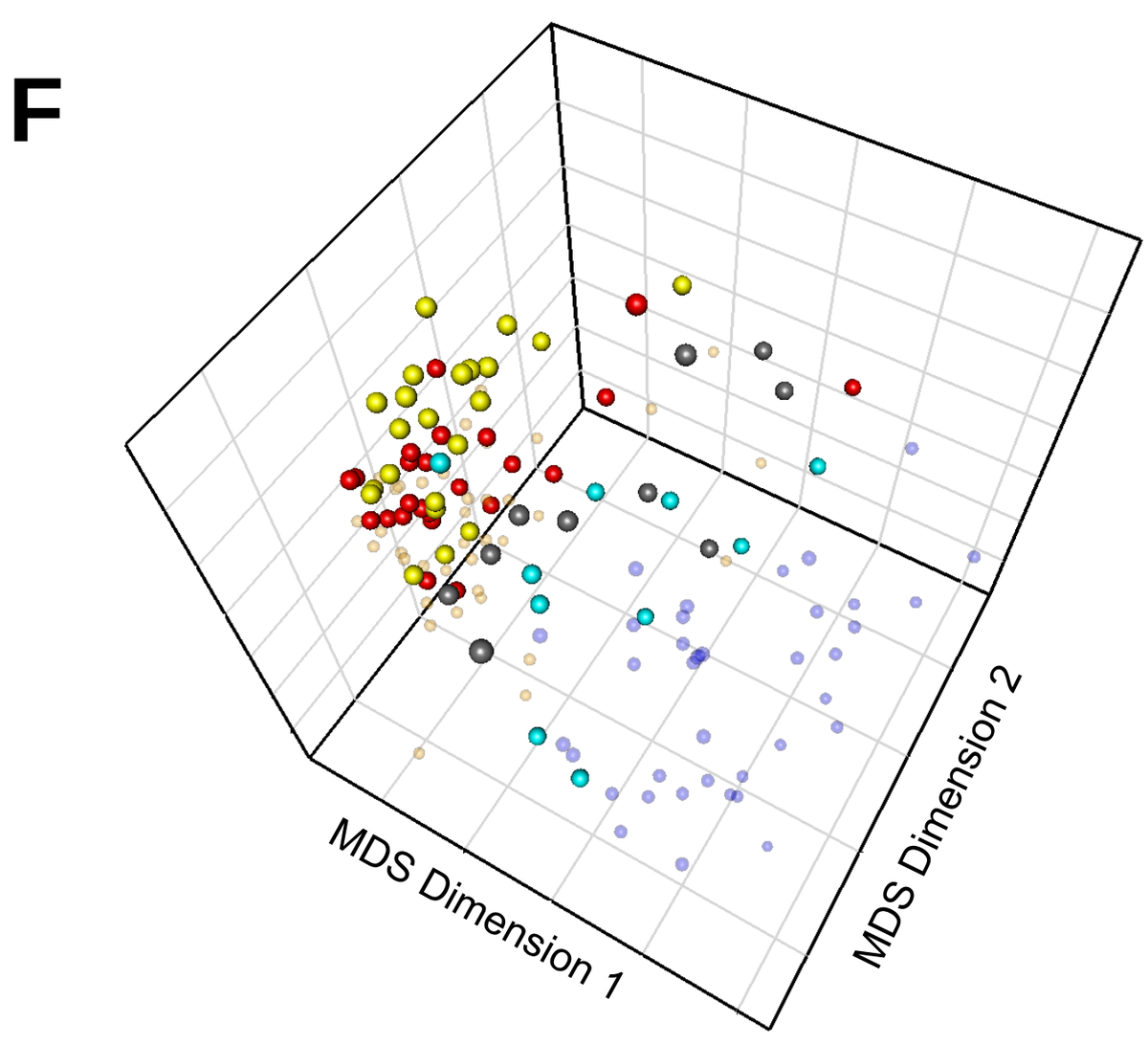
F
MDS Dimension 1
MDS Dimension 2
MDS Dimension 3

Figure S7

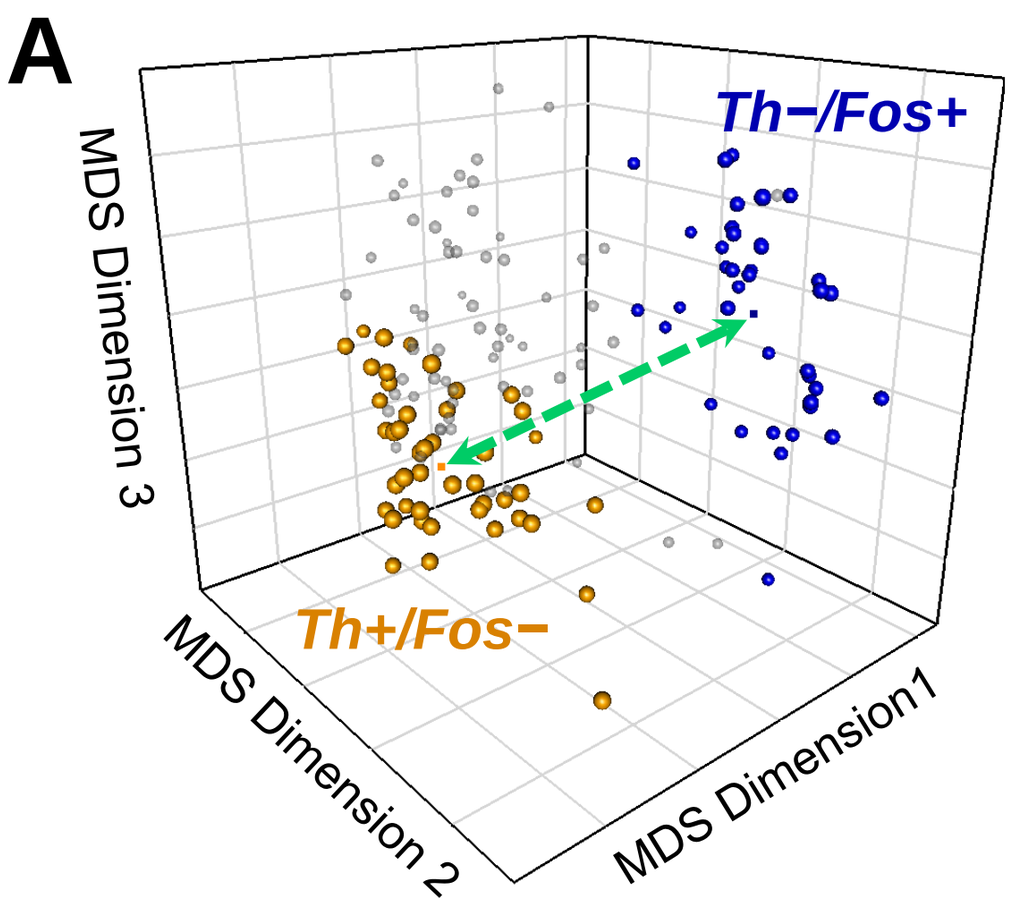

Original data

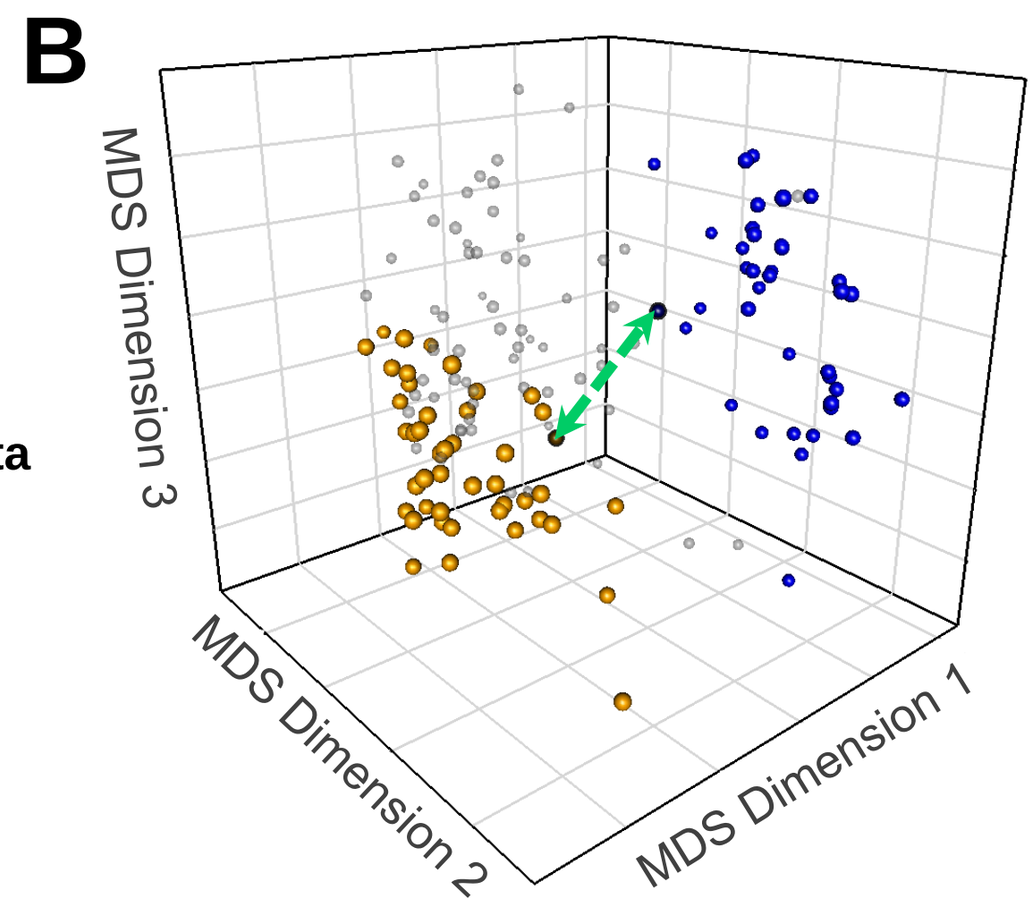

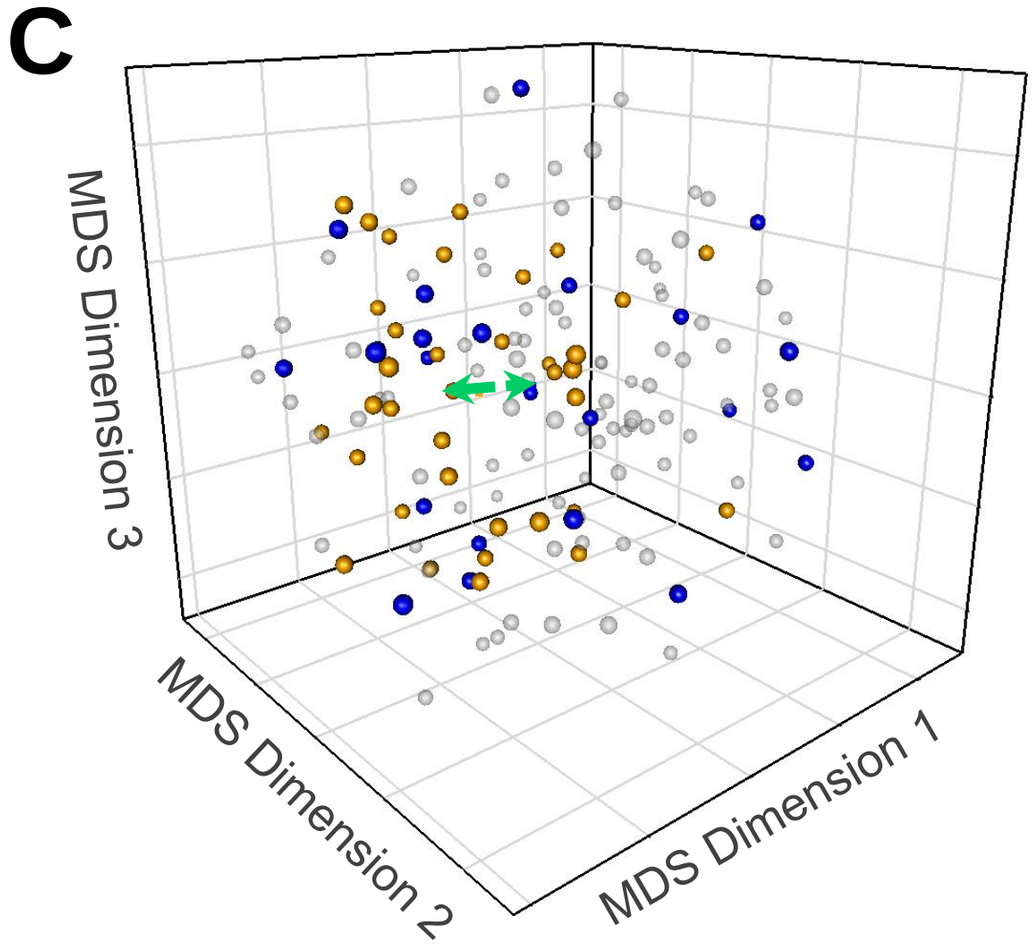

Representative permuted data

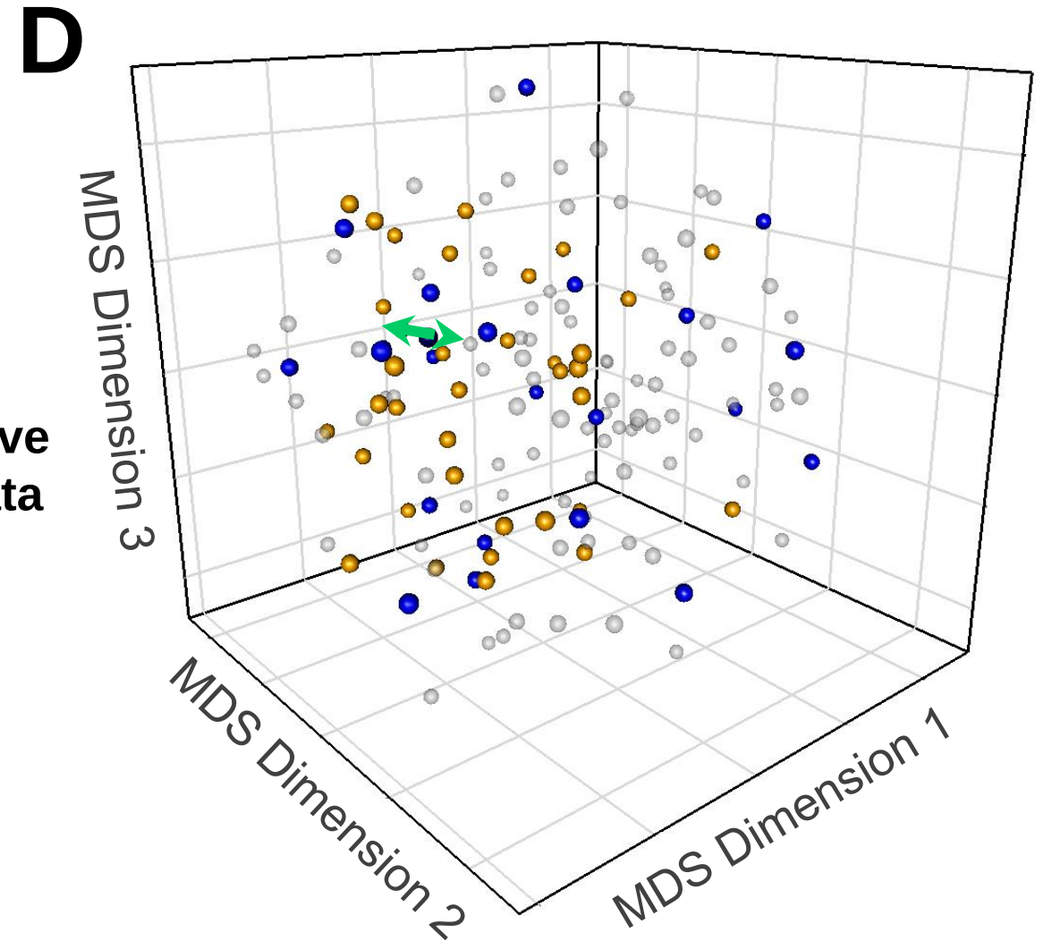

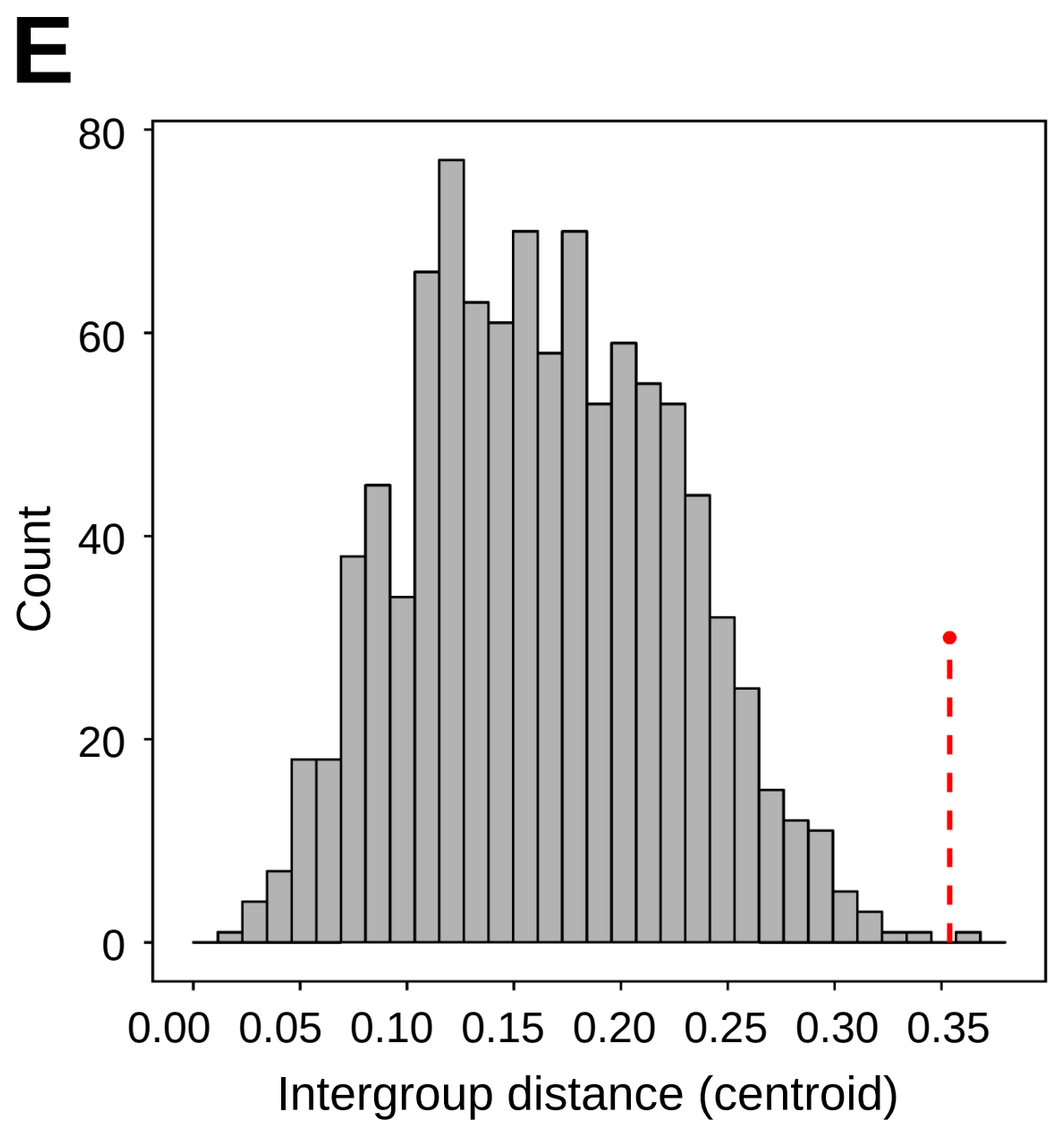

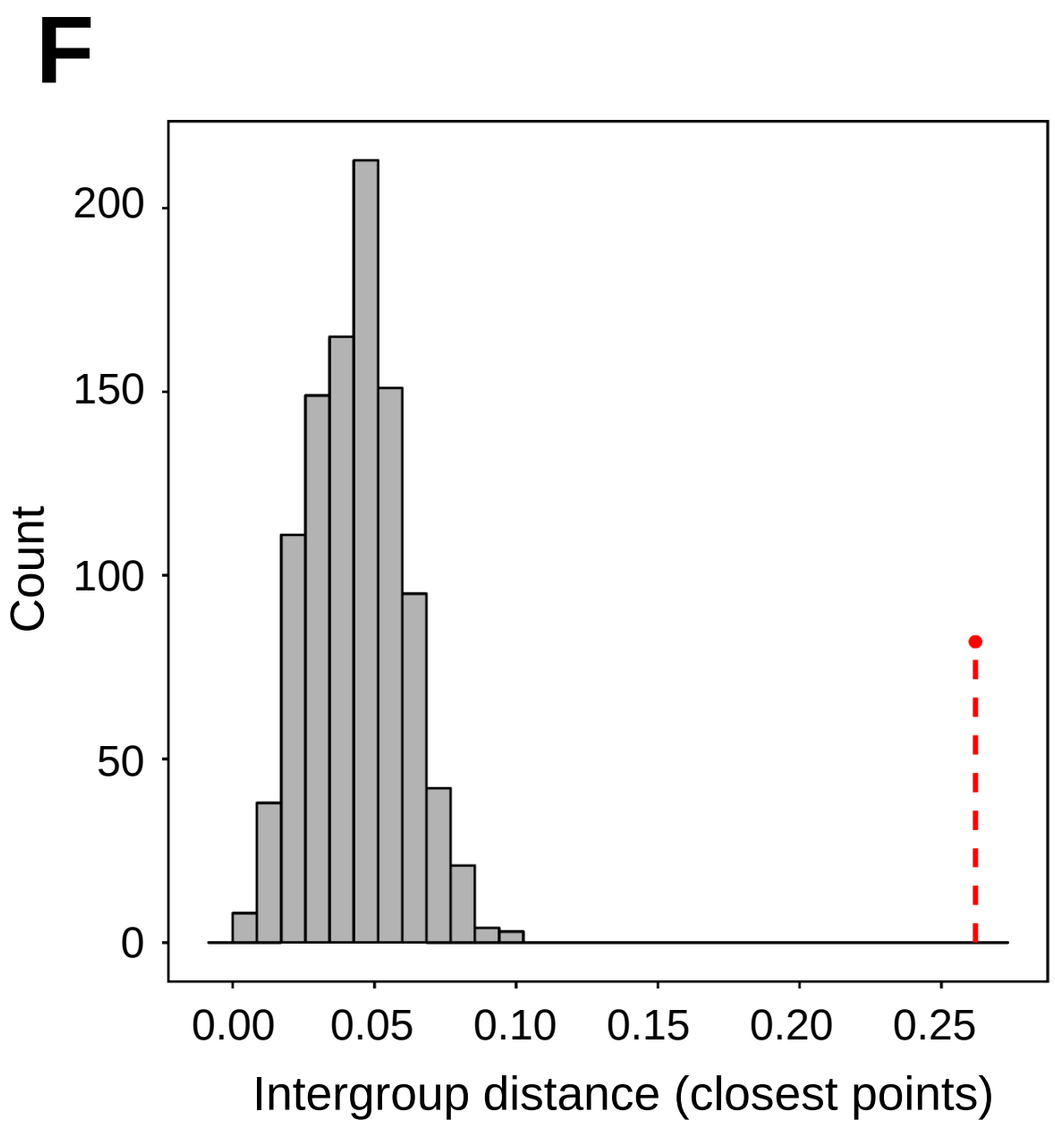

Figure S8

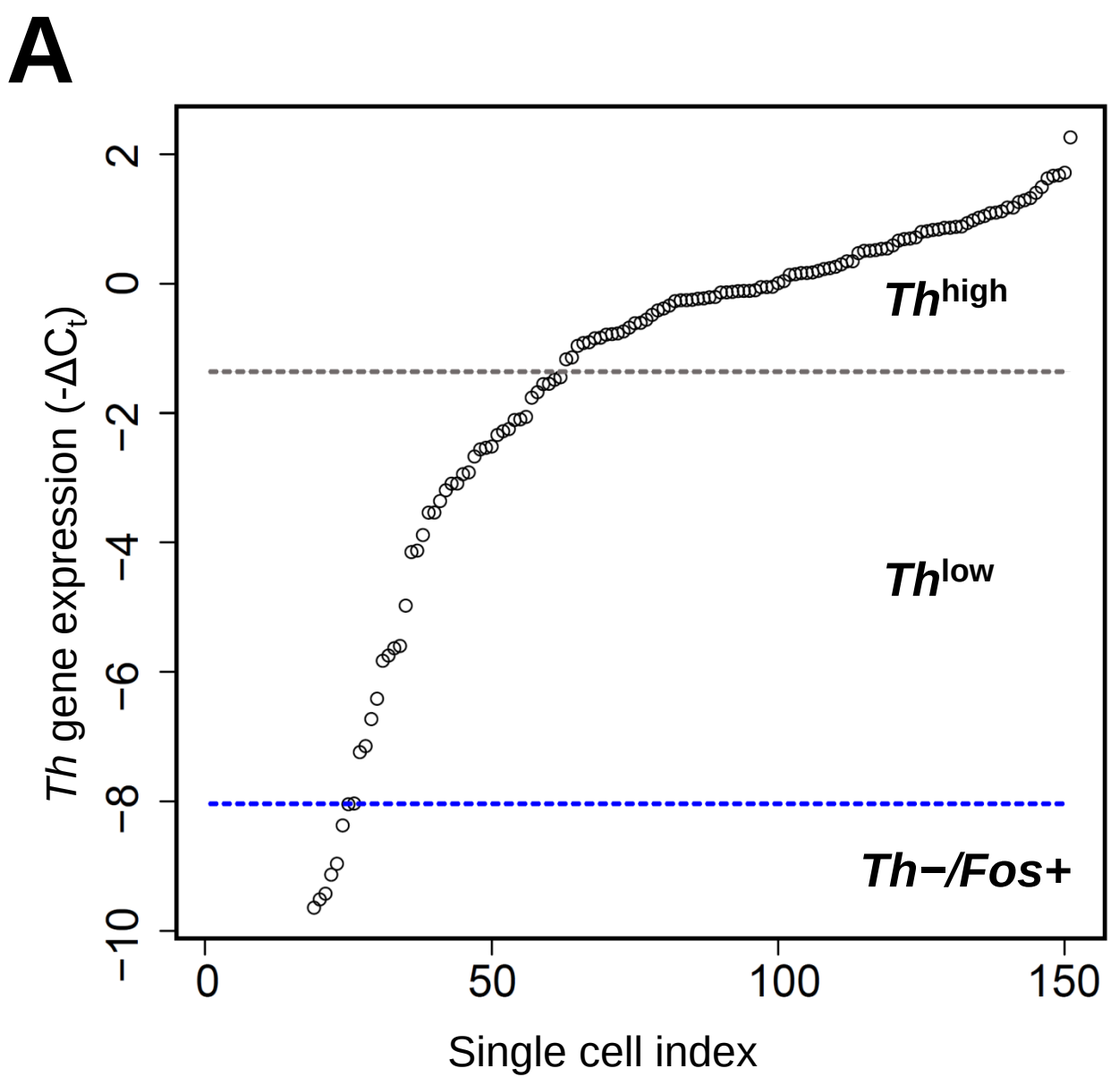
A
Th gene expression (-ΔCt)
Th^high
Th^low
Th−/Fos+
Single cell index

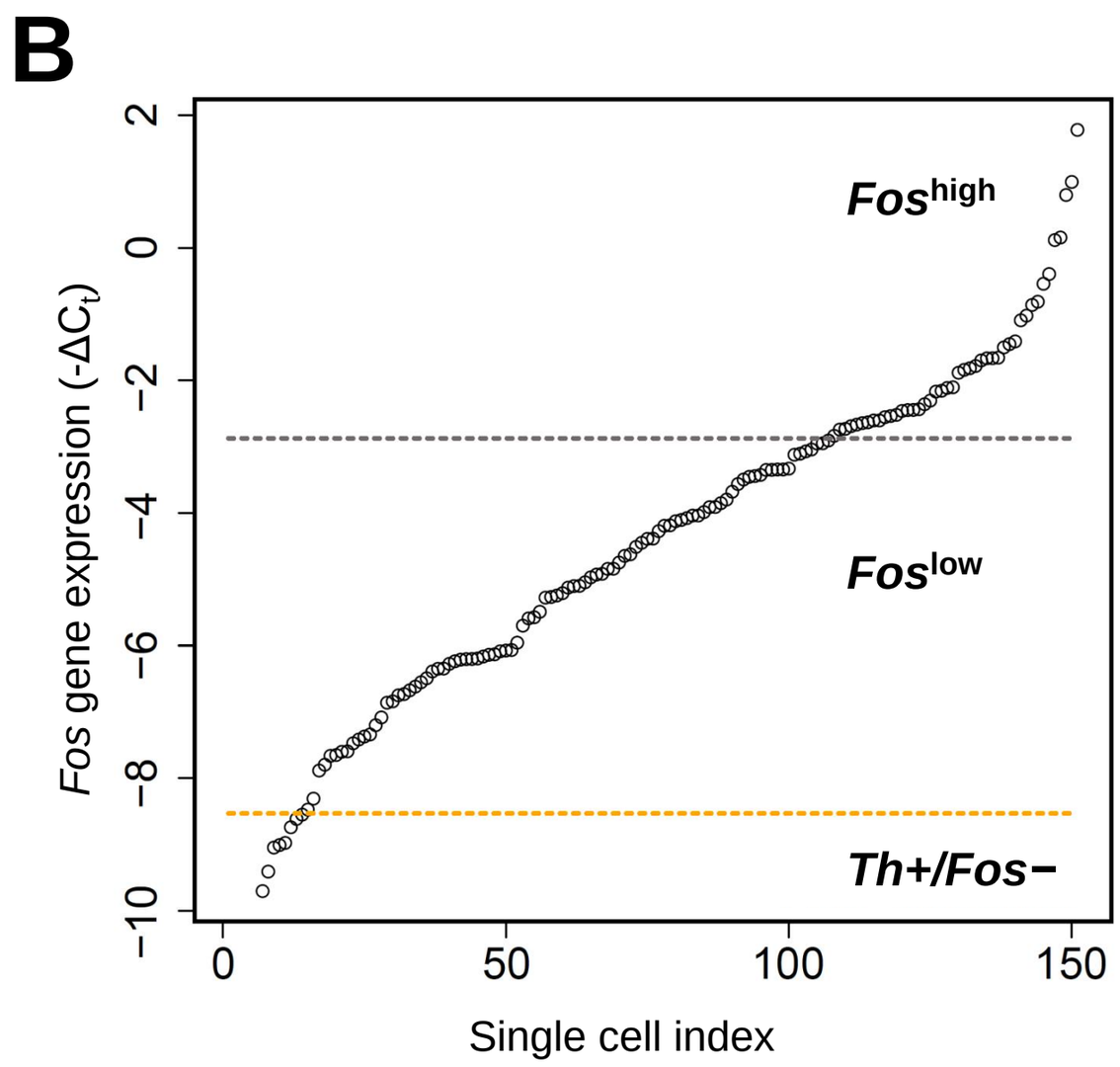
B
Fos gene expression (-ΔCt)
Fos^high
Fos^low
Th+/Fos−
Single cell index

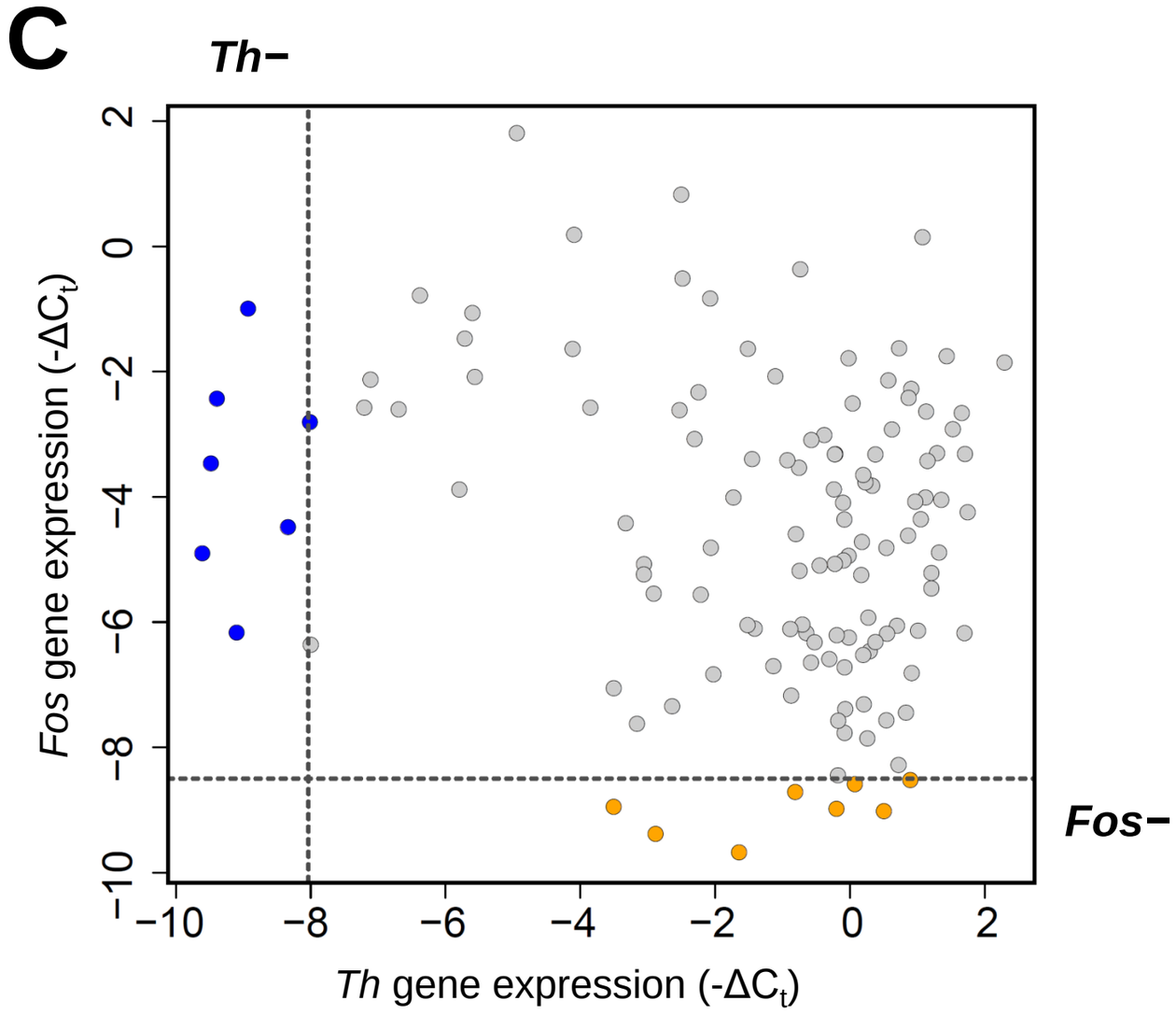
C
Th−
Fos gene expression (-ΔCt)
Fos−
Th gene expression (-ΔCt)

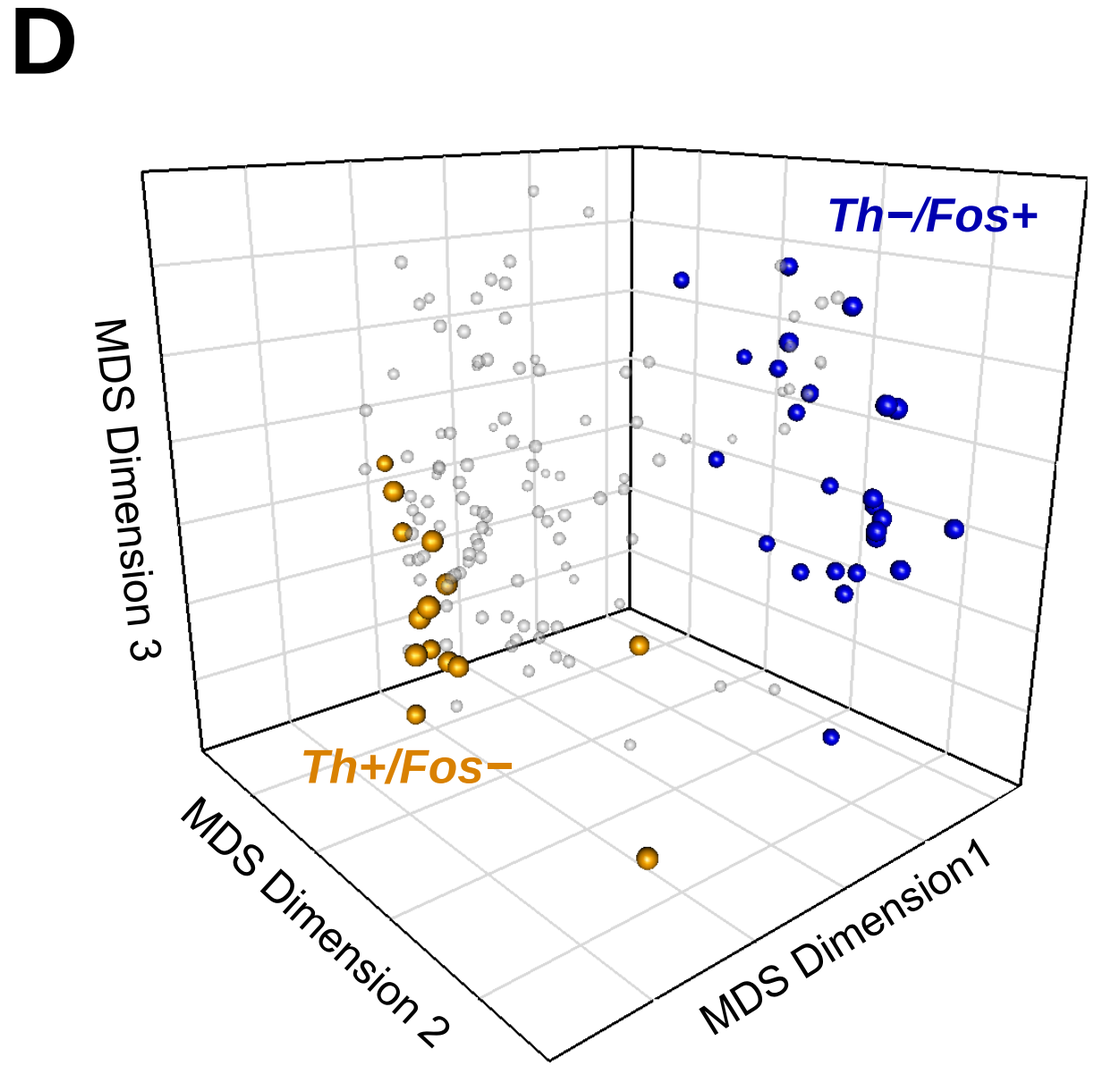
D
Th−/Fos+
Th+/Fos−
MDS Dimension 3
MDS Dimension 2
MDS Dimension1

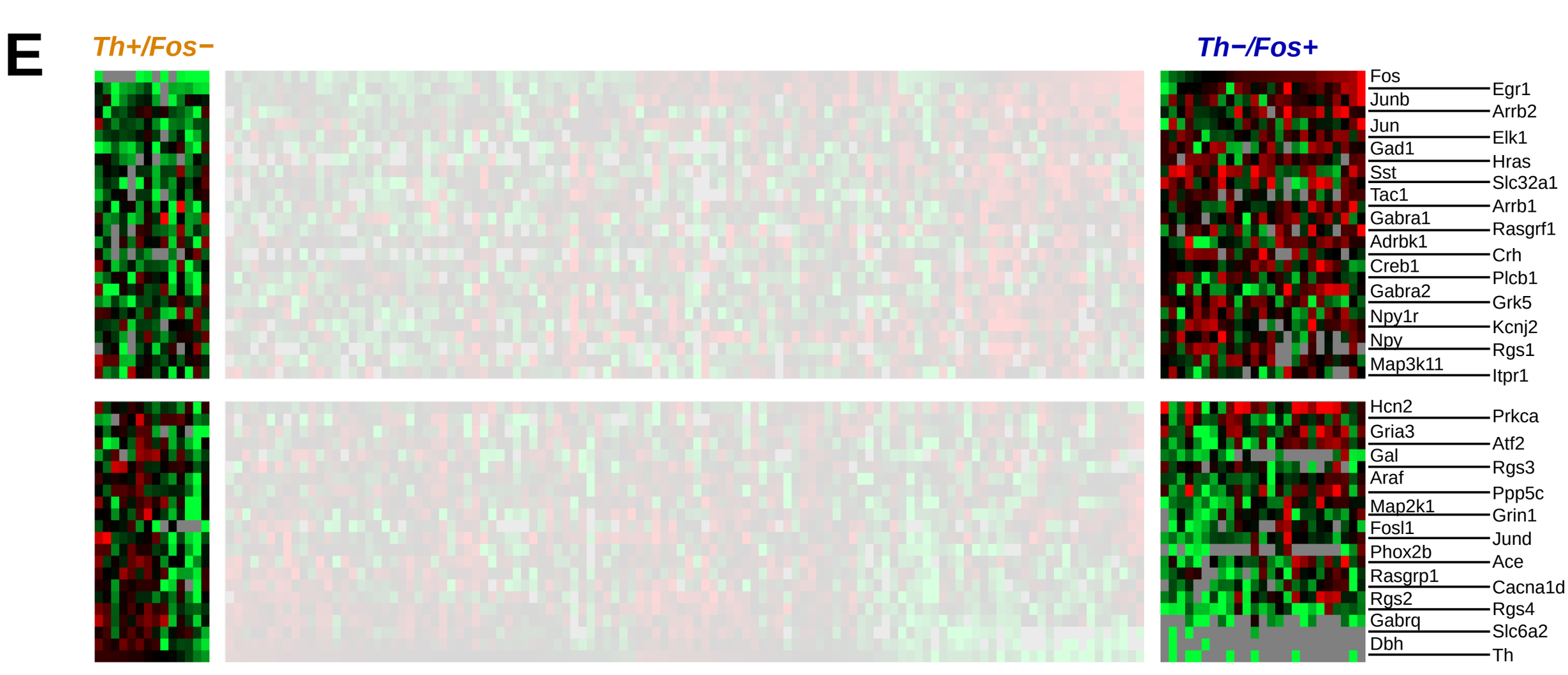
E
Th+/Fos−
Th−/Fos+
Fos
Egr1
Junb
Arrb2
Jun
Elk1
Gad1
Hras
Sst
Slc32a1
Tac1
Arrb1
Gabra1
Rasgrf1
Adrbk1
Crh
Creb1
Plcb1
Gabra2
Grk5
Npy1r
Kcnj2
Npy
Rgs1
Map3k11
Itpr1
Hcn2
Prkca
Gria3
Atf2
Gal
Rgs3
Araf
Ppp5c
Map2k1
Grin1
Fosl1
Jund
Phox2b
Ace
Rasgrp1
Cacna1d
Rgs2
Rgs4
Gabrq
Slc6a2
Dbh
Th

Figure S9

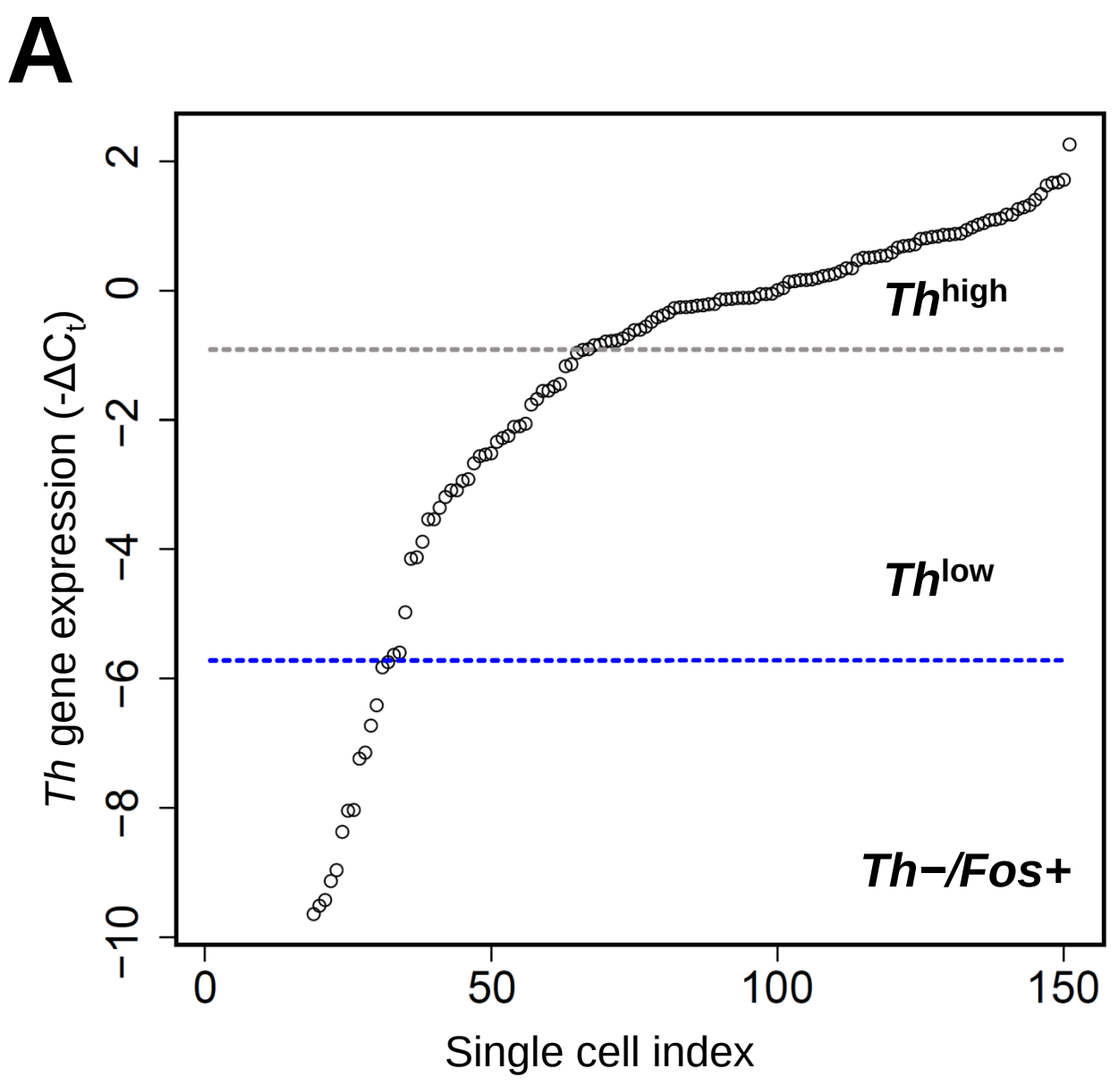
A
Th gene expression (-ΔCt)
Th^high
Th^low
Th−/Fos+
Single cell index

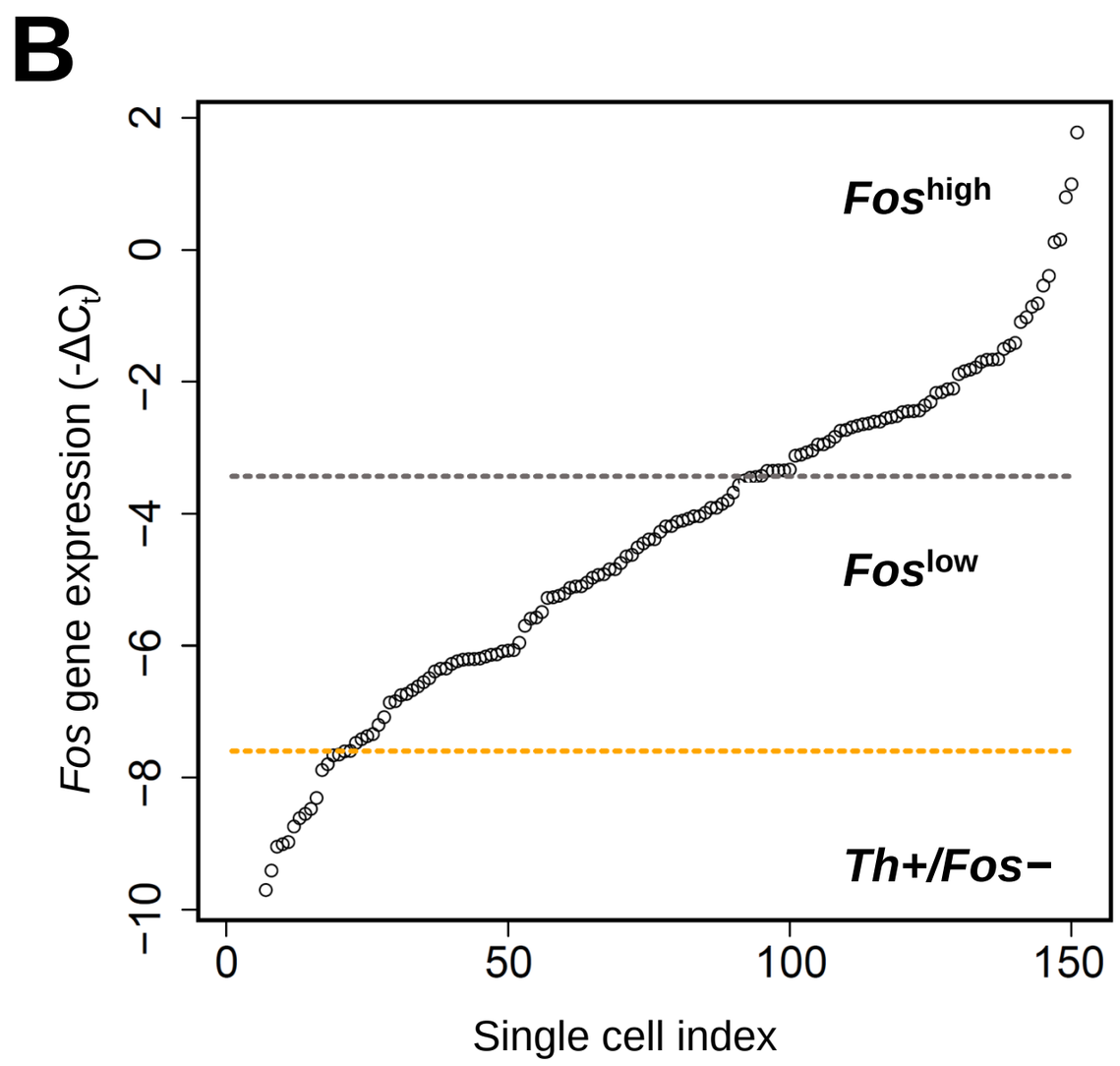
B
Fos gene expression (-ΔCt)
Fos^high
Fos^low
Th+/Fos−
Single cell index

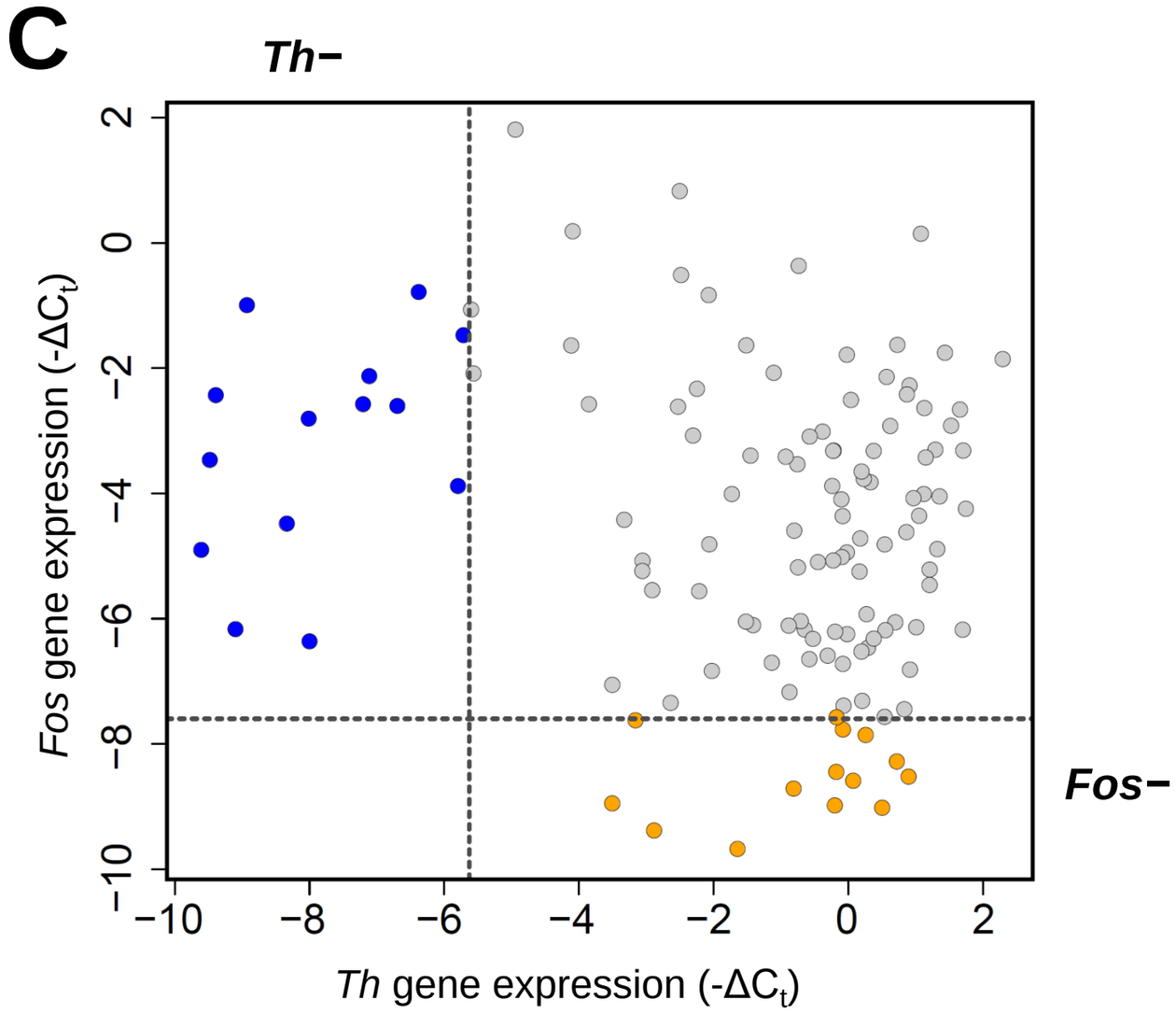
C
Th−
Fos gene expression (-ΔCt)
Fos−
Th gene expression (-ΔCt)

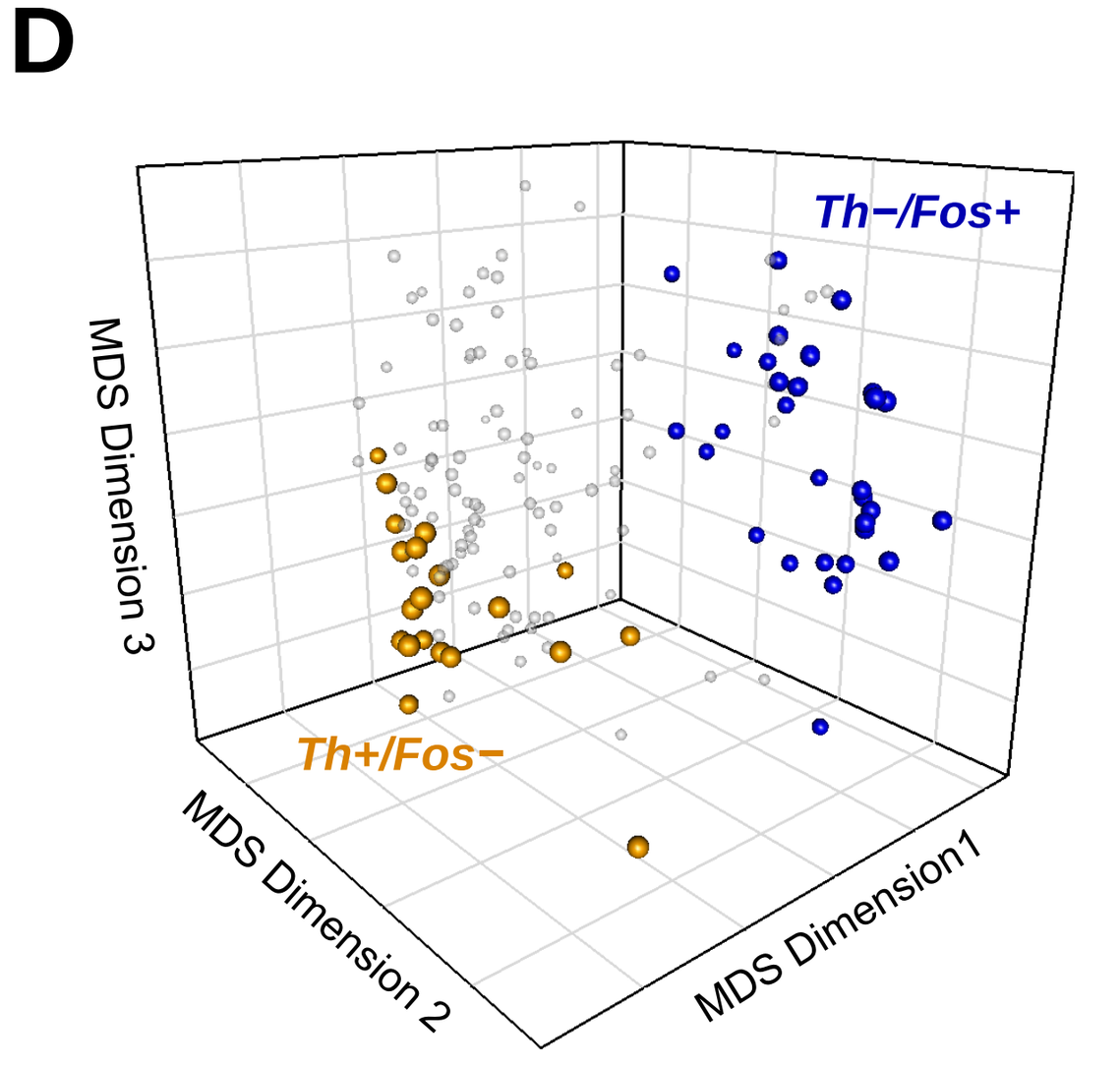
D
Th−/Fos+
Th+/Fos−
MDS Dimension 3
MDS Dimension 2
MDS Dimension1

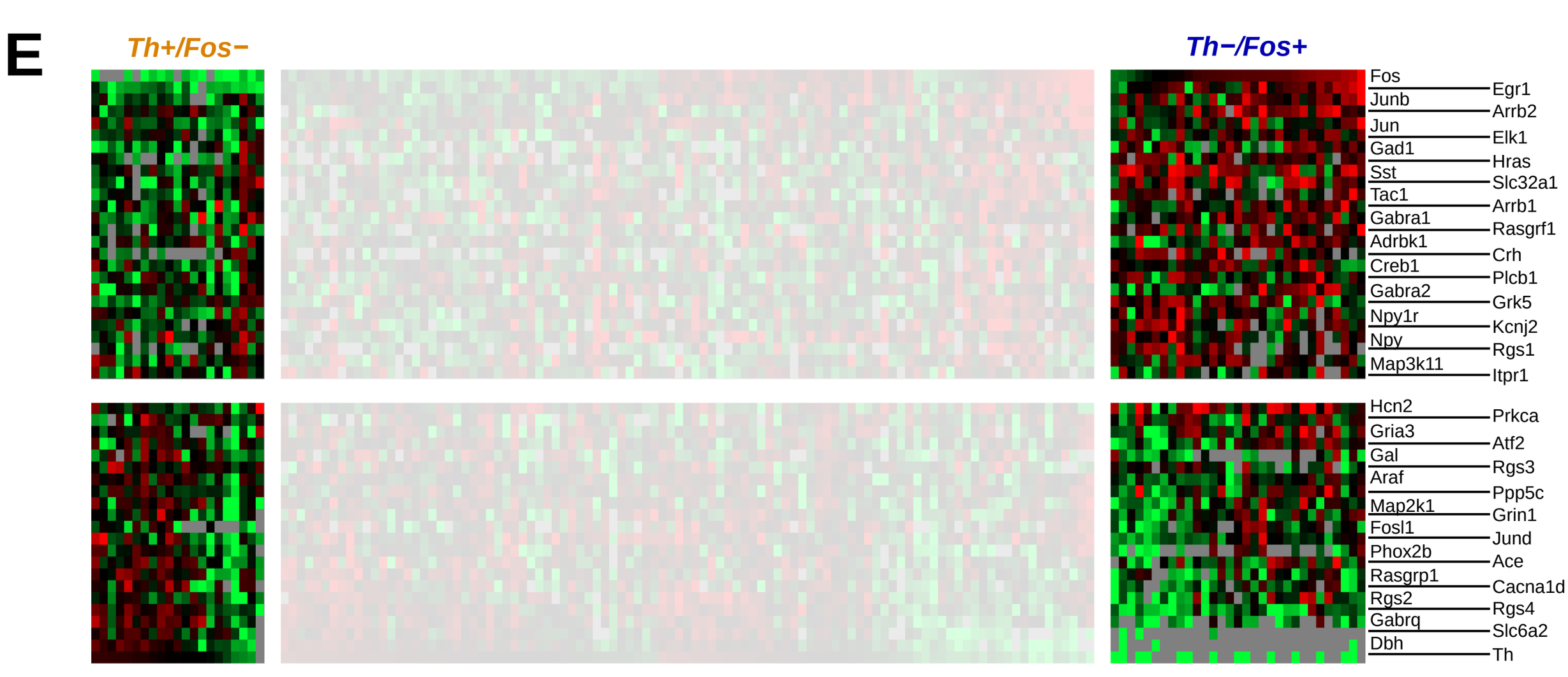
E
Th+/Fos−
Th−/Fos+
Fos
Egr1
Junb
Arrb2
Jun
Elk1
Gad1
Hras
Sst
Slc32a1
Tac1
Arrb1
Gabra1
Rasgrf1
Adrbk1
Crh
Creb1
Plcb1
Gabra2
Grk5
Npy1r
Kcnj2
Npy
Rgs1
Map3k11
Itpr1
Hcn2
Prkca
Gria3
Atf2
Gal
Rgs3
Araf
Ppp5c
Map2k1
Grin1
Fosl1
Jund
Phox2b
Ace
Rasgrp1
Cacna1d
Rgs2
Rgs4
Gabrq
Slc6a2
Dbh
Th

Figure S10

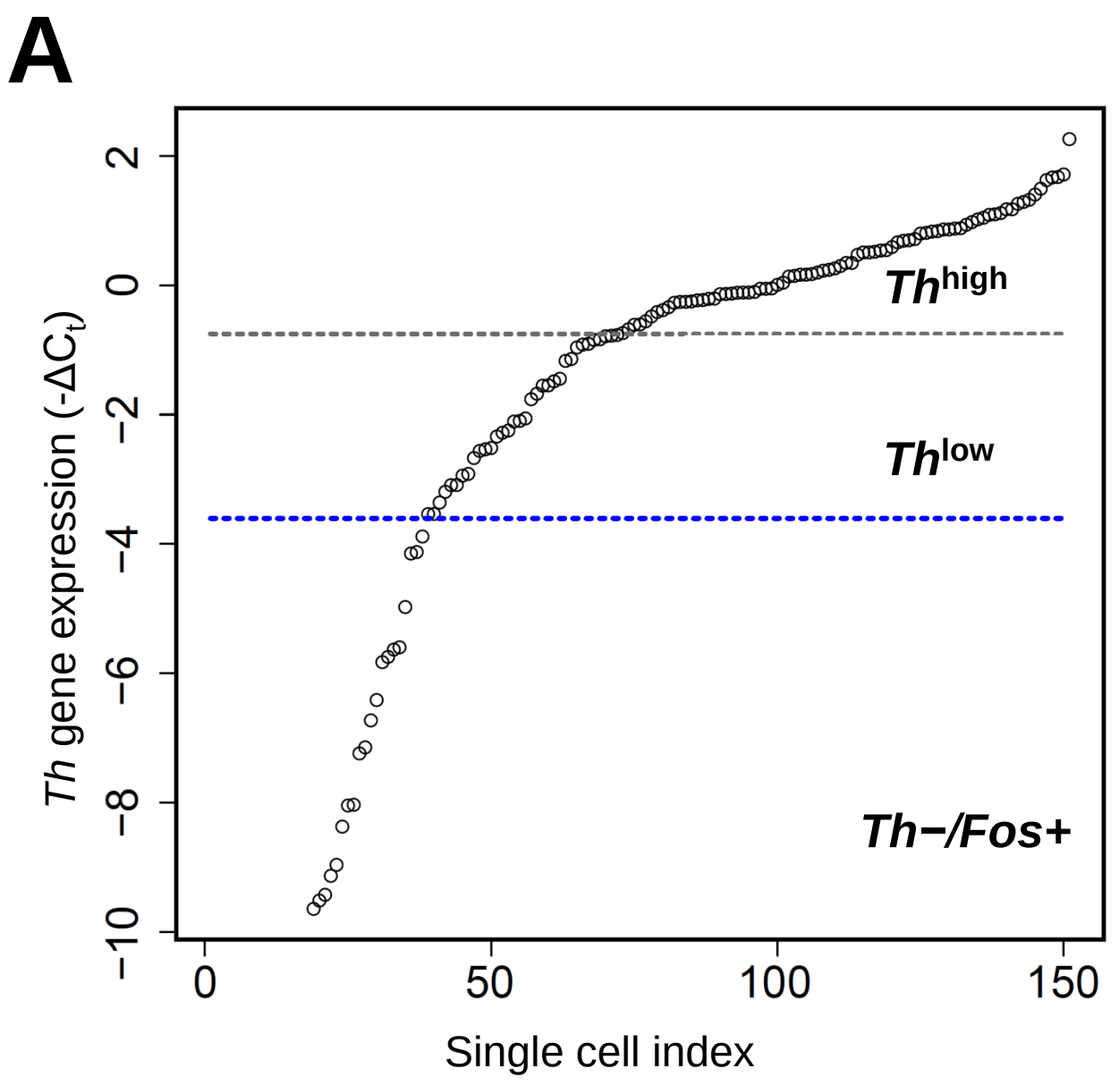
A
Th gene expression (-ΔCt)
Th^high
Th^low
Th−/Fos+
Single cell index

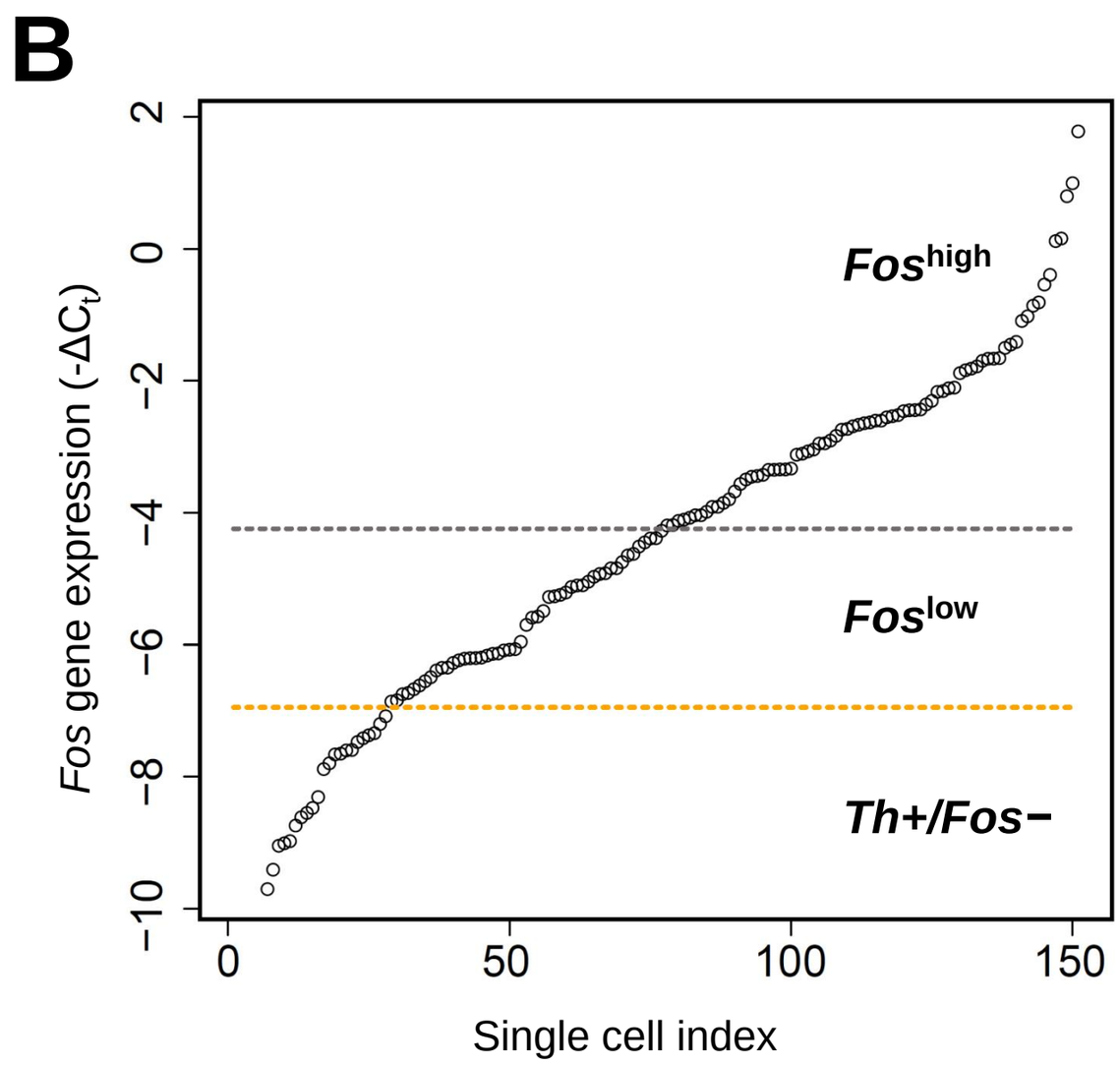
B
Fos gene expression (-ΔCt)
Fos^high
Fos^low
Th+/Fos−
Single cell index

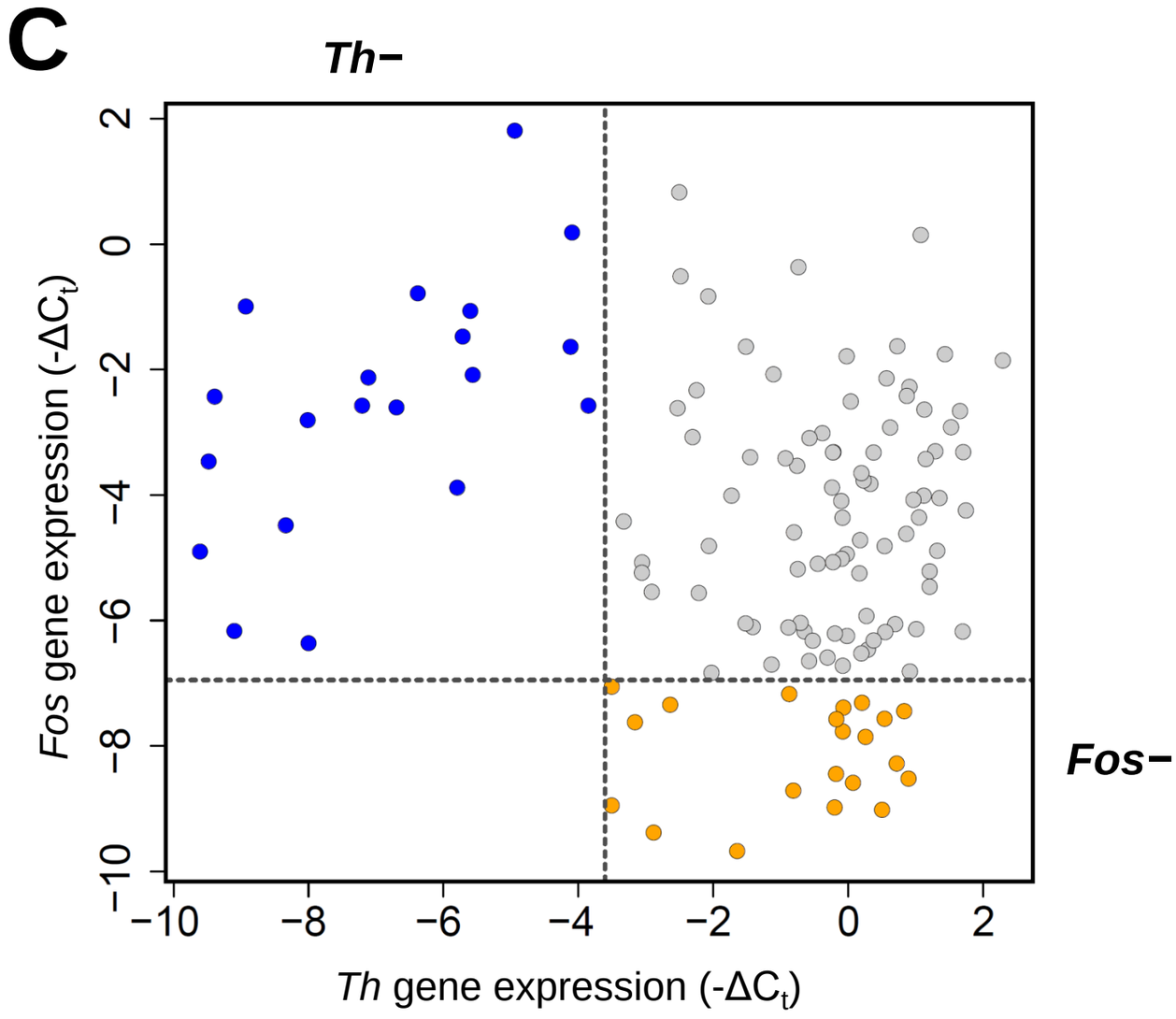
C
Th−
Fos−
Fos gene expression (-ΔCt)
Th gene expression (-ΔCt)

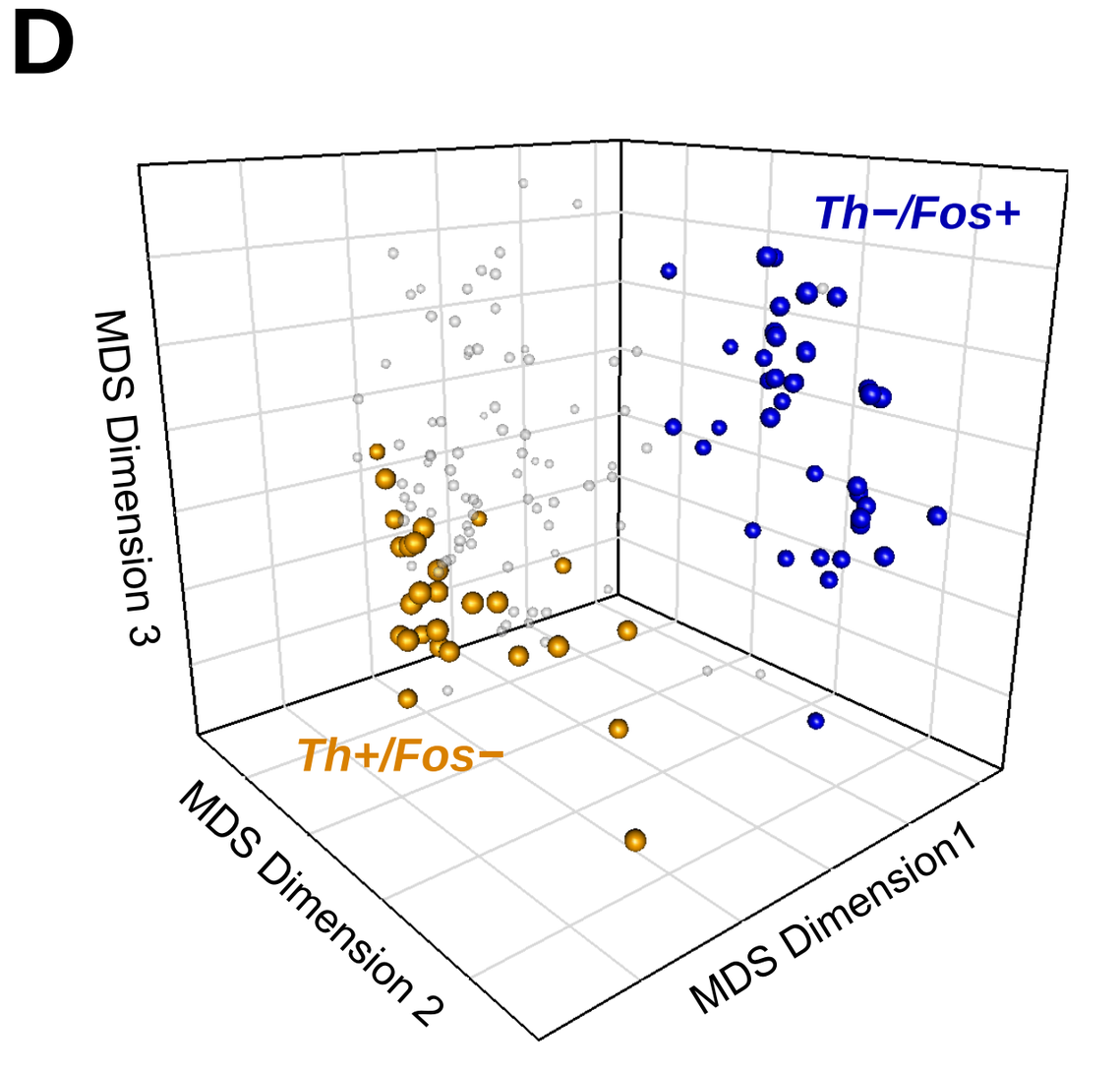
D
Th−/Fos+
Th+/Fos−
MDS Dimension 3
MDS Dimension 2
MDS Dimension1

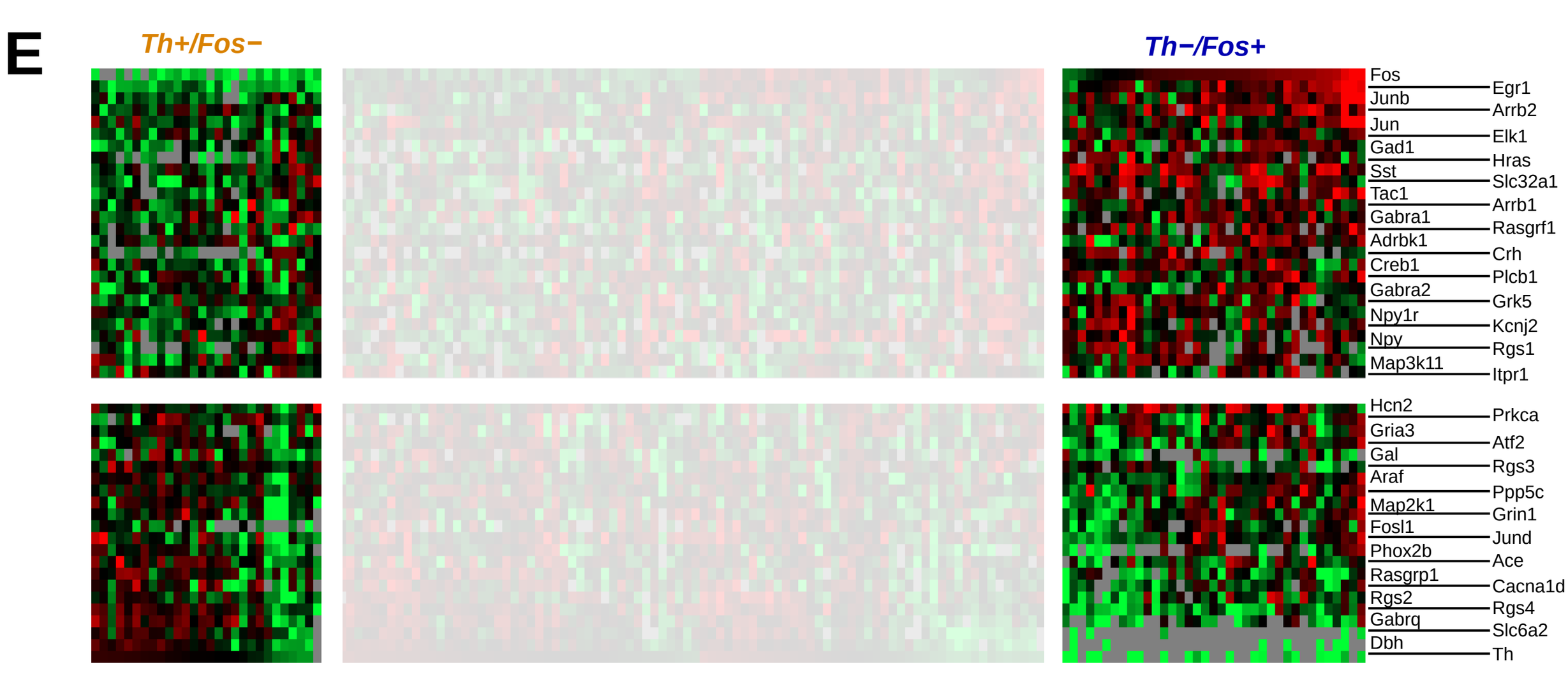
E
Th+/Fos−
Th−/Fos+
Fos
Egr1
Junb
Arrb2
Jun
Elk1
Gad1
Hras
Sst
Slc32a1
Tac1
Arrb1
Gabra1
Rasgrf1
Adrbk1
Crh
Creb1
Plcb1
Gabra2
Grk5
Npy1r
Kcnj2
Npy
Rgs1
Map3k11
Itpr1
Hcn2
Prkca
Gria3
Atf2
Gal
Rgs3
Araf
Ppp5c
Map2k1
Grin1
Fosl1
Jund
Phox2b
Ace
Rasgrp1
Cacna1d
Rgs2
Rgs4
Gabrq
Slc6a2
Dbh
Th

Figure S11

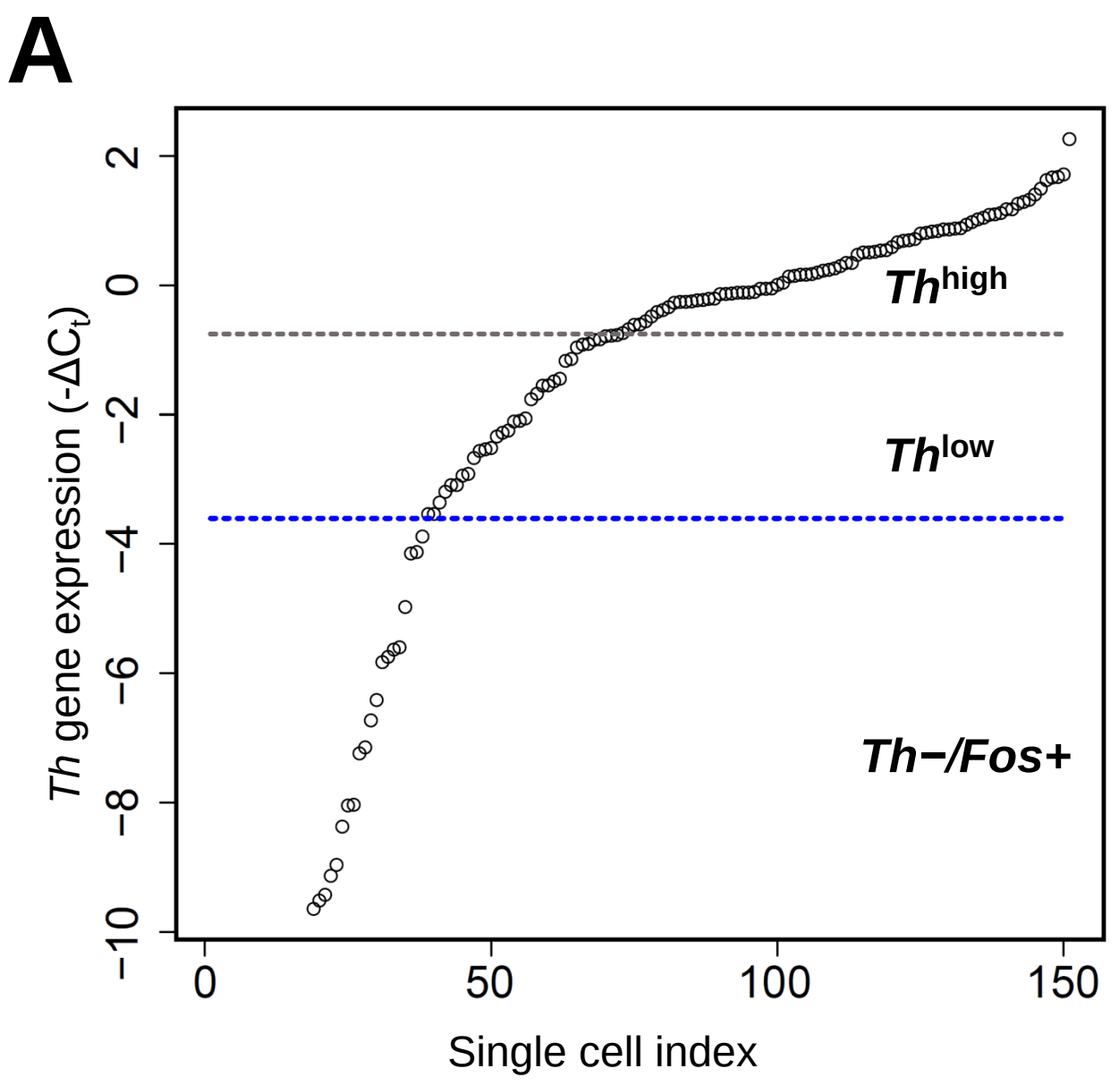
A
Th gene expression (-ΔCt)
Th^high
Th^low
Th−/Fos+
Single cell index

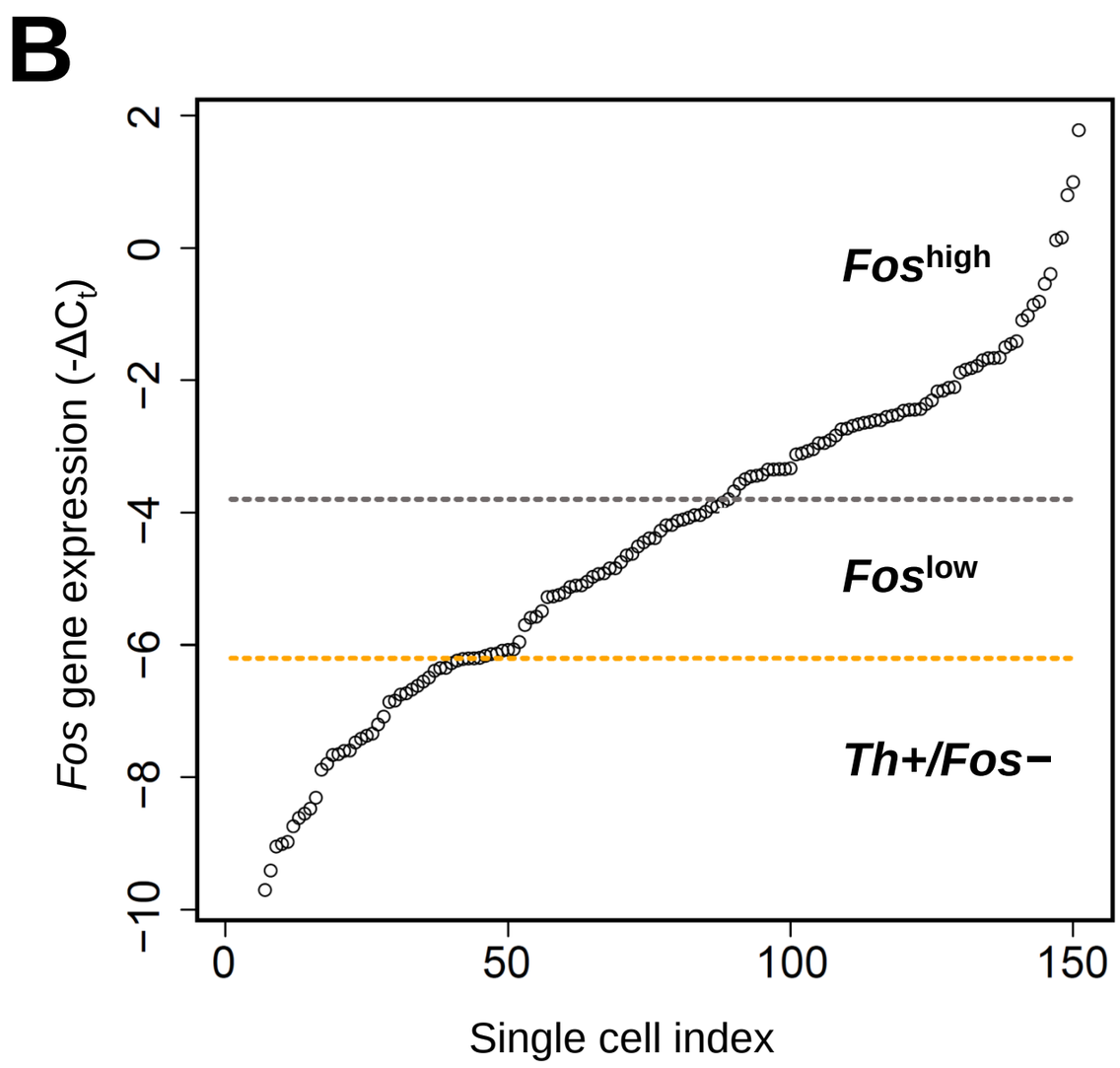
B
Fos gene expression (-ΔCt)
Fos^high
Fos^low
Th+/Fos−
Single cell index

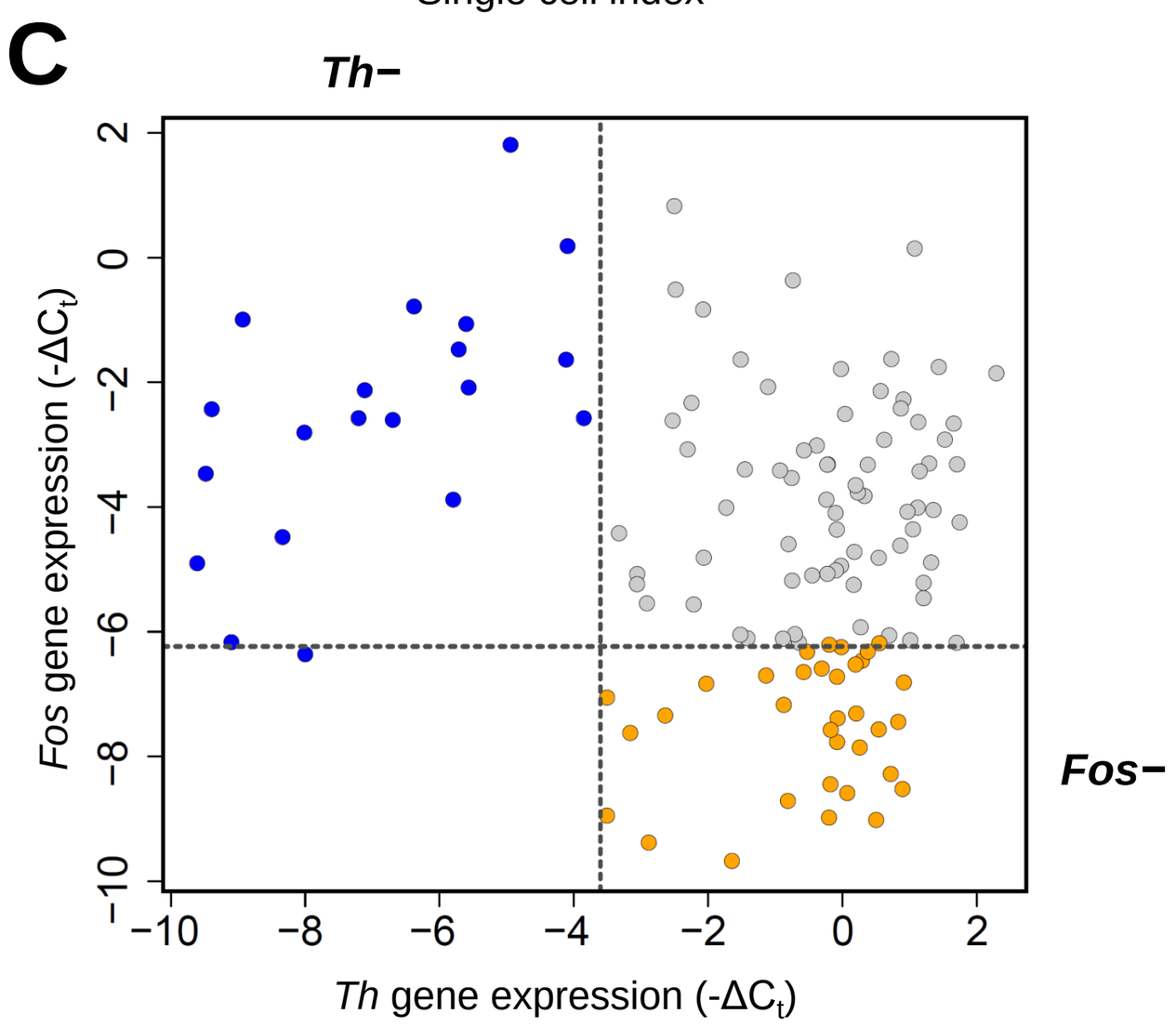
C
Th−
Fos gene expression (-ΔCt)
Fos−
Th gene expression (-ΔCt)

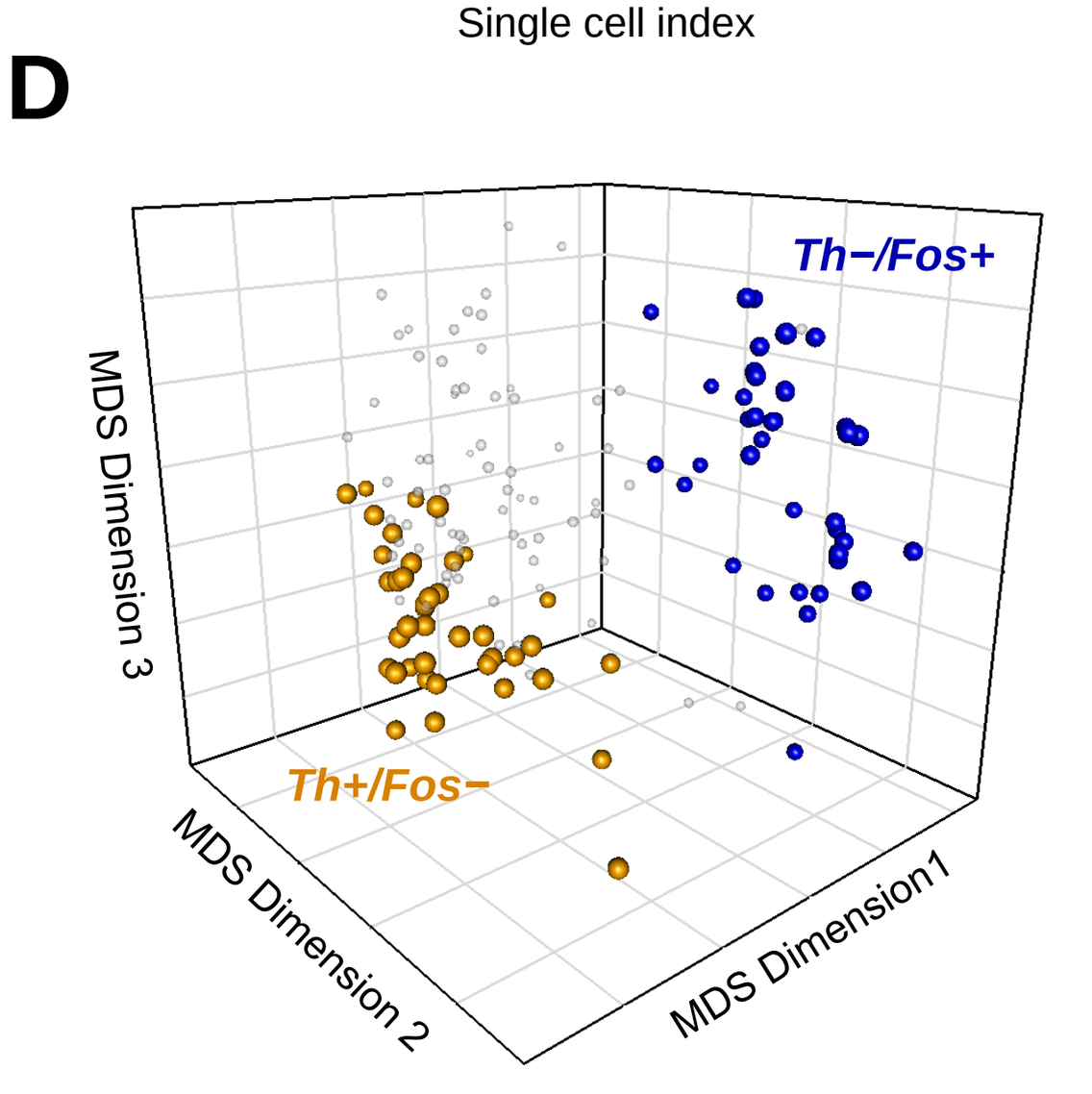
D
Th−/Fos+
Th+/Fos−
MDS Dimension 3
MDS Dimension 2
MDS Dimension1

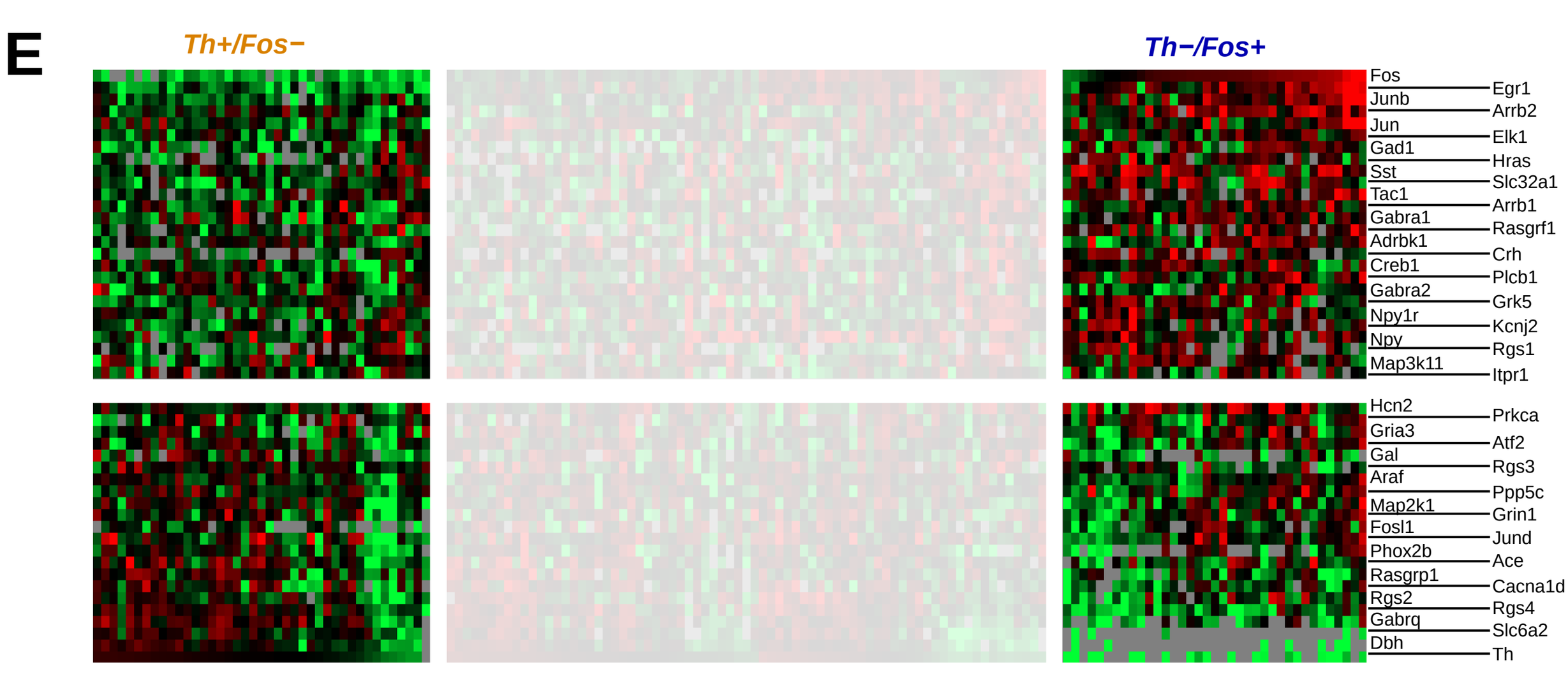
E
Th+/Fos−
Th−/Fos+
Fos
Junb
Jun
Gad1
Sst
Tac1
Gabra1
Adrbk1
Creb1
Gabra2
Npy1r
Npy
Map3k11
Egr1
Arrb2
Elk1
Hras
Slc32a1
Arrb1
Rasgrf1
Crh
Plcb1
Grk5
Kcnj2
Rgs1
Itpr1
Hcn2
Gria3
Gal
Araf
Map2k1
Fosl1
Phox2b
Rasgrp1
Rgs2
Gabrq
Dbh
Prkca
Atf2
Rgs3
Ppp5c
Grin1
Jund
Ace
Cacna1d
Rgs4
Slc6a2
Th

Figure S12

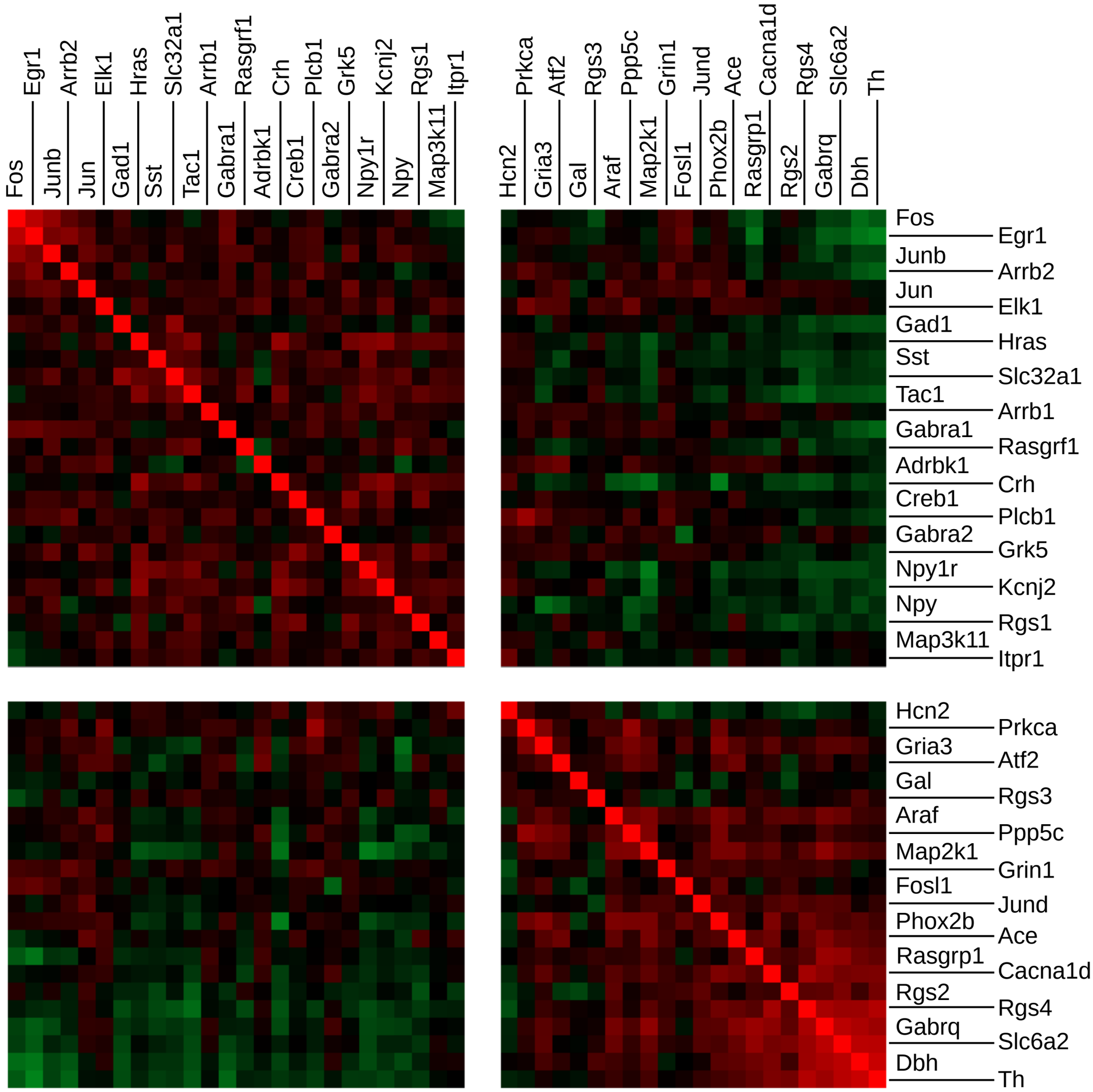
Fos
Egr1
Junb
Arrb2
Jun
Elk1
Gad1
Hras
Sst
Slc32a1
Tac1
Arrb1
Gabra1
Rasgrf1
Adrbk1
Crh
Creb1
Plcb1
Gabra2
Grk5
Npy1r
Kcnj2
Npy
Rgs1
Map3k11
Itpr1
Hcn2
Prkca
Gria3
Atf2
Gal
Rgs3
Araf
Ppp5c
Map2k1
Grin1
Fosl1
Jund
Phox2b
Ace
Rasgrp1
Cacna1d
Rgs2
Rgs4
Gabrq
Slc6a2
Dbh
Th
Spearman Rank Correlation
-1
1

Figure S13

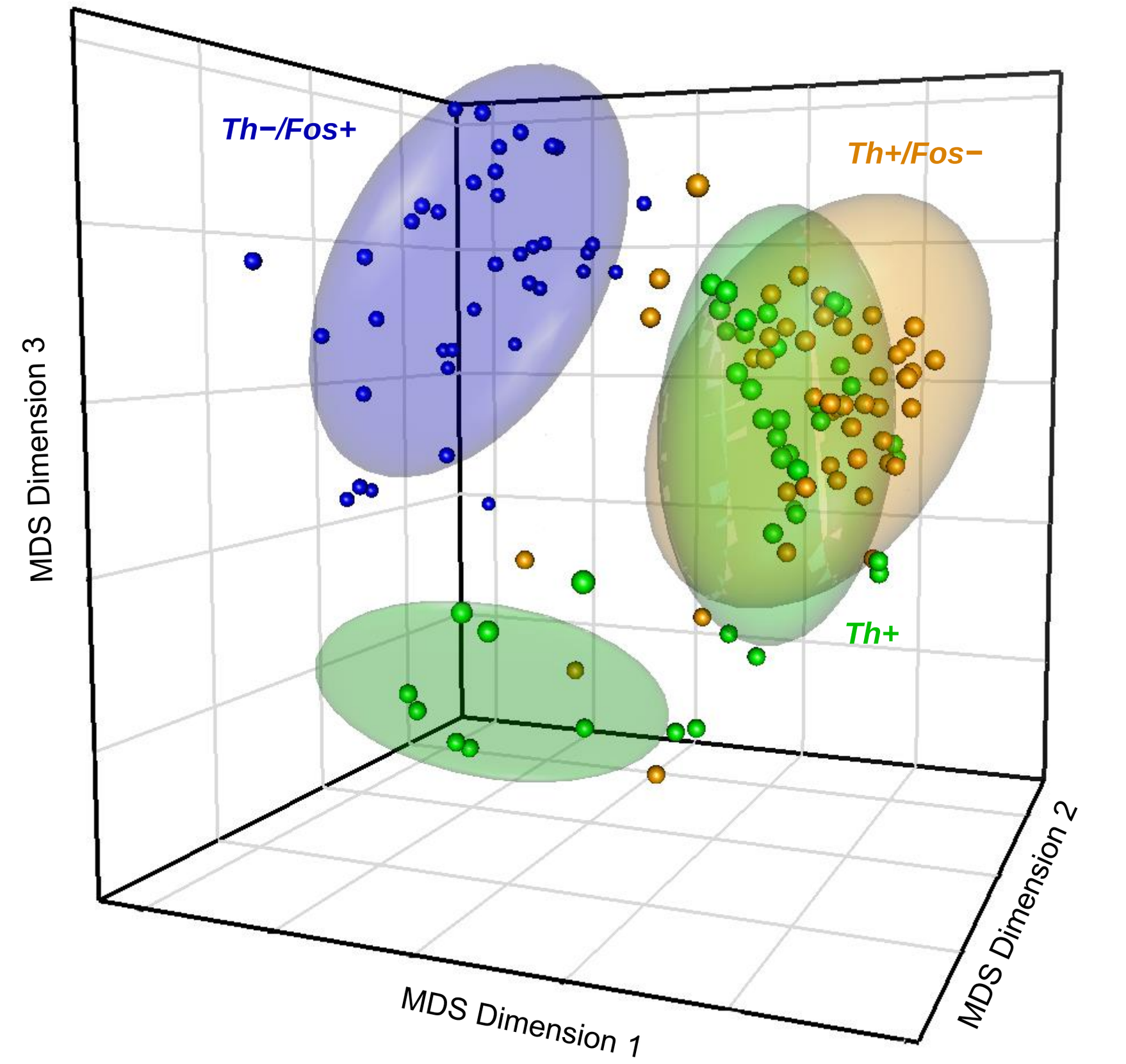
Th−/Fos+
Th+/Fos−
Th+
MDS Dimension 3
MDS Dimension 1
MDS Dimension 2
Hypertensive Th+/Fos–
Hypertensive Th–/Fos+
Baseline Th+

Figure S14

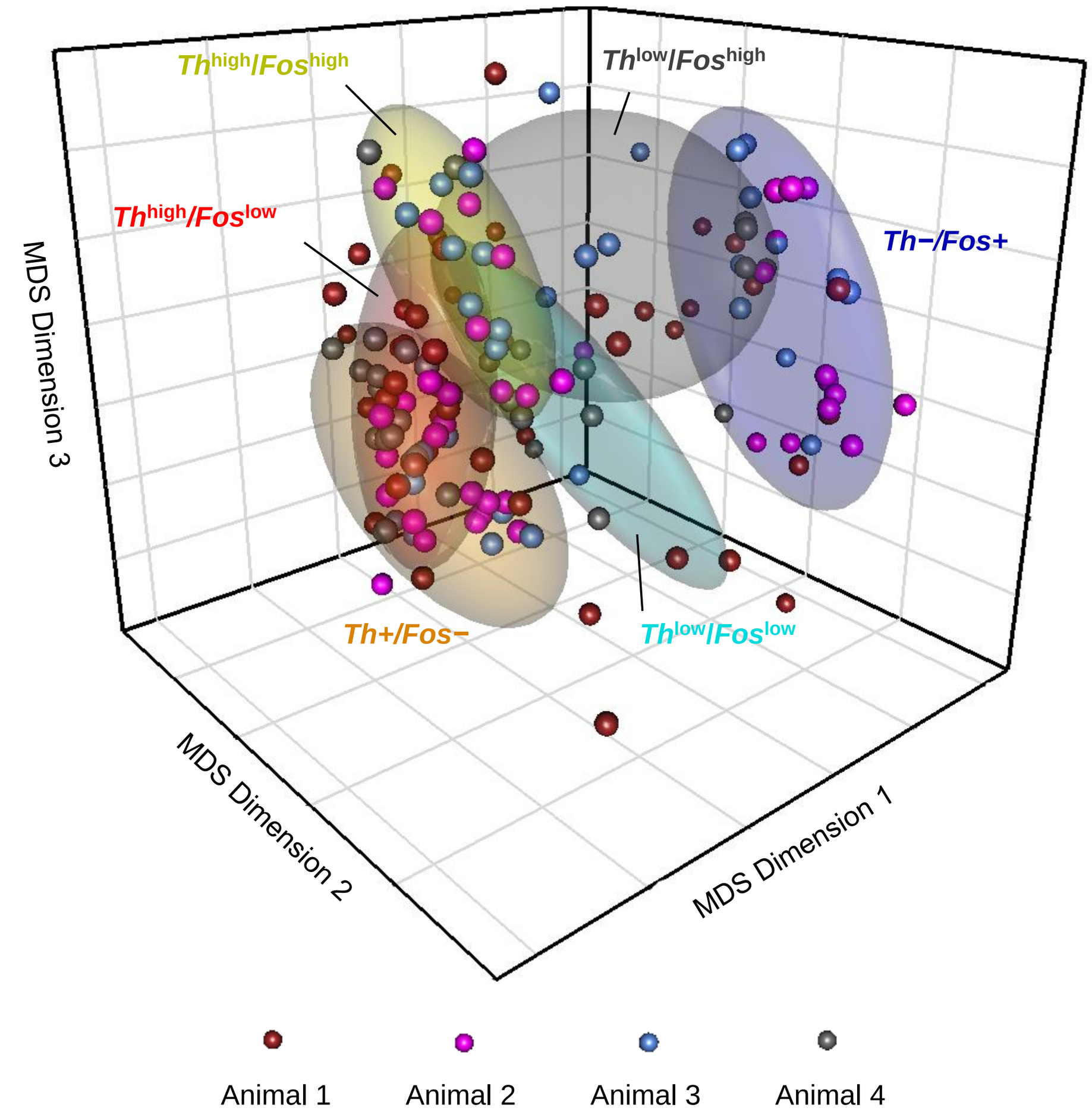
Th^high/Fos^high
Th^low/Fos^high
Th^high/Fos^low
Th−/Fos+
Th+/Fos−
Th^low/Fos^low
MDS Dimension 3
MDS Dimension 2
MDS Dimension 1
Animal 1
Animal 2
Animal 3
Animal 4